Patchy Surfaces

THÈSE N^{O} 8183 (2018)

PRÉSENTÉE LE 2 MARS 2018
À LA FACULTÉ DES SCIENCES ET TECHNIQUES DE L'INGÉNIEUR
LABORATOIRE DES NANOMATÉNAUX SUPRAMOLÉCULAIRES ET INTERFACES - CHAIRE CONSTELLIUM
PROGRAMME DOCTORAL EN SCIENCE ET GÉNIE DES MATÉRIAUX

ÉCOLE POLYTECHNIQUE FÉDÉRALE DE LAUSANNE

POUR L'OBTENTION DU GRADE DE DOCTEUR ÈS SCIENCES

PAR

Nikolaos NIANIAS

acceptée sur proposition du jury:

Prof. V. Michaud, présidente du jury
Prof. F. Stellacci, directeur de thèse
Prof. F. BISCARINI, rapporteur
Prof. F. Schreiber, rapporteur
Prof. H.-A. Klok, rapporteur

ÉCOLE POLYTECHNIQUE
FÉDÉRALE DE LAUSANNE

Suisse
2018

Acknowledgements

Isn’t everything self-assembly?... that is what G. M. Whitesides and B. Grzybowski wondered. Can order come from disorder? You can read this thesis and a few hundreds of books and maybe drive to a conclusion. In this part, I will refer to as many people I can remember that helped me directly or indirectly with thesis or during my research. I wish I will grow to be even a small percentage of a scientist as my supervisor. Francesco is a Scientist, the result of hard work and intelligence, matched with a very good character. I would like to thank him for everything he taught me and the way he supervised and mentored me. I will always owe him a lot. Staying in the Sunmil group, I would like to thank all colleagues and friends. In particular Evi Athanasopoulou the best Athenean who also worked on surface science. I am also very grateful that I finished my PhD and I am writing these acknowledgements on THIS universe. In a universe where one of the Khoolest awesome human ever was my friend and not my arch enemy or something like that…you helped, karma is building up, brace for it and keep it up beata. Quy Ong deserves many thanks and a shrine built somewhere in my village for all the help and guidance that he gave me. He taught me many things and pointed me on the right path, at numerous instances during my PhD and PhD thesis. Anna, thank you for all the help on many things, like AFM imaging and TERS analysis, Zhi you are going to be doctor soon. Of course I am forgetting things that people have done for me but everyone deserves a big thank you Pelin, Elif, Ahmet, Ozgun, the new sunmil PhDs and the postdocs that offered their help in many ways. The “old” Sunmil group also deserves a lot of thanks. Before I close the Sunmil support group, I have to refer to people like Paulo and Sergio who showed me that there are people of my kind at other places too. I was considered a bridge and among the last of the initial (Vaud) Sunmil group and the new Sunmil group. I want to thank them as well, because they helped at the beginning a lot. People like Tam, Randy, Mauro, Martha, Maria, Stefan and the rest of them of course.

Fernando Cometto, the Argentinian professor that showed me a lot and taught me even more. So many questions, met with an answer and a side joke to lighten the mood. Thank you Fernando for the intellectuall honesty and free knowledge. Also I should admit that during my bachelor and master I interacted with some good professors that helped me be were I am today.

I want to thank my family (for working all their lives to provide for me) and my friends. Giotis, Mitsos, Tasos and Migish they offered their precious help a lot during my PhD. Last but not least, I want to thank Katerina. One of the toughest, smartest and beautiful people I have met. I owe her so much, she helped significantly in situations and ways that others could not. I thank her for everything.

This thesis, in terms of character and experience building, made me pursuit new solutions to basic science in the discipline of surface science. Made me appreciate the efforts and the sacrifices science needs. Made me more motivated to become one day a researcher and a professor like my mentor and others like him.

Abstract

Tailoring solid surfaces attracts a number of technological and scientific interest with numerous applications. One method to modify a solid surface is via the formation of a molecular film. The adsorbed molecules assemble spontaneously (self assemble) forming a monolayer that is called self-assembled monolayer (SAM). When dissimilar molecules are employed to form a SAM on a surface, separation into domains takes place, but the domain shapes that have been reported vary from irregular patches with highly non-uniform size distributions to disordered stripes or worm-like domains. It was postulated that the various morphologies observed to date were due to kinetic trapping. The scope of this thesis was to investigate the thermodynamic equilibrium for such monolayers. High quality one- and two-component thiol SAMs on flat Au(111) was produced and studied. The thiols that were used were Octanethiol (OT), 4-Cyano-1-butanethiol (CN4T), para-nitrothiophenol (NB4M) and 3-mercaptopropionic acid (MPA). The SAMs were produced via solution immersion. XPS and contact angle measurements verified the SAM formation. Cyclic voltammetry has been employed for the reductive desorption of the bounded thiols. The reductive potentials of the thiols have been measured at -0.97 V for OT, -0.79 V for CN4T, -0.75 V for the NB4M and -0.78 V for the MPA. The difference in the peak potentials facilitates our studying of binary SAMs by this method. Binary SAMs of OT:CN4T, OT:NB4M and OT:MPA at different feed ratios was produced via solution immersion. The surface composition of the OT:CN4T and OT:NB4M binary SAMs was determined by XPS. The CV analysis of the binary SAMs showed two distinct separated peaks at the reductive potentials of the two constituting thiols, which indicates the existence of phase separated macro domains onto the Au(111) surface. A large series of one- and two-component SAMs were thermally treated inside neat solvent at 60°C (annealing) for various amounts of time. XPS and contact angle measurements verified that the annealing process did not cause any alterations on the composition or the quality of the SAMs. Upon annealing, the evolution of the binary SAM surfaces was found to lead to new nanoscale thermodynamic phases as indicated by the voltammograms. The two-peak profiles that were seen at the non-annealed binary SAMs changed to three-peak profiles, with the appearance of a new peak at an intermediate potential. As the annealing time increased a single peak profile was received. The one-peak CV profiles remained unaltered (one peak at an intermediate potential) upon further annealing. The new phase is therefore the thermodynamically equilibrium phase. The new equilibrium phase was identified by STM. The new phases were found to depend on the choice of ligand and the composition. STM imaging elucidated further that the new phase can morphologically be stripes with an average width of ∼3 nm for annealed SAMs of OT:CN4T and OT:NB4M, prestripes for OT:NB4M binary SAMs with higher OT concentration, while OT:CN4T at 20 days of annealing and OT:MPA 10:90 led to micellar domains in the size range from 4 to 8 nm as the thermodynamic phase. The work presented in this thesis has shown how the process of annealing leads to new thermodynamically equilibrium phases in binary SAMs. Due to this process, nanostructured surfaces with a variety of domains can be achieved in binary SAMs of thiols on flat Au(111) surfaces.

Keywords: Binary self-assembled monolayers, thiol, phase separation, electroreductive desorption, STM

Sommario

La possibilità di ingegnerizzare le superfici solide attrae l'interesse scientifico e tecnologico in vista di numerose applicazioni. Un metodo per modificare le superfici solide è la formazione di film molecolari. Le molecole adsorbite si assemblano spontaneamente (auto-assemblaggio) formando un monostrato chiamato monostrato auto-assemblato (Self-Assembled Monolayer, SAM). Quando molecole diverse sono utilizzate per formare un SAM su una superficie si ottiene una separazione in domini, ma le forme riportate per i domini variano da macchie irregolari con distribuzioni di taglia altamente non uniformi fino a strisce disordinate o domini vermiformi. È stato postulato che le diverse morfologie osservato finora siano dovute a trappole cinetiche, lo scopo di questa tesi era dunque quello di studiare l'equilibrio termodinamico per questi monostrati. SAM di alta qualità composti da uno o due componenti tiolati su oro piatto (Au(111)) sono stati prodotti e studiati. I tioli utilizzati sono ottantiolo (OT), 4-Ciano-1-butantiolo (CN4T), para-nitrotiofenolo (NB4M) e acido 3-mercaptopropionico. I SAM sono stati prodotti tramite immersione in soluzione. Misure di XPS e di angolo di contatto confermano la formazione dei SAM. La voltammetria ciclica (CV) è stata impiegata per il desorbimento riduttivo dei tioli legati. I potenziali riduttivi dei tioli sono stati misurati a -0.97 V per OT, -0.79 V per CN4T, -0.75 V per NB4M e -0.78 V per MPA. La differenza nei picchi del potenziale facilita il nostro studio dei SAM binari con questo metodo. SAM binari di OT:CN4T, OT:NB4M e OT:MPA a diversi rapporti di concentrazione in soluzione sono stati prodotti tramite immersione in soluzione. La composizione sulla superficie dei SAM binari di OT:CN4T e OT:NB4M è stata determinata tramite XPS. L'analisi CV dei SAM binari mostra due picchi distinti separati ai potenziali di riduzione dei due tioli costituenti, indicanti la presenza di separazione di fase in macro domini sulla superficie Au(111). Un gran numero di SAM ad uno o due componenti sono stati sottoposti a trattamento termico immergendoli in solvente pulito a 60°C per diversi intervalli temporali (ricottura o annealing). Misure di XPS e angolo di contatto dimostrano come il processo di ricottura non causi l'alterazione della composizione o della qualità dei SAM. Durante la ricottura, l'evoluzione delle superfici di SAM binari porta alla comparsa di nuove fasi termodinamiche alla nanoscala, come indicato dai voltammogrammi. I profili a due picchi misurati su SAM binari non ricotti diventano profili a tre picchi, con la comparsa di un nuovo picco ad un potenziale intermedio. Aumentando il tempo di ricottura sono stati ottenuti profili a picco singolo. I profili CV a picco singolo sono rimasti inalterati (un picco a potenziale intermedio) anche applicando ulteriori processi di ricottura. La nuova fase è dunque la fase di equilibrio termodinamico ed è stata identificata tramite STM. Le nuove fasi si sono rivelate dipendenti dalla scelta dei leganti e dalla composizione. Le immagini STM hanno rivelato come le nuove fasi possano essere, morfologicamente, strisce con una larghezza media di ~3 nm in SAM di OT:CN4T e OT:NB4M o prestrisce per SAM binari di OT:NB4M con concentrazione maggiore di OT, mentre OT:CN4T dopo 20 giorni di ricottura e OT:MPA 10:90 portano a domini micellari con dimensioni comprese tra 4 e 8 nm come fase termodinamica. Il lavoro presentato in questa tesi ha mostrato come il processo di ricottura porti a nuove fasi all'equilibrio termodinamico in SAM binari. Grazie a questo processo, superfici nanostrutturate con una varietà di domini possono essere ottenute su SAM binari di tioli su superfici piatte di Au(111).

Parole chiave: Monostrati auto-assemblati binari, tiolo, separazione di fase, desorbimento elettro-riduttivo, STM

Contents

Acronyms

SAM	Self-assembled monolayer
OT	octanethiol
AFM	atomic force microscopy
C12	dodecanethiol
C9	nonethiol
CN4T	4-Cyano-1-butanethiol
CV	Cyclic voltammetry
KOH	potassium hydrxide
LSV	Linear sweep voltammetry
MPA	3-mercaptopropionic acid
MUA	mercapto undecanoic acid
NB4M	para-nitrothiophenol
SPM	Scanning probe microscopy
FWHM	full width at half maximum
HWHM	half width at half maximum
STM	Scanning tunneling microscopy(e)
XPS	X-ray Photoelectron Spectroscopy

1. Introduction

The boundary between two states of matter is called interface. A surface is established as a solid-gas, solid-liquid or liquid-solid, liquid-gas interface. Surface science is devoted on the study and engineering of these interfaces at macroscopic and/or microscopic level. Tailoring solid surfaces attracts a huge technological and scientific interest with numerous applications in wetting, electronics, catalysis, corrosion control, lubrication and others [1]–[6]. One method to modify a solid surface is via the formation of a molecular film. The immense interest in molecular-scale coating arises from the fact that is an immediate and simple method to alter the physicochemical properties of a surface and tune its properties. Functionalisation of a surface with a thin organic film can be achieved by the absorption of molecules onto a solid. The molecules will assemble spontaneously (self assemble) forming a monolayer that is called self-assembled monolayer (SAM)[7]. It is not possible to engineer many interfacial properties with a single-molecule monolayer. Functionalisation of a surface with a binary-component SAM (i.e. a SAM that is comprised of two molecules) will give rise to groundbreaking contributions on new applications. When we have two dissimilar molecules, considerations of conformational entropy lead to the formation of phase-separated domains. A series of properties are believed to arise and depend on these nano-sized patterns. Patchy surfaces are defined here as surfaces processing domains that are chemically or physically different from the surrounding.

This thesis deals with the basic science of SAMs composed of binary mixtures of molecules on flat surfaces. It is a morphological study on the key parameters that determine the kinetically trapped morphologies. The link between surface morphologies and ligand length mismatch is also investigated. The main research question of this thesis is whether a new phase is achieved under thermal treatment in solvent (annealing) and what are the equilibrium patterns that are achieved. Sound characterisation approaches are employed for the investigation of the surface composition, surface morphologies and stability of SAM.

Thesis Outline.

This thesis is structured as follows:

- Chapter 2, Introduces the reader to self-assembly, one-component SAMs and the basics of thiols SAMs on gold. The second part focuses on phase separation in binary systems, previous experimental and theoretical work on binary SAMs of thiols on gold. The last part is a description of the surface analysis techniques that have been employed.
- Chapter 3, contains the experimental procedure, details about the synthesis, analytical methods description and methods validity with examples.
- Chapter 4, presents the results on the binary SAMs. A discussion about the annealing process that does not have a negative result on the SAM but it allows it to reach equilibrium that is easily and quickly identified with cyclic voltammetry. The chapter finishes with the STM images of this new phase that the annealing led to.
- Chapter 5, contains the final conclusion from the studies on binary SAMs and the outlook
- Appendix A contains the reagents and materials, experimental procedure and supplementary material.
- Appendix B contains additional STM images.
- Appendix C contains all the voltammograms of all the surfaces/samples.

2. Self-assembled monolayers

2.1. Self-Assembly

Self-assembly is defined as the spontaneous association of disordered "building blocks" into defined 2- or 3-dimensional geometries. The components can be molecules, particles or even planetary bodies. Since the middle of 1980s, research in self-assembly has been insuppressibly leaping forward. Self-assembly is a strategy that can be applied at all scales. But it originated from organic chemistry and molecular studies. Self-assembly epitomizes the interplay between enthalpy and entropy, where order emerges from disorder using energy to compensate reduction in entropy[8]. Self-assembly is an effective approach that has the potential of producing novel materials with tuned properties and specific patterns.

Molecular self-assembly is a thermodynamics process where the molecules and the self-assembled domains are in equilibrium. Self-organization differs to self-assembly in terms that it requires a situation far away from thermodynamic equilibrium with external forces acting on it. A leading example is pattern formation in reaction-diffusion systems, by Turing[9], [10]. Whitesides et al. . managed to comprehensively explain the concept of self-assembly and even categorise its types at their publication *"Self-Assembly at All Scales"*[11].

Self-assembly of amphiphilic molecules leads to a variety of structures. Strong hydrophobic attraction promotes the organisation into spherical, rod-like micelles, bilayered membranes and other continuous structures. The covalent bonds between immiscible blocks in block copolymers leads to micro-phase separation. A variety of patterns in the bulk is achieved by controlling the composition of the two blocks and the temperature[12]. Self-assembly is responsible for nature's ability to construct large complex structures with biological functionality. The covalent or ionic bonds between the building blocks as well as, interactions like van der Waals, London, π-π and hydrogen bond play an important role in self-assembly [13]. In nature, a protein takes part in essentially every structure and activity of life. Proteins have a unique signature that derives from their primary, secondary, tertiary, and quaternary structures. Intensive studies are trying to shed light on the properties that are attributed to the surface of the proteins that is composed of hydro-philic,-phobic patches/areas. One very interesting finding was that the proteins' ability to form patterns and self-assemble is allowing them to identify and communicate information in their environment. Research on nanomaterials with amphiphilic surface can assist in understanding the connection between surface composition and properties[14][15].

2.2. Organic self-assembled monolayers

Self-assembled monolayers (SAMs) are molecular assemblies formed spontaneously on surfaces by adsorption and are organized into domains. The essential component of SAM (called ligands) consists of: the anchoring-head group, which attaches the molecules to the surface, the functional group, which defines the state of functionalization of the new outer surface and the spacer chain, which via Van der Waals' interactions, provides an additional driving force for the adsorption reaction, that creates a certain degree of order in the system

2.2.1 One-component thiol SAMs on Au

The purpose of this sub-chapter is to introduce the reader to the basics of thiols SAMs on gold. The work that is being done on single-component SAMs leads to a level of understanding that is, in most of the cases, clear and remarkable. A plethora of new mechanisms, models and applications for single SAMs is constantly proposed by researchers.

The most studied and known SAM is monolayers of an alkanethiol on Au(111). The thiol group bonds almost covalently with the gold atoms (bond energy ~50 kcal/mol). The steps of the SAM formation are physisorption via solution immersion or vapors, chemisorption of the thiol and the formation of bond. As the binding sites decrease the density of the monolayer increases and the thiols transit form the ordered lying-down phase to the stand-up phase. The phases are shown at Figure 1.

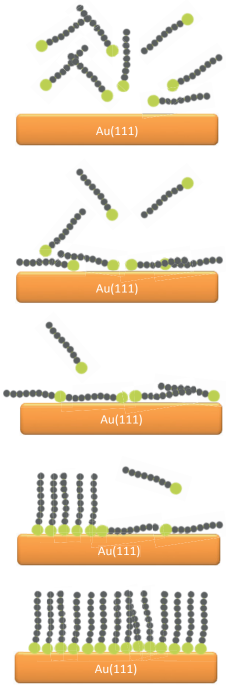

Figure 1. Scheme of the different steps during the self-assembly of alkanethiol on Au(111). Physisorption(top), chemisorption, lying down phase formation, nucleation of the standing up phase, completion of the standing up phase.

The transition to the fully ordered crystalline condition depends on the substrate, chain defects, terminal group and the chain-chain interactions. The van der Waals interactions are the reason why longer alkanethiols will form crystalline phases at lower times[16]. Increase in temperature can also speed up the transition to the ordered phase, provided that thermal decomposition does not occur. Thermal decomposition of a alkanethiol SAM has been reported to happen at 170-230^{o} C [17]. The reaction of Au with a thiol is not fully understood, but it is believed that it occurs via oxidative addition, followed by reductive elimination of 1/2 H_2. The fate of the hydrogen is also a matter of controversy, but recent studies on aromatic nitro-containing thiols showed partial reduction of the nitro terminal group into amine. The released hydrogen from the formation of Au-S bond on the surface environment is believed to be the reason for the reduction[18]. As mentioned before, the monolayer undergoes a two-step growth process. The sites that the ligands will prefer to attach are the defective and exposed sites (i.e. the step edges). The islands of lying-down ligands are formed and increase in density leads to the stand-up phase. A TOF-DRS study on the H signal from a methyl-terminated thiol has shown the two steps (Figure 2). The first plateau pin-points the completion of the lying-down phase, as the exposure increases the stand-up phase is achieved. The second plateau is at the most dense phase that all molecules are upright and the surface coverage is $\theta \sim 1/3$[19].

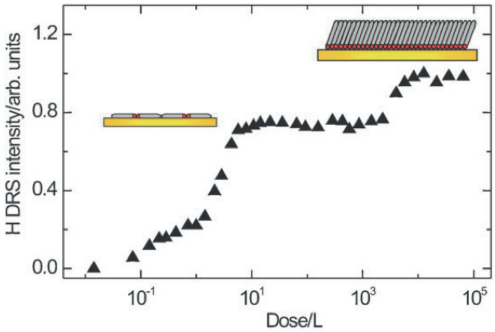

***Figure 2. Hydrogen DRS intensity from Au(111) versus exposure to hexanethiol in UHV. The lying-down and stand-up phases are at the two plateaus. Reproduced with permission from** [19].*

Initially it was believed that the thiol can bind in Au111 at three possible sites. The energy minima at the Au(111) hollow sites, renders it the site of selection for the absorption. One thiol occupying every sixth hollow site results in a $\sqrt{3}x\sqrt{3}R30^0$lattice[20]. Further studies showed that four molecules in two indistinguishable pairs resulting in a rectangular unitmesh. The notation of the new super lattice was c(4x2). Recent studies have shown that the surface undergoes reconstruction during the SAM formation. The reconstruction includes vacancy formation and adatoms of gold. The most recent proposed model are shown at Figure 3.Two independent studies using S2p photoelectron diffraction and S1s NIXSW concluded that the S atom occupies the a-top site. A NEXAFS study came later to lead to the same conclusion[21][22][23].

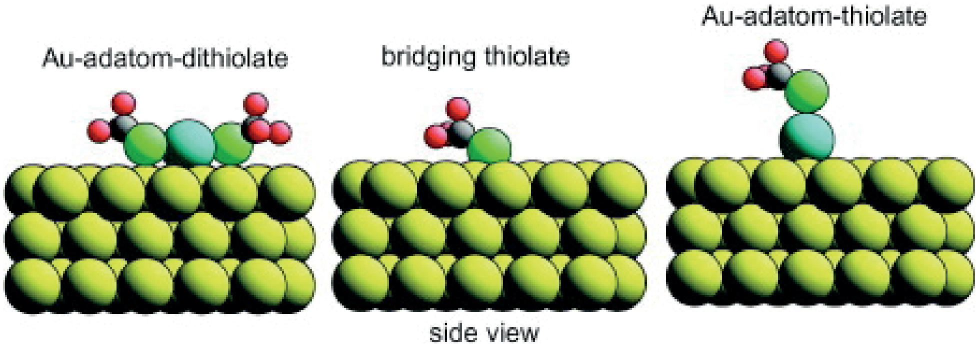

***Figure 3. On the left is shown the Au-adatom-dithiolate model in which two thiolate species lie on either side of a bridge-bonded Au adatom with the S atoms in near-atop sites relative to the underlying Au(1 1 1) surface. On the right is shown the Au-adatom-thiolate model in which the thiolate lies atop an Au adatom which occupies a bulk-continuation fcc hollow site. In the centre is the simple bridging thiolate that has been proposed to coexist on the surface with the Au-adatom-dithiolate species. With permission from** [22].*

The ongoing research will prove, enrich or disprove the new models. Until then it is accepted that for short thiols the presence of adatoms is evident and plays crucial role in the SAM formation process. The surface complexes $RS\text{-}Au_{ad}\text{-}SR$ are not only present on flat surfaces but they have been identified on gold nanoparticles[24]. The RS-Au$_{ad}$-SR moieties are also assumed to be present in long thiol SAMs. The bridge-bonded model is also expected to be generated during SAM formation[25], [26].

Initial reports on small carboxyl-terminated thiols showed a variety of structures (3x3), $2\sqrt{3}x2\sqrt{3}R30^0$, $p\ x\sqrt{3}$ and $p\ x2\sqrt{3}$. Rigorous research has proven that single-component SAMs of ligands that bare a carboxyl terminal group form the $\sqrt{3}x\sqrt{3}R30^0$ and the c(4x2) lattices like the methyl-terminated thiols. Azzaroni et al. provided the verification employing STM and electrodesorption analysis on mercaptoundecanoic acid (MUA) and mercaptopropionic acid (MPA) [27]. Sawaguchi et al. showed the packing arrangements of MPA on a (3x3) structure that is close to the $\sqrt{3}x\sqrt{3}R30^0$ with every three MPA molecules snuggled up in a triangle position[28]. Last but not least, Stellacci et al., using STM in air showed that the $\sqrt{3}x\sqrt{3}R30^0$ structure featuring a c(4x2) supperlattice is received in MPA SAMs. Figure 4 [29].

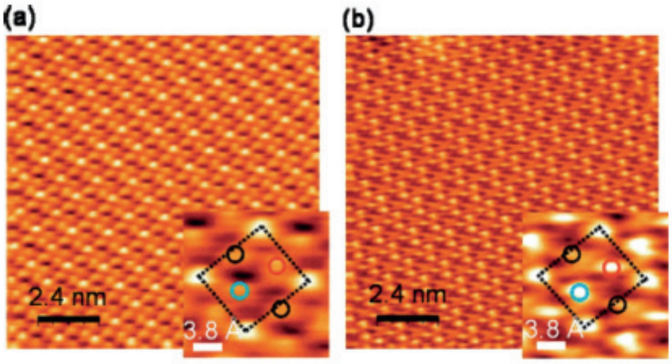

***Figure 4. Different contrasts for the molecules in the c(4×2) structure have been observed at different locations on a MPA SAM: The two polymorphs are shown at (a) and (b). (a): β-contrast and (b): ζ-contrast (Vb=500-700 mV, It =500 pA.) . Reproduced from** [29].*

Nitro aromatic single SAMs have been studied mainly due to the fact that the nitro group may reduce to an amino group as has been already mentioned in this chapter. Either on gold or silver the aromatic nitro-containing thiols can be reduced partially to amino terminated thiols or dimerize or crosslink. Electrochemically, chemically, using low energy electrons or during SERS/TERS the nitro group can be reduced and the gold might catalyze the transformation[30]–[36].

Cyano-terminated single-component SAMs have not been reported despite the importance and the agility that a cyano group can offer in terms of properties and further chemical reactions.

2.2.2 Phase separation in binary systems

From a thermodynamic point of view, the molecular phase separation is the result of the competition between enthalpic energy gain and the entropy of mixing, favoring the random distribution. Phase separation occurs only if the enthalpy of mixing exceeds the entropy of mixing. The energy gain dictates the degree of phase separation i.e. small or large areas of a single-component phase. In a binary system, for the two phases to equilibrate the enthalpy of mixing has to overcome the entropy of mixing. The free energy of mixing is presented at Figure 5. The Ca and Cb wells correspond to a phase of only ligand-a and only ligand-b, respectively. When the average SAM composition is between the Ca and Cb then the monolayer phase separates in order to reduce the free energy[37].

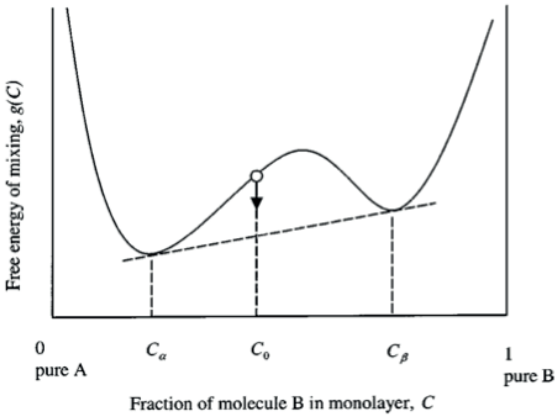

***Figure 5. The free energy of mixing for a monolayer composed of two molecular species, A and B. The pair has a large enthalpy of mixing, so that the free energy of mixing has two wells at Ca and Cb , corresponding to two phases. Reproduced from** [37].*

Block copolymers are binary systems that undergo micro-phase separation and their two components self-assemble into a variety of nanoscale morphologies. The self-assembly process is driven by an unfavorable mixing enthalpy and a small mixing entropy, while the covalent bond connecting the blocks prevents macroscopic phase separation.

A polymer blend, during mixing can phase separate or lead to a homogenous mixture. The Flory-Huggins equation for a blend of two polymers PA and PB is given below:

$$\Delta G_{mix} = \Delta H_{mix} - T\Delta S_{mix} \qquad \text{(eq 2.1)}$$

If the Gibb's free energy is negative then the blend is homogenously miscible. The $T\Delta S_{mix}$ is always positive. If the entropic contribution of free energy surpasses the enthalpic contribution ($\Delta H_{mix} < T\Delta S_{mix}$) then a single phase is received. A similar (mean free) approach by Flory and Huggins, that considers that the volume does not change, is given by:

$$\Delta H_{mix} = f_A f_B \chi_{AB} \qquad \text{(eq 2.2)}$$

The occupied volume fractions of PA and PB are the fA and fB. χ is an interaction parameter that specifies the degree of incompatibility between the PA and PB, temperature is implemented in this parameter.

$$\chi_{AB} = \frac{Z}{k_{BT}}(w_{AB} - 0.5(w_{AA} - w_{BB})) \qquad \text{(eq 2.3)}$$

Z is the nearest neighbor contacts, and w_{xx} are the interaction energies between monomers. The entropy of mixing si given by:

$$\Delta S_{mix} = -k_b\left(\frac{f_A}{N_A} lnf_A + \frac{f_B}{N_B} lnf_B\right) \qquad \text{(eq 2.4)}$$

where Nx is the degree of polymerization of the two polymers. From the equations 6.1 and 6.4 we arrive to the expression of the mixing behavior of blends[38].

$$\frac{\Delta G_{mix}}{KBT} = \chi f_A f_B + \frac{f_A}{N_A} lnf_A + \frac{f_B}{N_B} lnf_B \qquad \text{(eq 2.5)}$$

Block copolymers are a polymer category. They consist of different long macromolecules. The prefix (di-, tri-, multi- etc.) added corresponds to the number of macromolecular chains (blocks). The correct nomenclature for block copolymers is: "polyA-block-polyB". Many different molecular structures of block copolymers can be synthesized by anionic polymerization. Linear AB block copolymers are the simplest block copolymer structures where blocks of different chemical structures are linked together in line, when more than two dissimilar blocks are bind through a common junction point more complicated structures are received[39]. Most block copolymers have an ordered equilibrium microdomain structure. The phase behavior of diblock copolymers has been the subject of numerous theoretical and experimental studies over recent decades, and is relatively well understood[40], [41]. This self-assembly process is driven by an unfavorable mixing enthalpy and a small mixing entropy, while the covalent bond connecting the blocks prevents macroscopic phase separation[42][43].Since the first synthesis block copolymers have been intensively investigated[44]. They are widely used and their study allowed for (i) a deeper understanding of phase-separation, (ii) a revisit of the physical understanding of a phase, (iii) a revisit of the concept of hierarchical assembly and (iv) the development of the concept of directed assembly[45].

As we mentioned earlier, in the bulk, block copolymers with immiscible blocks can self-assemble into a variety of ordered nanoscale morphologies with a tremendous scientific and technological impact. The microphase separation of diblock copolymers depends on three parameters: (i) the volume fractions of the A and B blocks (fA and fB,), (ii) the total degree of polymerization (N = NA + NB), and (iii) the Flory–Huggins parameter (χAB) which specifies the degree of incompatibility between the A and B blocks, which drives the phase separation. Temperature is implemented in this parameter[46], [47]. The representation of the most distinct morphologies in di-block copolymers in the bulk is provided at Figure 6.

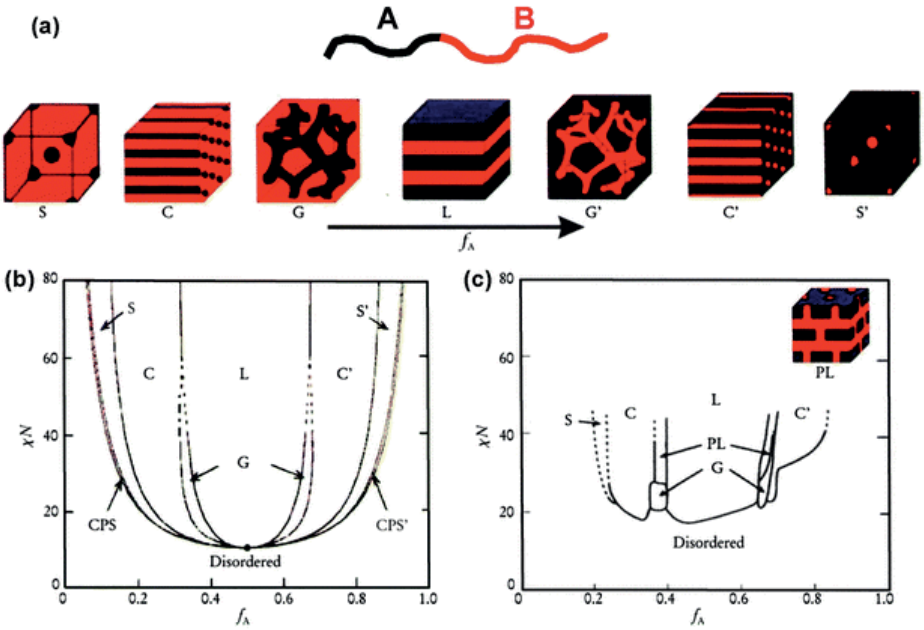

***Figure 6. (a) Equilibrium morphologies of AB diblock copolymers in bulk: S and S′= body-centered-cubic spheres, C and C′= hexagonally packed cylinders, G and G′= bicontinuous gyroids, and L = lamellae. (b) Theoretical phase diagram of AB diblocks predicted by the self-consistent mean-field theory, depending on volume fraction (f) of the blocks and the segregation parameter, CPS and CPS′= closely packed spheres. (c) Experimental phase portrait of polyisoprene-block-polystyrene copolymers, in which fA represents the volume fraction of polyisoprene, PL = perforated lamellae. Reproduced from** [46].*

The block copolymer system that has been described above is one of the binary systems in which self-assembly is dictating the formation of defined geometries. Self-assembly has also been proven to be the morphology-defining factor in systems such as proteins' quaternary structure, liquid crystals and lipid aggregates. Equivalently, separation into domains takes place spontaneously in the case of binary SAMs on solid surfaces.

2.2.3 Binary thiol SAMs on Au(111)

The level of understanding of and control over single component SAMs is, in most of the cases, clear and remarkable. However a binary SAM will provide an inhomogeneous coating. When dissimilar molecules are employed to form a SAM on a surface, separation into domains takes place spontaneously, but the domain shapes that have been reported vary from irregular patches with highly non-uniform size distributions to disordered micellar or worm-like domains. Therefore, as soon as mixtures of different molecules are used to coat surfaces, most of the control we had on single components SAMs is lost.

The purpose of this sub-chapter is to present all the studies on binary SAMs on gold. The phase separation and the domain shape and sizes that have been identified at various pairs of thiols are discussed and STM images are supplied.

The main characteristic of phase separated SAMs is the observation of patchy domains. Jeong Sook Ha et. al. showed that patchy domains of 40 nm^2 are received in the case of Octanethiol(OT):Dodecanethiol(C12) SAMs on Au(111), at various molar ratios of the thiols in the solution via solution co-absorption at room temperature (Figure 7)[48].

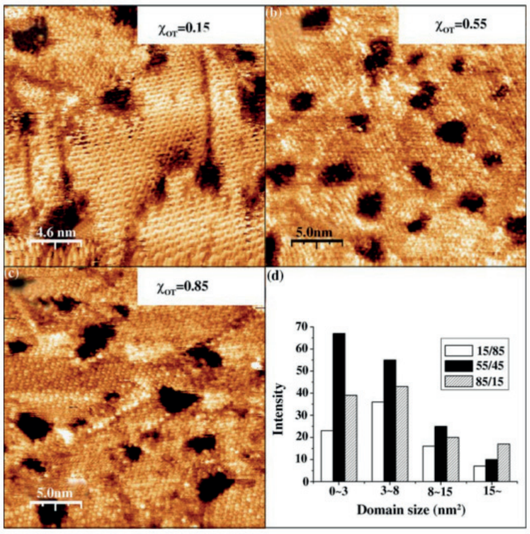

Figure 7. STM images taken from the binary SAM of OT:C12 on Au(111) surface with variation of mole fraction of OT in solution: (a) 0.15; (b) 0.55; (c) 0.85; (d) domain size distribution of the minor-component on each binary mixed SAM surfaces. Reproduced from *[48].*

Binary SAMs with an aliphatic and an aromatic thiol have also been studied in regards of phase separation and resulting surface morphologies. Gaby Avila-Bront et. al. via STM have shown patches on a OT:biphenyl-4-thiol SAM. The OT was initially deposited via vapor deposition. The second step involved the immersion of the OT SAM in a solution of the biphenyl-4-thiol. The place exchange reaction of these thiols that have different molecular lengths, lead to phase separation and the clear identification of disordered patches surrounding flat patches (Figure 8) [49].

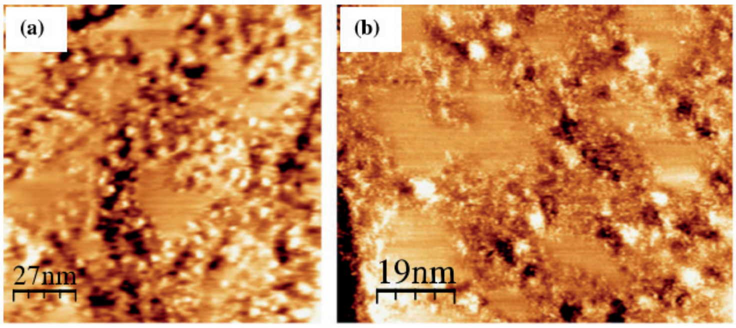

***Figure 8. OT monolayer immersed in 100 μM BPT solution for 20 minutes. Areas of disorder surround flat domains. Images of different areas of the same surface. Reproduced from** [49].*

Bjorn Lussem et. al. have shown that patchy domains and isolated ligands are received via solution immersion of a C12 preformed SAM in a 4-methyl-1,1'-biphenyl-4-butane solution. The patches of the later introduced thiol result because of its insertion at defect sites on the C12 SAM. Isolated molecules are inserted at C12 domains (Figure 9) [50].

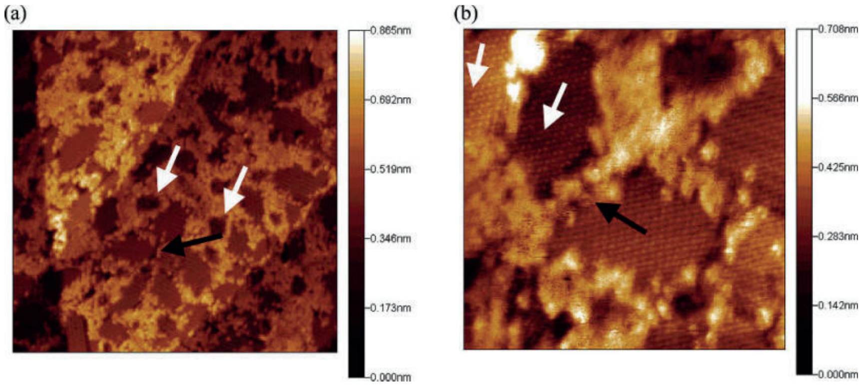

***Figure 9. STM scans {(a) 100 × 100 nm2 and (b) 30 × 30 nm2}of a C12:BP4 SAM. The film shows separate BP4 and C12 domains. Higher appearing domains consist of BP4. In the higher-resolution scan, the c(4 × 2) structure of C12 is visible (white arrows in b). Black arrows mark the nucleation of BP4 domains at C12 domain boundaries, and the white arrows in part a mark the nucleation of BP4 domains at holes in the gold surface. Reproduced from** [50].*

H.Yamada et al., using a Kelvin probe force microscope combined with the non-contact atomic force microscope reported that patchy domains are received on binary C12:C8 and C12:C14 SAMs. The procedure involved the thermal treatment of the pre-formed singe-component SAM, in order to introduce defects, and the addition of the second thiol. The length mismatch and the procedure are the main factors of the patchy morphologies [51].

Binary SAMs that include one or both thiols with a heteroatom (O or N) either at the spacer or at the terminal group also phase separate. Rafael Madueño et al. analysed binary SAMs of 1-decanethiol and 11-mercaptoundecanoic acid, using cyclic voltammetry, electrochemical impedance spectroscopy and infrared reflection−absorption spectroscopy. He reported that, according to the intermolecular interactions, the two possible surface morphologies that the SAM can have are small nanodomains (patches) or a molecularly mixed monolayer (Figure 10) [52].

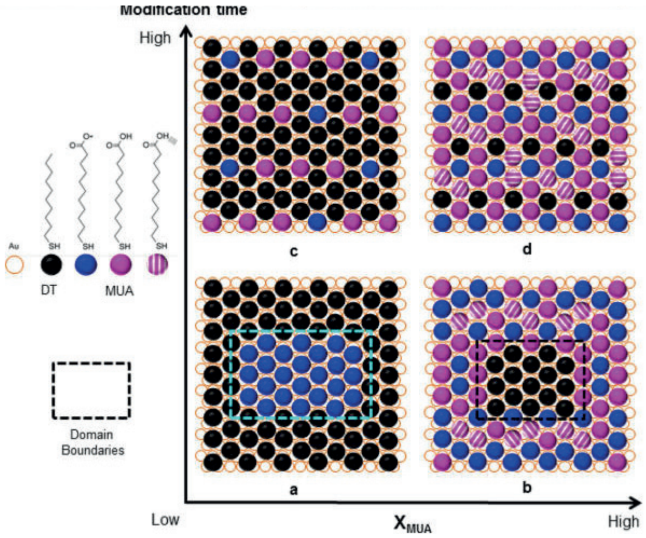

Figure 10. Homogeneously MUA:DT Mixed SAMs Composed by segregated nanodomains (Lower Depicted Figures) and molecularly distributed (Upper Depicted Figures) Arrangements at Different MUA Surface Compositions, XMUA: (a) 0.25, (b) 0.84, (c) 0.23, and (d) 0.8. Reproduced from *[52].*

Kakiuchi et. al. scanned with STM binary SAMs of C11:MUA and C16:MPA thiol pairs. The images revealed macroscopically homogenous mixed phase with maybe 10 molecules segregation in the case of C11:MUA and macroscopically phase-separated domains in the case of C16:MPA SAMs Figure 10 [53], [54].

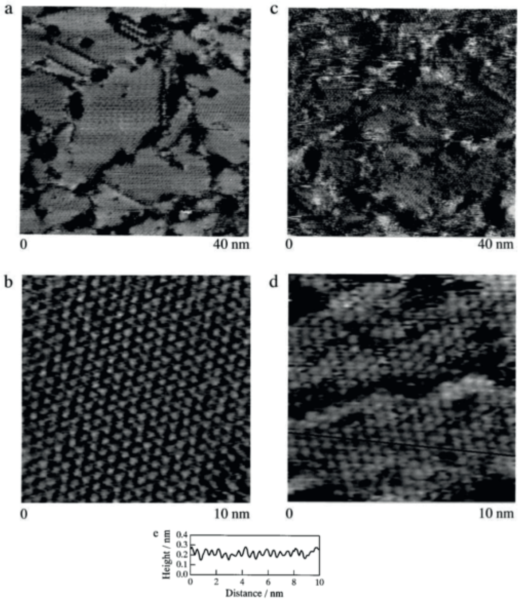

Figure 11. STM images of C11 monolayer (a and b) and mixed monolayer of MUA and C11 (c and d). Height profile (e) is from Figure 4d. Bias voltage was 1.5 V. Setpoint was 11 pA. Reproduced from *[53].*

A combination of a long alkanethiol with a short carboxyl-terminated thiol, as the ligands of the binary SAM always results in patches. S. Kuwabata et al. showed the distinct patchy domains via STM imaging of MPA with C8 or C10 or C12 binary SAMs. The mole fraction and the length mismatch are the conclusive factors of the phase separation into patches. The STM images have been taken after the MPA was selectively desorbed (Figure 12) [55].

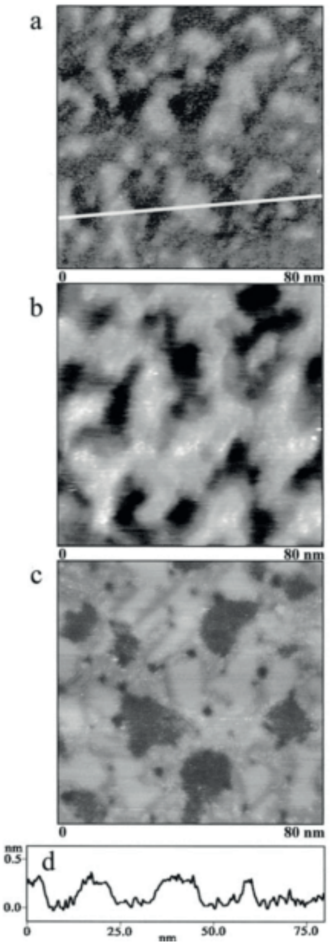

Figure 12. STM images of OT-MPA Au electrode surfaces in 80 nm squares taken after subjecting the electrode to selective desorption of MPA by polarizing at −0.60 V vs. Ag AgCl in 0.5 mol dm−3 KOH. The electrodes were prepared from immersion baths contain- ing 1 mmol dm−3 MPA and (a) 0.1, (b) 0.2, and (c) 0.3 mmol dm−3 OT. Cross-sectional profile (d) along the line drawn on the STM image (a). Reproduced from [37].

Graham J. Leggett et al. has shown that the presence of a terminal group (hydroxyl group) can also lead to phase separation. The binary SAM that comprises of C12 and mercaptoundecanol (same molecular length) was characterized by friction force microscopy and chemical force microscopy. The results indicated the presence of small (approx. 15 nm^2) phase separated domains[56]. Binary SAMs formed by solution co-absorption of C18 with 16-mercaptohexadecanoic acid or MUA also phase separate into domains. Holger Schönherr et al. published an AFM study that showed the patchy domains of the C18:MUA binary SAM and the C18:16-mercaptohexadecanoic acid SAM that did not segregate laterally down to a length scale of 8−10 nm. As reported: the patchy domains are the result of the phase separation on a SAM, where the ligand terminal group differs and the molecular length of the thiol pair is greater that 3 carbon atoms [57].

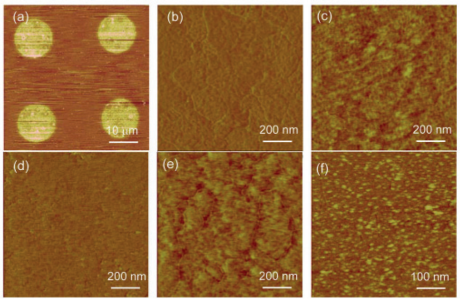

Figure 13. Friction force AFM images of C18/MHDA on TSG. Micropatterns with (a) MHDA in the circular areas, (b) C18 SAM, (c) binary SAM with an xC18 of 0.5, (d) binary SAM with an xC18 of 0.2, (e) MHDA SAM, and (f) binary C18/MUDA SAM (1:1 molar ratio) on TSG. The phase patches have apparent sizes of 10–30 nm. Reproduced from *[57].*

With the proposal of 3 possible mechanisms on domain formation in binary SAMs, P.S. Weiss et. al. has shown the large patches that are received in the case of two thiols that have similar lengths, they are not both alkanethiols and they do not form hydrogen bonds. The thiol pair that was reported was comprised of C16 and $CH_3O_2C(CH_2)_{15}SH$ (Figure 14) [58].

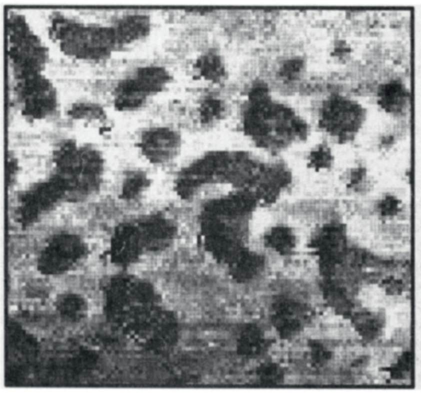

Figure 14. STM of a 440x410 A^2 area of a SAM with 25% C16 and 75% $CH_3O_2C(CH_2)_{15}SH$. The regions that appear higher in the image are $CH_3O_2C(CH_2)_{15}SH$ domains and the lower regions are C16 domains. Reproduced from *[58].*

Hydrogen bonds and van der Walls interactions between the ligands of a monolayer are considered as one of the definite factors that will result in phase separation. These interactions affect the domains' size, shape and stability. As shown by Weiss et al., co-absorption via solution immersion of alkanethiols with amide containing thiols lead to highly ordered patchy morphologies (Figure 15) [59], [60].

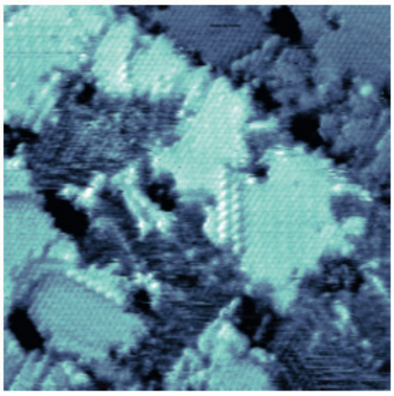

Figure 15. STM image of a 300 Å × 300 Å area of a phase-separated SAM formed by coadsorption from an equimolar solution of 1ATC9 and C10(1mM in total thiol). The image was recorded at a sample bias of +1.0 V and a tunneling current of 1.0 pA. Topographically higher regions correspond to the brighter areas. Reproduced from [60].

The progression of domains from micellar to patches and worm-like are reported by D.M. Ratner et. al. with regard to ligand ratio and time. The binary SAMs of oligo ethylene glycol & 2 different oligo ethylene glycol thiolated glycans phase separate in both cases, and they evolve with time (Figure 16) [61].

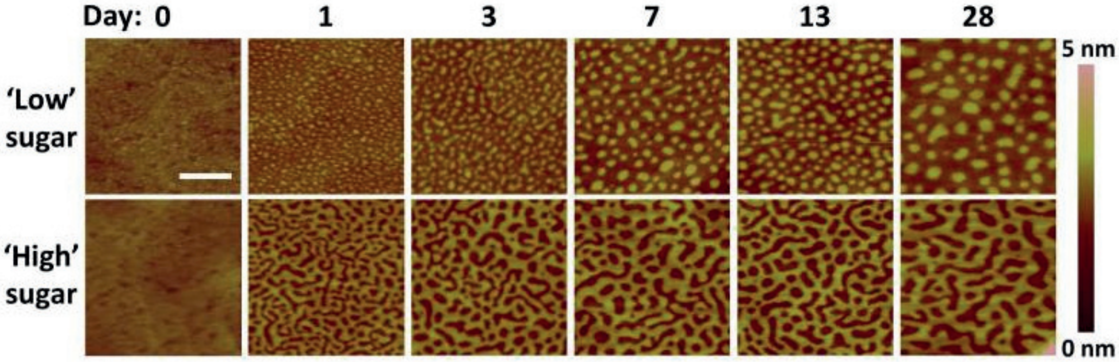

Figure 16. Time-course topographic AFM analysis of mixed SAMs on ultraflat gold. 'Low' sugar SAMs were prepared using a 2:3 molar ratio of sugar (3) to OEG (2), while 'high' sugar SAMs were prepared using a 4:1 sugar:OEG molar ratio. The surface topography exhibits time-dependent clustering behavior. Scale bar = 100 nm. Reproduced from [61].

Micellar domains due to phase separation have also been reported in binary SAMs formed via solution co-absorption. Various pairs of thiols such as: C18 : 4-amintothiophenol by Curtis Shannon et. al. [62]. C4 : C18 (at multiple ratios) by Masahiko Hara et. al. [63] and C8 : C18 or C16 or C14 or C12 (Figure 17) by Shaoyi Jiang et al. [64].

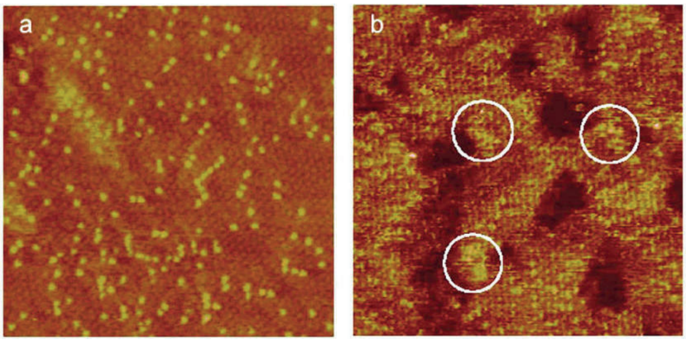

***Figure 17. (a) STM image of mixed SAMs of C8/C12 formed at 50 °C, showing the random distribution of C12 in the mixed SAMs. White spots are long chains of C12 while the background is composed of short chains of C8 with a sqrt3 ×sqrt3 lattice. The ratio of C8 to C12 is about 8.5:1 at the center of the Au(111) terrace while it was 7:1 in solution. (b) STM image of mixed SAMs of C8/C12 formed at room temperature. The ratio of C8 to C12 was 7:1 in solution. Pits in the SAMs are defects of SAMs. The circles indicate clusters of C12. The dimension of the images is 20 nm × 20 nm. Reproduced from** [64].*

The conclusion from reviewing the morphological reports on binary SAMs are presented below:

- Despite the vast literature concerning the binary SAMs on flat Au(111) the details of how the separation proceeds and what equilibrium phase might form are still not well understood.
- The final composition of the film depends on many factors including the solubility of the thiols, the surface diffusion, and the exchange of adsorbates with solution.
- The substrate plays important role on whether phase separation will occur.
- The patches are mainly received if temperature is applied and the thiols have different lengths. Although, phase separation in same length thiols has been reported.
- Co-absorption via solution immersion is adequate to result in phase separation.

As mentioned before binary SAMs of C12:C18 and C12:C22 resulted in phase separation and the energy gain due to the van der Waals interactions by the hydrocarbon chains were more than sufficient to drive the system to phase separate. The majority of the reported binary SAMs are probably in a metastable, kinetically trapped state that by thermodynamics has to phase separate. Slow diffusion and/or intra-molecular interactions are believed to be the suspects of the hindrance of thermodynamic equilibration.

Alkanethiol molecules form strong bonds to gold surface. For a ligand to diffuse on a plane via hopping can be evaluated from the mean square of travelling distance divided by 4t (travelling time). $D = \langle x^2 \rangle / 4t$. The diffusivity of different alkanethiols on gold has been estimated to be:

- 10^{-18} cm^2/s at 60^o C for C11:MUA SAM in water[65].
- 10^{-17} cm^2/s for C15:C15-COOCH3 SAM[58].
- $3 \pm 2 \times 10^{-17}$ cm^2/s for C12 SAM[66].

Increasing the temperature during the incubation or introducing an annealing step is capable of by increasing these estimated values. The quality of the substrate and the number of etch-pits also plays a role on the diffusion.

When a surface is immersed in a solution that contains one ligand the physiroption and chemisorption will lead to the formation of a monolayer. When the SAM is formed, the connection between the surface and the ligand tank is broken. In the case of a binary SAM the solution contains two types of ligands. If the surface will not be removed then a single phase SAM will be produced due to ligand exchange form the available reservoir i.e. the ligands in the solution. That is the main reason why the incubation time is crucial and should not be altered if we want to have control over the surface composition by controlling the solution ratio. Annealing the surface in the absence of other ligands can promote the diffusion and desorption-reabsorption but the amount of ligands remains constant.

2.2.4 Simulations on binary-component SAMs

Numerous theoretical studies cope with molecular self-assembly and phase separation in binary SAMs. They present the most important factors that will lead to various types (in terms of shape and size) of surface domains. In that way, the experimentalist is equipped with a powerful tool on producing a patterned surface.

The well-established theoretical studies by Glotzer et al. on binary SAMs onto flat, nanospherical and nanocylindrical surfaces has shown that an entropic force due to the difference on the molecular length and the terminal group of two dissimilar ligands lead to phase separation and the formation of micellar domains, patchy domains and stripes. Chetana Singh from Glotzer's group has applied the DPD simulations on SAMs onto flat surfaces. She studied in depth the patterns received in terms of surface composition and density, immiscibility and physicochemical properties of the ligands.

The dissipative particle dynamics (DPD) is a particle-based method. An atom or atoms is considered a single particle that is referred as bead. They calculate the movement of the beads at different time instances (time-steps). The change in the position of a bead is given after calculating the net force on the bead due to neighbor beads and solving Newton's equations of motion. The molecule that is modeled as a collection of beads attached by springs is constrained to move in the 2-dimensional surface using constrained dynamics. The final position of the beads is given after the estimated constrain force is applied on the initially unrestricted bead that was assuming its position as described before. In DPD the interatomic forces are replace by net forces acting on the beads. For every bead i, the total force Fi is given by equation 1.1. We notice that Fi is the sum of the conservative ($\mathrm{f^c}$), dissipative ($\mathrm{f^D}$) and random ($\mathrm{f^R}$) forces between the bead i and the neighbor bead j. The equations of $\mathrm{f^c}$, $\mathrm{f^D}$ and $\mathrm{f^R}$ are given by equations 1.2 , 1.3 and 1.4.

$$\boldsymbol{Fi} = \sum_{j\neq i}\left[f^C(r_{ij}) + f^D(r_{ij}, v_{ij}) + f^R(r_{ij})\right] \qquad \text{(eq 2.6)}$$

$$\boldsymbol{f^C(r_{ij})} = \begin{cases} a_{ij}(1 - r_{ij})\boldsymbol{\hat{r}_{ij}} & r_{ij} < r_C \\ 0 & r_{ij} > r_C \end{cases} \qquad \text{(eq 2.7)}$$

$$\boldsymbol{f^D(r_{ij}, v_{ij})} = -\gamma\omega^D(r_{ij})(\boldsymbol{v_{ij}} \cdot \boldsymbol{r_{ij}})\boldsymbol{\hat{r}_{ij}} \qquad \text{(eq 2.8)}$$

$$\boldsymbol{f^R(r_{ij})} = \sigma_N\omega^R(r_{ij})\varepsilon_{ji}\boldsymbol{\hat{r}_{ij}} \qquad \text{(eq 2.9)}$$

A brief explanation on the forces is essential to describe their role and importance in the DPD simulation. The conservative force ($\mathrm{f^c}$) is the pair potential for bead i and j. r_i and r_j are the position vectors of bead i and j. Where $r_{ij} = r_j - r_i$, $\boldsymbol{\hat{r}_{ij}}$ is the unit vector in the r_{ij} direction and r_C is the distance of the beads at which $\mathrm{f^c}=0$. The velocity of the beads does not affect the $\mathrm{f^c}$, only the relative positions of the beads i and j does. a_{ij} is a parameter of interaction. The interaction parameter consists of two parts: α, that is independent of the types of interacting beads and Δα (=repuslion parameter) that is depended. A large Δα indicates strong repulsion between two beads. Beads of two differnet ligands have larder Δα than the beads of the same ligand. The $\mathrm{f^c}$ is a repulsive only force and because is finite even for $r_j = 0$ is allowing the beads to be able to diffuse into each other. Due to the two aforementioned characteristics of $\mathrm{f^c}$ the size of the time step is significantly improved.

The dissipative force (f^D) is the frictional force on a bead i because of another bead j. The velocity and the position of the beads are affecting the f^D. The degree of the frictional force between the beads is controlled by coefficient γ. $\omega^D(r_{ij})$ is a weight function that describes how the friction coefficient varies according to bead distance.

The random force (f^R) is applied to conserve momentum and temperature. It can be considered as a simulation of the effect of collisions of the beads with the solvent. σ_N is the degree of the pairwise f^R of the beads and is related to the temperature. ε_{ji} is a random variable with uniform distribution. $\omega^R(r_{ij})$ is linked to $\omega^D(r_{ij})$ as such: $\omega^D(r_{ij}) = [\omega^R(r_{ij})]^2$. The f^D and f^R conserve momentum and thermodynamics [67].

The results of DPD simulations on the phase separation on binary SAMs are reported below. SAMs of an equal number of two ligands that are immiscible and have different molecular lengths phase separate into stripes. Complete phase segregation is not received due to entropic factors. Thermodynamics dictate that a binary system will phase segregate if its two components are incompatible. By minimising the interface of the two components the overall free energy of the system is achieved. The simulation snapshots at Figure 18 are showing the complete phase segregation that is received when two ligands of the same length are trying to occupy an area. φ is the asymmetry fraction i.e. the surface composition. The long ligand is colored yellow and the short ligand is colored as red. If φ=1 then the SAM is single-component SAM comprised only of the long ligand. If φ=0 the SAM is comprised only of the short ligand. The length difference will be mentioned in terms of number of beads difference.

Figure 18.Simulation snapshots of phase separation in symmetric (φ = 0.5) mixture at surface density of r = 4.0 of immiscible (Δa = 15) surfactants. The surfactants have the same molecular length. The number in the top right corner is the time step at which the snapshot was taken, where K refers to thousands and M to millions of time steps*[68].*

Phase segregation under the aforementioned conditions is inevitable unless there is a symmetry-breaking parameter such as an external field[67] and/or chemical bond[69][70] and/or anisotropic surface stress[71]. Glotzer theory proposes that a symmetry-breaking parameter in the SAMs onto surfaces is the length mismatch and the bulkiness difference. In a monolayer that has one long (or bulkier) and one short ligand the first will place itself next to the short ligand gaining free volume and an entropic freedom. The length of the interface is increased (microphase separation) and it is energetically costly but it is hypothesised that the entropic gain might outweight that energetic cost. Chetana S. applied the DPD simulations to study if the conformational entropy of the long ligand will lead to domain formation[68]. Her research on the patterns that can be received in terms of surface composition and density, immiscibility and physicochemical properties of the ligands yielded results that our group has experimentally supported.

The progression of phase separation in time is shown at Figure 19. The SAM is comprised of a short (4 beads) ligand and a long (9 beads) one. All simulation that are at 1:1 surface ratio and involve ligands that have five or more beads length mismatch reach the equilibrium phase of stripes. As previously discussed, the length mismatch and the progression of time leads to the increase of the interface between the two ligands as compared to phase segregated SAM in figure $.

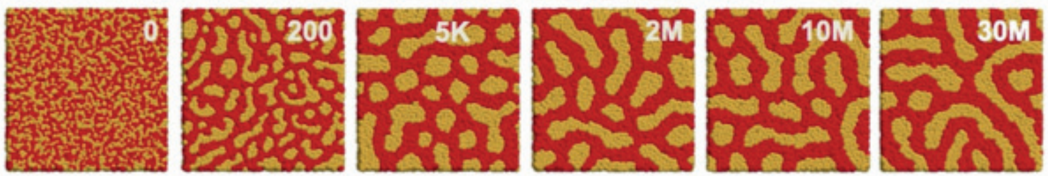

Figure 19.Simulation snapshots of phase separation in symmetric mixture at surface density of r = 4.0 of immiscible (Δa = 15) surfactants with lengths 4 beads (red) and 9 beads (yellow).

A collection of results at different asymmetry fractions φ and at different lengths of the two ligands is presented at Figure 20. Examining these snapshots it is obvious that for a length difference of less than 3 beads we have complete phase segregation at all φ values. For length mismatch of equal or larger than 3 beads and for φ<0.5 micellar domains are received at equilibrium. For a length difference between 3 and 5 beads stripes are received while patches are formed for all larger values of φ. micelles are entropically preferred over stripes for highly asymmetric mixtures with a majority of long surfactants. When Dl is large (> 4 beads), the gain in conformational entropy for long surfactants by forming patches is large. However when Dl is just sufficient for microphase separation (2 < Dl < 5), the conformational entropy gain for the long surfactants by forming micelles is small and stripes are energetically and entropically favored.

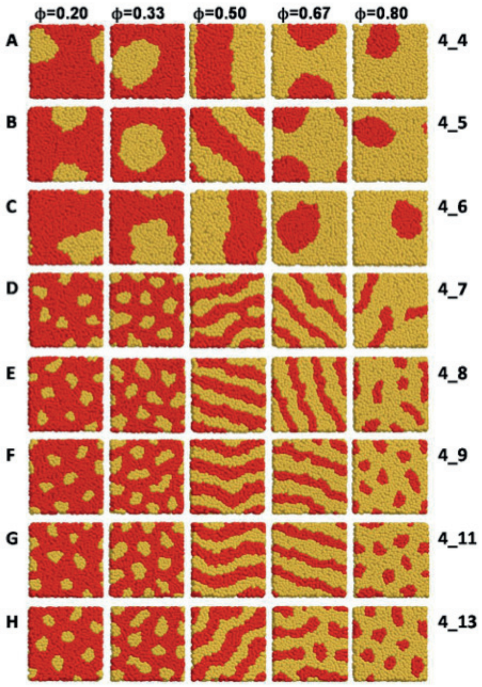

***Figure 20. A. to H.: Equilibrium patterns formed at different φ of surfactants with increasing length differences. The numbers at the right are the beads number of the short _ long ligand**[68].*

Finally, having established the meaning of repuslion parameter Δα at the beginning of 2.2.4, Figure 21 presents the pattern formation according to the surface composition and at different Δα values.

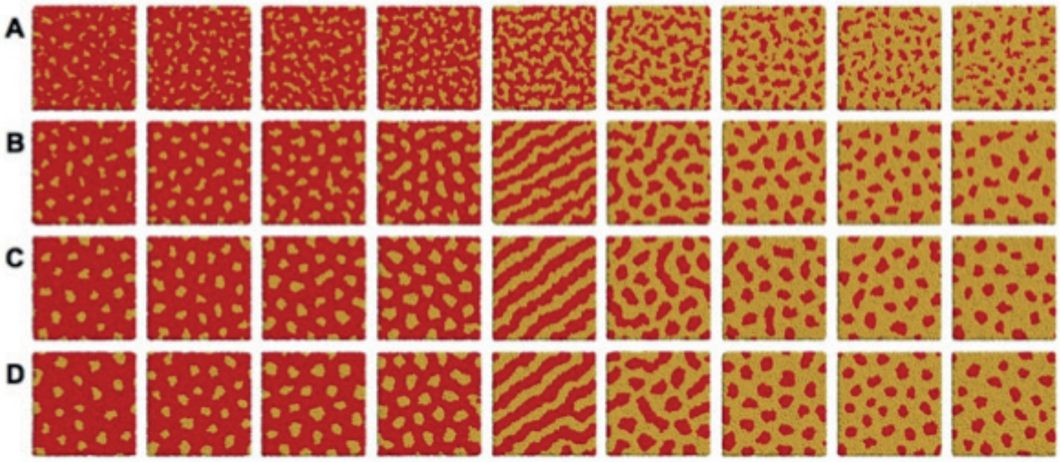

***Figure 21.Simulation snapshots of microphase separation in binary SAMs of 4 bead (red) and 13 bead (yellow) ligands. The fraction of long surfactants is increasing φ = 0.17, 0.20, 0.25, 0.33, 0.50, 0.67, 0.75, 0.80, 0.83 (from left to right). The repulsion parameter is increasing from A to D (A. Δα = 5; B. Δα = 10; C. Δα = 15; D. Δα = 20**[68].*

The results of the DPD simulations presented at chapter 2.2.4 indicate that:

- The length difference of the ligands and/or the difference in the terminal group leads to microphase separation and domain formation due to entropic factors.
- Kinetically arrested patches are frequently obtained in binary SAMs on flat surfaces. High surface coverage, lack of curvature and small ligand length mismatch are the main reasons for the patches formation.
- A 1:1 surface ratio of dissimilar ligands with sufficient length mismatch and given sufficient time, the patches are kinetically arrested but they will evolve to stripes.
- At different surface compositions either ordered micelles or stripes are formed depending on the fraction φ and number of beads difference (length mismatch).
- The domain shapes that have been reported in STM studies on binary SAMs on flat surface vary from irregular patches to disordered stripes or worm-like domains. Additionally, all prior studies are inconclusive about the equilibrium structures in phase separated SAMs. Slow dynamics compound the problem, often obscuring the thermodynamically preferred phase.

Other theoreticians have also studied phase separation in binary monolayers. The majority of the publications use Monte-Carlo (MC) methods. The conclusion is that phase separation takes place and domains are formed. In particular, Aoki et al. uses simulations backed-up by cyclic voltammetry analysis by Hobara et al.[72]. As it is discussed in-depth in this thesis, an intermediate peak during the reductive desorption of the thiols of a binary SAM indicates a mixed phase or the existence of small domains that changes the behavior of its components during desorption. The MC simulations show phase separation that leads to large and small areas/patches of the two components of the SAM[73]. Tokumoto H. et al. showed the stripes that can be formed when the system reaches thermal equilibrium. The symmetric mixture of initially perfectly mixed components is arranged on a flat triangular lattice surface[74]. Shaoyi Jiang et al. focused on how length mismatch affects phase separation[75]. According to his configurational-bias Monte Carlo simulations, neglecting the kinetic factors, found that phase segregation that results into patchy domains occur if the two thiols have a difference larger than 3 carbon atoms in their hydrocarbon chain, Figure 22. Therefore in the binary SAMs of C10 thiol with C11, C12, C13 mixed configuration is expected, whereas in the case of SAMs of C10 thiol with C14, C15, C16, C17 and C20 thiols the patchy domains are expected.

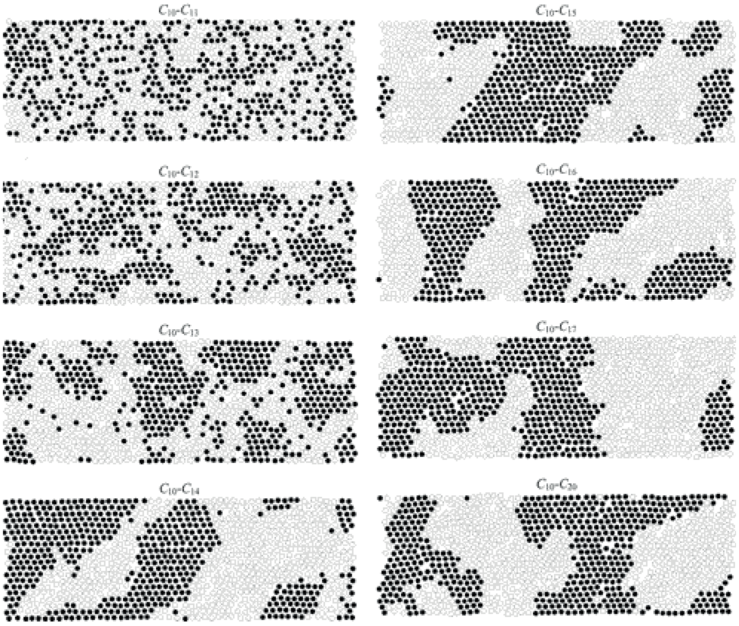

***Figure 22.Monte-Carlo simulation of binary SAM of C10 and an alkanethiol of increasing chain length (C11 to C20). The surface composition for all mixtures are xC10,SAM = 0.5 and simulation temperature of 300 K. Head groups of the thiols are represented by open (for short-chain) and filled (for long-chain) circles. Reproduced from reference** [75].*

Cacciuto A. et al. used numerical simulations to compute the free energies on a binary system of polymer brushes grafted onto a cylindrical surface. It was reported that the most favorable state for the system is when the cylinder has more thinner lines as the length difference of the two components increases [76].

Egorov applied a computationally more efficient approach, self-consistent field (SCF) theory. According to his findings, thinner stripes are received as the chain length difference and the density increases. His system is also two types of polymer brushes on cylindrical surfaces. His results are in accordance to Glotzer's theory on stripe formation on flat and curved surfaces. He also reports that if the lengths of the two molecules does not differ then macro-phase separation will occur[77].

Yaliraki et al. via mean field theory, attempted to theoretically evaluate the phase diagram of binary SAMs that are applicable to the system of benzenethiol/dodecanethiol and corenoid/alkanethiol mixures[78]. Reviewing his work, a temperature-composition phase diagram is given in Figure 23. From that phase diagram, one can identify a range of unstable composition and temperature conditions where the phase separation is thermodynamically expected. The region between the binodal and spinodal curves (solid and dashed curve respectively) is where the monolayer is metastable. At this region patchy domains are expected to form. By altering the benzenethiol concentration on the surface, one can move outside the phase separation region and achieve a thermodynamically stable one-phase monolayer that contains both ligands. It still remains a challenge, for the experimentalists, to construct a phase diagram on a binary SAM of thiols on gold surface.

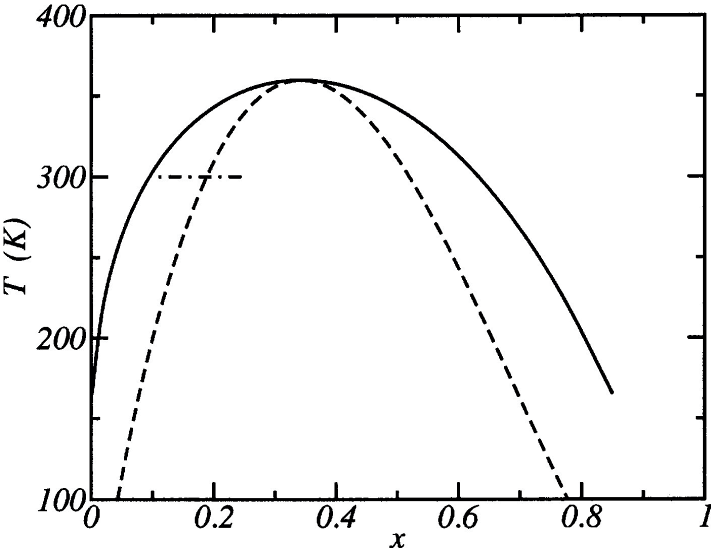

Figure 23.Partial phase diagram calculated for a binary system of benzenethiol/dodecanethiol. Spinodal and binadal curves are represented by a dashed and solid curve, respectively. The experimental data are illustrated by thre horizontal line for composition x 0.11 to 0.25 (mole fraction of benzenethiol). Reproduced from reference[78].

Nassoko et al. investigated, using periodic DFT-D calculations, the pattern formation of 20 different linear thiol pairs on a defect-free surface[79]. Based only on the energy of adsorption and not taking into consideration the conformational entropy of the long ligands on the interface with the shorter ones, he reported that all combinations lead to phase separation. As it was mentioned at the discussion on Glotzer theory, a ligand of higher molecular length when it stands next to a shorter ligand it is expected to be disordered due to high conformational entropy. Focused only on that matter, MC studies concluded that a long ligand is more disordered at the boundary with the short ligand than being inside a domain of other long ligands[80]. Targeted research on the state of the molecules at the interface on binary systems is imperative. STM imaging of decanethiol:dodecanethiol SAM on gold has shown clear molecularly sharp interfaces rather than disordered molecules at the boundary[81].

In practice, a phase diagram of a system of two ligands is of great utility but not yet constructed experimentally. It remains an experimental challenge to actually record the molecular phase separation states for a range of temperature and composition presented in such a simple phase diagram. Most of the binary SAMs reported are believed to be in some kinetically trapped state. In this work the introduction of an annealing step in a free from thiols solvent aims to assist the SAM to reach thermodynamic equilibrium. Increasing the diffusion of thiols will probably lead to the evolution of the SAM into the thermodynamically preferred domains.

2.3. Characterisation

Scanning probe microscopy (SPM)

This sub-chapter contains a brief mention of the SPM methods and a detailed description of Scanning Tunneling Microscopy (STM). The morphological study of SAMs on surfaces relies mainly on STM. Consequently, STM is the main analytical tool of the research that is presented on this thesis.

SPM contains all the analytical techniques that measure the chemical and/or physical properties of a surface by the use of a probe. A tip is interacting with a nanometer or micrometer area of a surface, it performs the scan and a detector is constantly detects and records these interactions. The family of SPM techniques mainly includes (alphabetically): Atomic force microscopy (AFM), chemical force microscopy (CFM), electrochemical STM (ECSTM), lateral force microscopy (LFM), magnetic force microscopy (MFM), scanning tunneling microscopy (STM) and scanning near field optic microscopy (SNOM). AFM is the second most popular surface analytical technique with nanometer resolution after STM. AFM contact mode and AFM lateral force mode are mostly used for SAMs imaging[82] [57].

The STM was invented G. Binnig (1947) and H. Rohrer (1933). For their invention they have been awarded the Nobel Prize at 1986. The STM is based upon scanning with a metallic sharp tip interacting with a conductive surface at a distance of .1 Å. A voltage is applied and a small current flows either from the tip to the surface or from the surface to the tip. This is tunneling current because there is not contact between the tip and the surface but the small distance is adequate for an electron to tunnel towards the opposite side. Semi conductive and conductive materials are possible to be scanned with STM. If a metallic surface is modified with a thin film or a layer of molecules or atoms the STM is capable performing the scan as long as the current can flow. There are two modes of operation on STM the constant current mode and the constant height mode. The constant current mode is the one that is employed for the surface analysis of the samples of this work. In constant current a feedback loop attempts to keep the tip at a specific constant distance from the surface. The tip is mounted at a non-moving head. A piezo-crystal-tube on top of which we have mounted the sample surface is the quick responsive and precise positioning system that can change the distance according to the change in the monitored current. The tip is scanning the surface line by line at alternating directions front and back (trace and retrace), until the whole specified area is covered. If, at any moment, the distance between the tip and the surface increases, the current decreases and the feedback loop (the piezo) raises the surface to restore the current at its initial value. At the constant height mode, the tip is not moving on the x direction and the surface morphologies are identified and recorded from the produced current fluctuations in the tunneling current[83][84][85]. STM measurements can be performed in air, in solution or in ultra-high vacuum and low temperature conditions[86].

After the description of the parts and the modes of operation of an STM, it is imperative to describe the STM basic physical principles and explain the z-height (distance between tip and surface). Research on studying the transconductance of hydrocarbon chains using STM can assist on the explanation of tip-surface distance changes during SAMs imaging[87][88]. The height of a molecule that STM is measuring (z-height) is a convolution of its molecular and electronic structure. STM scanning of thiol SAMs at high tunnel junction transimpedance places the tip outside the alkanethiol film, resulting in a tunnel junction that is composed of two layers: the film layer and the gap. The two-layer tunnel junction model is shown at Figure 24.

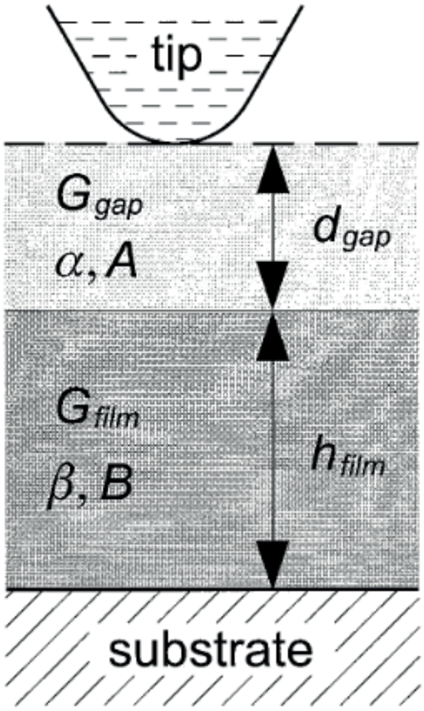

***Figure 24.The two-layer tunnel junction model. The STM tunnel junction consists of two distinct layers, the vacuum gap and the film with their corresponding transconductances** [87].*

The h_{film} is the physical thickness of the monolayer. The film transconductance G_{film} is determined by the molecule properties. The gap from the film to the tip is controlled by the STM to control a constant overall transconductance. Finally, The gap length determines the gap transconductance. It is obvious that an increase in the film thickness during a scan will change the tip trajectory to larger z-height but at the same time, if the transconductance decreases (thicker film=less conductive) then the STM will compensate by decreasing the d_{gap}. Alkanethiols that do not have a terminal group have been studied and the Δh (change of the z-height moving from one domain of decanethiol molecules to a domain of dodecanethiol molecules) has been successfully predicted, Figure 25 [87].

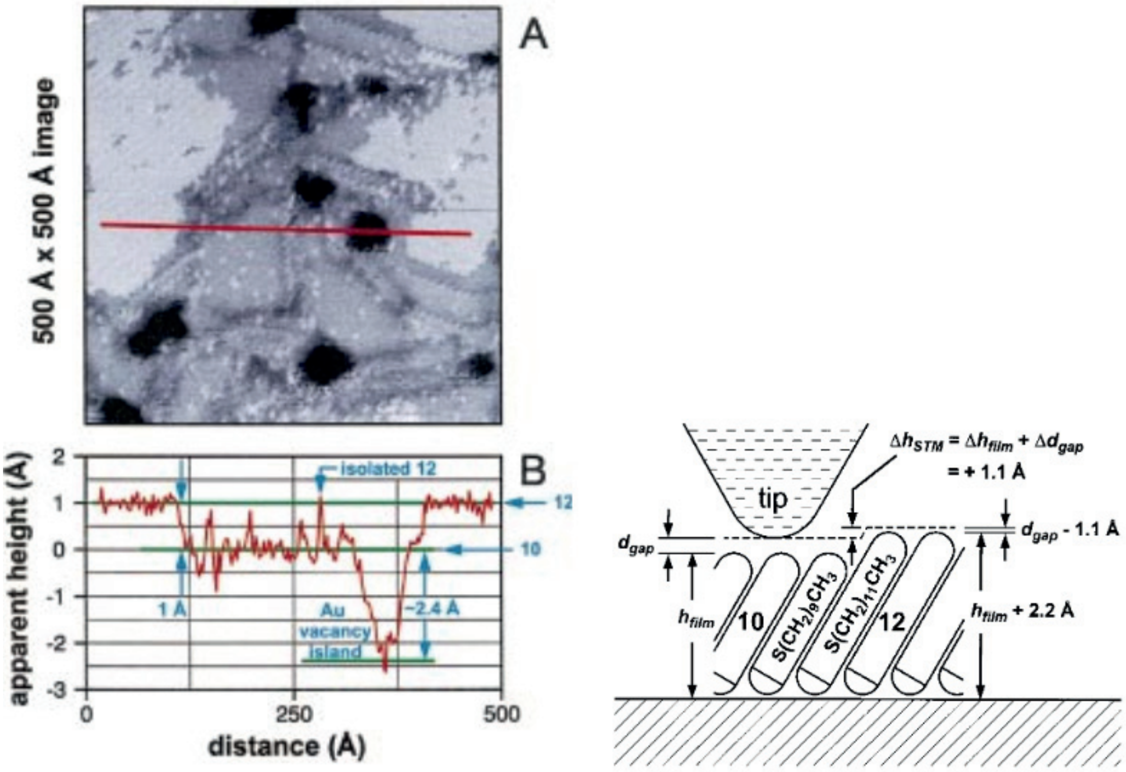

Figure 25. A. STM image of a 500 Å × 500 Å area of the mixed composition mosaic SAM of decanethiol and dodecanethiol showing the alkanethiolate molecular lattice. B. A topographic cross section extracted from A on the path shown by the red line. On the left, schematic diagram showing the STM tip trajectory (dashed line) corresponding to the constant tunneling current operating point 5 in image A. Adapted with permission from*[87]*. Copyright (2017) American Chemical Society.

Electrochemistry / Reductive desorption

This sub-chapter is a review on electrochemistry as a surface analysis technique. The reductive desorption of thiols from gold surfaces using Cyclic Voltammetry (CV) and Linear Sweep Voltammetry (LSV) is described more in detail. During the research for this thesis e-chem has provided valuable results on the qualitative determination of the chemisorbed thiols but mainly on the verification of a mixed or segregated phase either ordered or disordered.

Electrochemistry is an analytical technique that is divided in 5 major methods: voltammetry, potentiometry, coulometry, conductometry and dielectrometry. These methods use the measurement of potential, charge, or current to determine an analyte’s concentration or to characterize an analyte’s chemical reactivity[89].

The first use of CV on thiol SAMs by Porter et al. showed the inhibition of redox current of the ferricyanide redox couple according to the alkanethiol molecular length[90]. Cyclic voltammetry has been widely used for the characterization of a SAM and evaluation of its barrier properties by studying the electron transfer reactions using redox probes. Although this approach can give valuable information, the reductive desorption is going to be studied in this thesis. Electrochemistry has been used for the determination of thiol coverage and the (sqrt(3) x sqrt(3)) R30° structure at which alkanethiols assemble[91]. Since then, the electroreductive desorption in basic media has been used in SAMs and especially in thiolates on polycrystalline or crystalline Au[92][93]. In the case of a thiol monolayer on gold the reduction with the involvement of a electron occurs via:

$$Au - S - R \ + \ e^{-} \ \rightleftarrows \ Au \ + \ R - S - \qquad (12.1)$$

The potential of the reductive desorption on alkanethiols varies linearly with the length of the alkyl chain at values from -0.7 V to -1.2 V[94][95][96]. Among many uses, the electroreductive desorption is not only able to qualitatively identify the alkanethiol of the SAM but also to monitor the thermal stability and verify the decomposition by comparison of the peaks (Figure 26). Small changes in the alkanethiol length and decomposition of the monolayer are clearly identified as the temperature is increased [97].

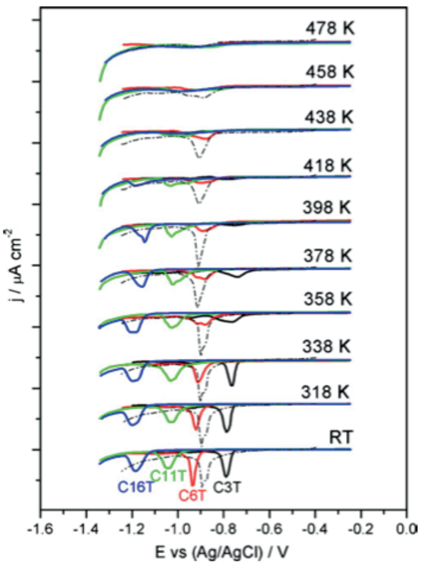

Figure 26.Set of cathodic sweeps showing the reductive desorption of the adsorbed species remaining after the thermal treatment of C3T (black lines), C6T (red lines), C11T (green lines) and C16T (blue lines) SAMs. The atomic S desorption

***profiles are given in dashed lines. Scan rate: 50 mV s−1 . Reference electrode: Ag/AgCl (NaCl 3 M). Heating time: 30 min at each temperature. Reproduced with permission from** [98].*

Focusing on binary-component SAMs, Hu-Lin Li et al. used CV with two different redox couples at a binary SAM that is comprised of a 1,3,4-oxadiazole ligand and dodecanethiol. Only by controlling the solution ratio of the two thiols he found that a specific ratio (20% of dodecanethiol), while the $Ru(NH_3)_6{}^{3+}$ penetrates the monolayer, the $Fe(CN)_6{}^{3-}$ does not. It was attributed to the possibility that the surface has larger areas with the mercaptan ligand than in SAMs that have been produced with higher dodecanethiol solution ratio[99]. Publications on electroreductive desorption in binary SAMs can provide valuable information that will later be used during the discussion of this thesis' results. Mercaptoundecanoic acid : octanethiol binary SAMs formed from solution under electrochemical control, resulted in SAMs with a mixed phase rich in octanethiol. The single peak at the voltammograms shift as the OT ratio is increased [100].

Yoenyama et al. studied binary MPA : hexadecanethiol (C16) SAMs. It was reported that phase segregation occurs. Two-peak voltammograms at the expected MUA and C16 reductive potentials was received at a SAM from 5:1 solution ratio. Higher C16 in the solution resulted in one single peak at the C16 reductive potential indicating that the SAM comprised only of one component. The procedure for the SAM synthesis did not entail annealing of the SAM and small incubation times. It is interesting to mention that if the incubation time was increased to 72 hours the voltammogram of the MPA:C16 also had two peaks but the area of the MPA peak was significantly smaller. That result demonstrates the fact that increasing the incubation times in a solution with dissimilar thiols will yield on a surface with a single-component SAM. It is believed that the longer thiol is the most thermodynamically favored, therefore the SAM will consist of the C16, a hypothesis that has been proved by the CV analysis[101]. Binary SAMs of Mercaptoundecanoic acid (MUA) : mercapto propionic acid (MPA) prepared from ethanolic solutions gave single peak voltammograms during CV. The peak potential between the peak potentials of the pure components desorption and the absence of domains during the STM imaging indicates that a homogeneous mixed SAM is formed. The hydrogen bonding between the terminal groups (-COOH) of adjacent MUA and MPA molecules has been proposed as the driving force for the homogenous mixtures[102]. By comparing the reductive desorption profiles with the distribution of the domain size by STM in a MPA:C16 binary SAM, it was found that domain areas larger than 15 nm^2 on a flat surface give rise to a single macroscopic peak in the voltammogram, allowing the unambiguous identification of phase-segregation and potentially morphological analysis by reductive desorption[72].

Synopsizing the binary SAMs electroreductive desorption research. The voltammogram during the CV or LSV can provide the analyst with the following information:

- The strength and stability of the Au-SR bond and the absorbate-absobate interactions from the desorption potential i.e. peak position.
- The molecular packing quality from the sharpness of the reductive peak[93].
- The surface coverage from the area of the peak with a know electrode area.
- The re-reduction, after the absorption of the first cycle, can also help in the identification of the desorbed molecules especially in binary SAMs. Referring to the second cycle, in the case of CV analysis.
- On binary SAMs. In the case of a phase segregated phase the reductive desorption of each component will occur independently at the potential at which each single-component SAM is reductively desorbed. In a homogeneously mixed phase, the desorption occurs at an intermediate potential of the desorption potential of each single-component SAM.

X-ray Photoelectron Spectroscopy (XPS)

XPS is briefly reviewed in this chapter. The samples of this thesis have been given for XPS analysis at the Molecular and Hybrid Materials Characterization Center (MHMC) laboratory of MX-epfl.

XPS is a spectroscopic technique. It measures the elemental composition or the chemical state of any solid or surface. The sample is irradiated with x-rays (in an ultra-vacuum chamber). The electrons that are ejected from the sample are plotted against their binding energy. The binding energy (in eV) is unique and specific to any element. The technique is one of the most vital surface analysis techniques since the depth of penetration and the sensitive allows for scanning molecular length monolayers and the interaction of them with the surface. Studies on thiol SAMs on gold with angle-resolved XPS allow the measurement of the thickens of the SAM. The ratio of the bounded sulphur to the Au $4f_{7/2}$ can give the thiol coverage. Whitesides et al. employed XPS to observe that both thiols and disulfides bond as a thiolate-Au on the surface[103]. Angle-resolved XPS has been also used for the study of cyano-terminated thiol :

alaknethiol binary SAMS. Although the Nitrogen region has not been presented the S2p region revealed the existence of desorbed sulfur for 48h incubation[104]. Despite the fact that the capability of the instrument, the angle of scan and the long times of scanning, XPS is able to provide useful compositional information of the chemisorbed ligands.

3. METHODS

Chapter outline

Chapter 3 contains the experimental preparation procedure and surface analytical techniques that have been employed for the compositional and morphological analysis of the prepared binary SAMs.

3.1 Reagents and Materials

All chemicals were purchased form Sigma-Aldrich (St.Louis, MO) and Acros Organics (West Chester, PA) in the highest available purity and used without further purification. The thiols that have been used for this study are: Octanethiol (OT), 4-Cyano-1-butanethiol (CN4T), para-nitrothiophenol (NB4M) and 3-mercaptopropionic acid (MPA). Anhydrous toluene 99.8% from Sigma-Aldrich was used after it was purged with Argon gas for at least 1 hour.

OT

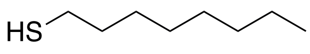

CN4T

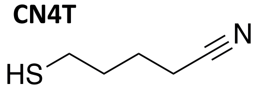

NB4M

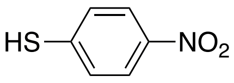

MPA

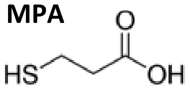

The Au (111) surfaces were purchased from Phasis (Geneva). Gatalog # : 20020015, size: 8 x 4 mm^2. The gold foil (200 nm thickness) is on top of high grade freshly cleaved mica without the use of adhesives. The surfaces are ready to use, without any cleaning or flame annealing pre treatment.

3.2 SAM preparation

The project is mainly focused on the preparation and characterisation of 3 binary SAMs on Au(111). The ligands that were used are presented below:

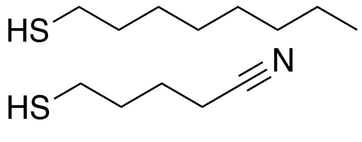

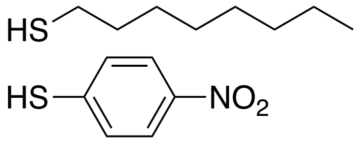

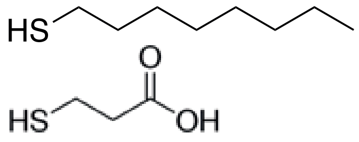

The procedure is divided in two distinct steps.

Incubation step: The solution co-adsortpion procedure was followed for the SAMs formation of this thesis. Au(111) surfaces from a freshly opened bottle were immersed in a degassed toluene thiol solution for 24 hours at 60° C. High pressure glass tubes from Aldrich were used for the incubation and annealing processes (Ace pressure tube-bushing type, volume ~15 mL). The feed ratio of the two thiols in the solution varies. The total thiol concentration is 50uM. After the incubation, the surfaces were rinsed with copious amount of toluene and dried under a stream of Argon. The surfaces that will not be annealed were kept in a desiccator and used immediately for characterization. These surfaces will be noted here as 0 days SAMs

Absolute precision over the thiol ratio in the incubation solution is important. The control over the surface composition is achieved via controlling the feed ratio of the two thiols and keeping the incubation period strictly for 24 hours.

Annealing procedure: The surfaces that will be annealed were placed in separate high-pressure tubes that contained pure degassed toluene (the solvent was degassed again to make sure that the oxygen has been completely removed) and put inside an oven at 60° C for various amounts of time. The final SAMs were analysed immediately after they were rinsed with toluene and dried under a stream of Argon.

An example of the notation that will be followed at this chapter is **OT:X 4060 (62%).** The pair of thiols followed by the feed ratio of the thiols and inside the parenthesis is the **surface ratio** from the N/S atomic percentage concentration XPS results only for the cases of OT:CN4T and OT:NB4M binary SAMs that bare the nitrogen at their terminal group. The surface composition of the OT:MPA SAMs could not be determined with a conventional XPS. The reason lies to the fact that the carboxyl terminal group, that could be used for the determination of the surface ratio of MPA is not clearly distinguishable in the C1s region. The large contribution to the peak at the C1s region by sp2 hybridized carbon atoms in C–C bonds tends to mask the expected peak of the -COOH at (289.13-289.33 eV). Therefore, the notation that will be used for the OT:MPA binary SAMs will reflect on the feed ratio of the sample. i.e OT:MPA 20:80-5days refers to a sample that has been formed via immersion of a Au(111) surface in a toluene solution that contains 20% OT and 80% MPA ad has been annealed for 5 days.

The surfaces were never allowed to be exposed in air for long times. The thorough drying of the surfaces with Argon and the use of vacuum desiccator was an essential part of the procedure. AFM images (Figure 27) of the modified surfaces that have not been dried thoroughly and not been placed in the desiccator for at least 2 days have presented large “blobs”. The use of desiccator resulted in the disappearance of these features. The thoroughly dried surface was less prone to ambient contamination.

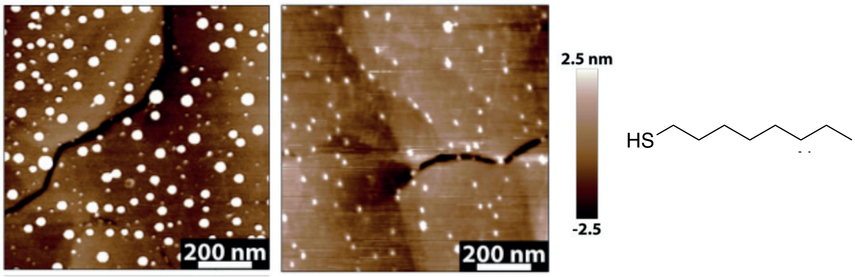

Figure 27. AFM images of OT-only SAM. The surface on the left was not dried thoroughly and not been placed in desiccator presenting large blobs. The surface on the right has been dried and placed in desiccator and the features have almost completely disappeared.

3.3 Analytical techniques

XPS

Primary necessity is the determination of surface composition of the prepared SAMs according to the feed ratio of the two thiols at different annealing times. XPS analysis of the non-annealed and annealed samples was performed and is presented at Figure 28 and Figure 29 A 10% air of uncertainty on the peak intensities has been given by the instrument’s manufacturer. In the case of division for the calculation of N/S ratio from the atomic percentage concentrations the error propagates resulting to a 14% error for the result.

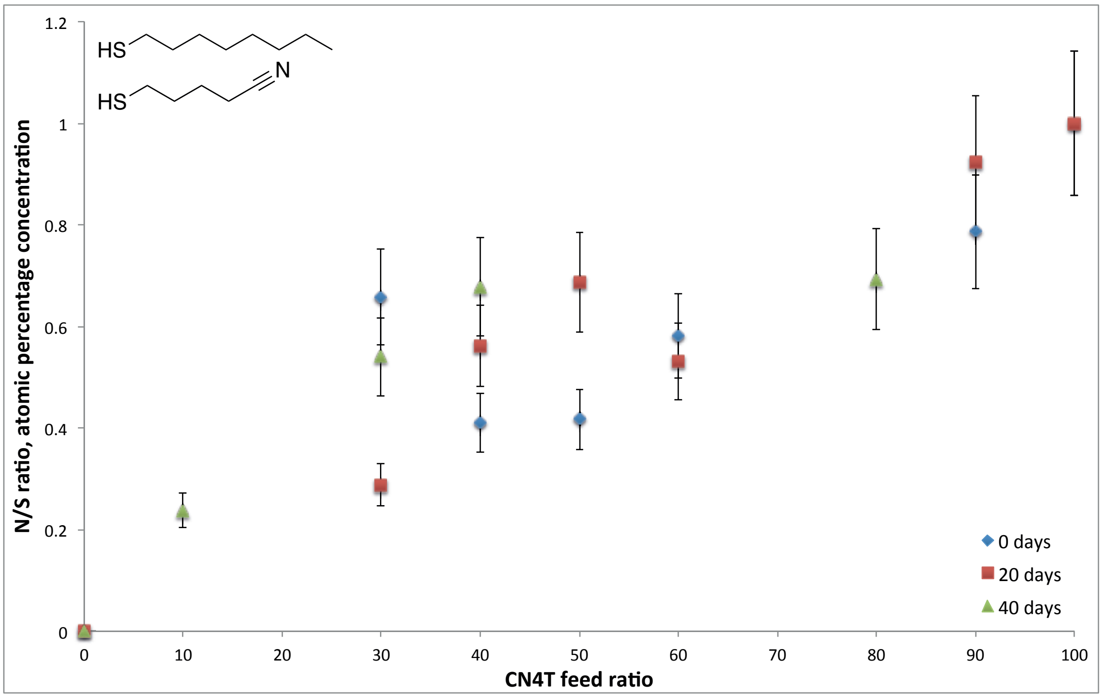

Figure 28. N/S atomic percentage concentration at different feed ratios of CN4T and different annealing times. The error bars are the error propagation for a 10% error, given by the instrument's manufacturer.

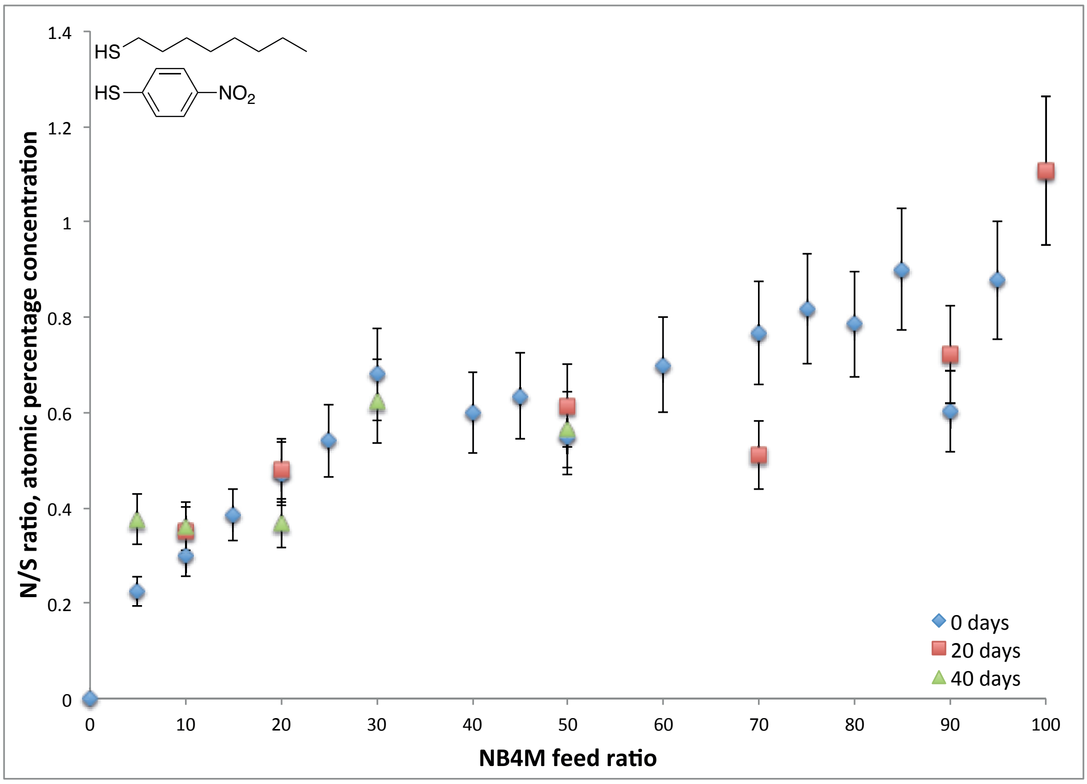

Figure 29. N/S ratio from the XPS atomic percentage concentration. The x-axis is the NB4M ratio in the feed solution. The samples that have been annealed for more days are also plotted and presented with different colours. The error bars are showing the uncertainty of 10% that propagates in the N/S atomic percentage concentration values.

For all the samples the XPS detected the gold substrate and the elements from the thiol monolayer (C, S, O and N). The spectra received, where shifted using the strong Au 4f7/2 peak at 84.0 eV. The surface composition was determined for the OT:CN4T and OT:NB4M binary SAMs based on the signal at the N1s region. The cyano and the nitro-groups give a peak at ~400 eV. A relatively poor signal-to-noise ratio of the N1s region has been attributed to large inelastic background[105]. The peak received from the XPS has 10% the values of the counts/second compared to the carbon peak, as seen at Figure 30.

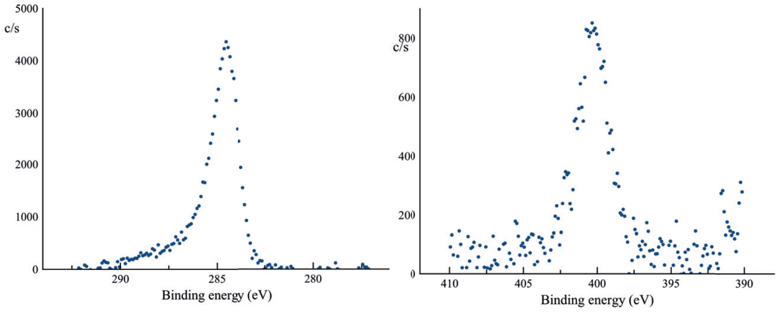

Figure 30. The N1s peak on the right compared with the C1s peak on the left. The counts per second are 85% less as seen by the values of the y axis.

The bounded S at the S2p spectra is observed as a doubled (S2p3/2 ad S2p1/2) at ~162 eV[106]. The N/S ratio from the atomic percentage concentrations is used to determine the surface composition of the binary SAMs. In some instances, different portions of the various core levels need to be used for quantification. Relative Sensitivity Factor takes into account mainly the atomic cross section (between others specific variables of every equipment) which is dependent of the source Thus, the area of a peak must be divided by the RSF in order to have the corrected area. All the samples were analysed by the same instrument and the atomic percentage concentration values have been corrected. The area and height sensitivity factors for all the used 5 elements are given at the paragraph “XPS” in appendix A. The manufacturer of the STM is indicating a 10% error on the calculated values. The error propagation for the N/S values is ±14.14% illustrated with the use of error bars at the plots of this thesis. For the OT:MPA binary SAMs, the conventional XPS cannot be used for the quantitative determination of the -COOH based on the C1S or O1S region. The S/Au ratio from the atomic percentage concentration has been used to verify that no desorption has taken place during the annealing Figure 31.

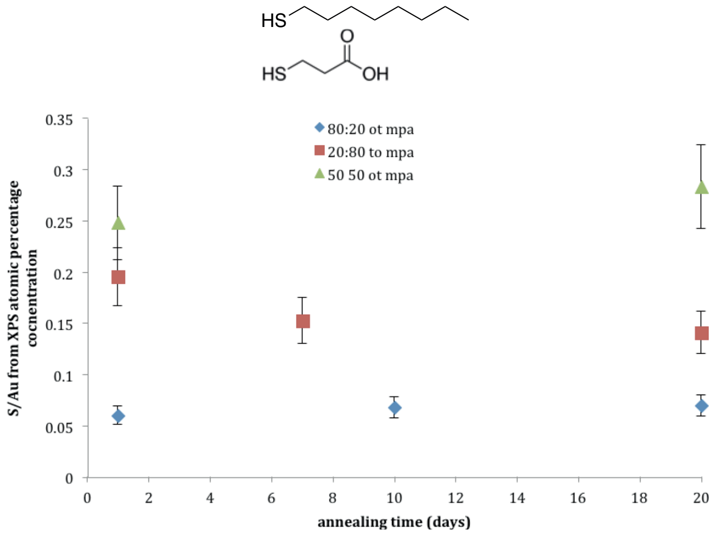

Figure 31. Sulphur to Gold ratio from the XPS atomic percentage concentration. The x-axis is the annealing time. The error bars are showing the uncertainty of 10% that propagates in the N/S atomic percentage concentration values.

The use of XPS in this thesis is not limited to determine the surface composition but also to verify that the annealing process does not decompose the SAM. The existence of oxidised sulfur species was examined along with the surface composition, according to annealing time. The peak was observed sporadically and with no apparent trend in regard to the thiols used or the annealing time. As seen in Figure 32, there is a small peak at the binary SAMs that have been annealed for 0 or 20 days but no peak for the sample that has been annealed for 40 days.

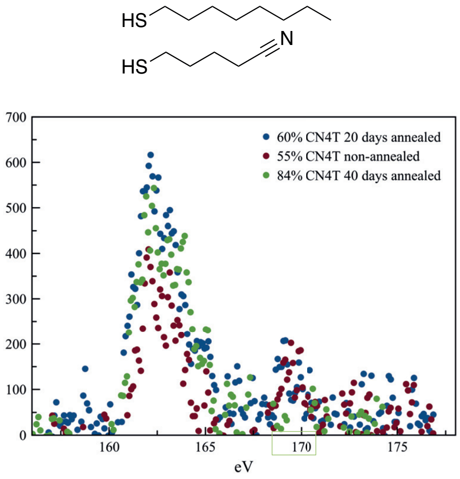

Figure 32. XPS of OT:CN4T binary SAMs that have a small peak at 168 eV that imply the existence of oxidised sulphur.

XPS analysis was performed using a monochromatic Al Kα X-ray source of 25.3 W power with a beam size of 100 μm. The spherical capacitor analyser was set at 45° take-off angle with respect to the sample surface. The pass energy was 46.95 to 90 eV. Curve fitting was performed using the PHI Multipak software.

Electroreductive desorption

Cyclic voltammetry and linear sweep voltammetry were employed for the characterisation of the prepared SAMs. All the voltammograms are presented at Appendix B according to the thiol pair in order to not disturb the flow of the discussion.

As described in detail at Chapter 2, the reductive desorption of thiols from Au(111) can offer valuable information about the species that are adsorbed onto the surface and the phases of the binary SAM. The one-component SAMs of all the thiols of this work show no significant differences upon annealing. The voltammograms are used for reference reasons throughout Chapters 3 and 4. The OT-only SAM desorbs at -0.97V, in good agreement with the literature[107], [108]. The voltammogram of the non-annealed CN4T-only SAM has no difference with the annealed CN4T-only SAM. The sample used here, has been annealed for 20 days and is characterised by a non-broad peak at -0.78 V. The peak of the p-nitrothiophenol SAM is a broad peak at -0.75mV. The peak appears to have a shoulder at -0.8 V. Other studies on the reduction of NB4M from gold surfaces have shown that for a bead crystal Au(111) in 50mM Na_2SO_4 (pH=7) electrolyte the reductive potential was found to be -0.65V versus SCE reference electrode[34]. The MPA desorption gives a sharp peak at -0.78 V.

The scan rate of the CVs is constant throughout the presented work at 50 mV/s. The desorption studies of this thesis involve a redox process. The reaction rate will not change noticeably if the scan rate changes. Figure 33 below testifies in favor of this. The “peak” that appeared in the -1.2 potential is seen some times and it is due to the delicate nature of the gold foil that slightly detaches at the hydrogen evolution potential.

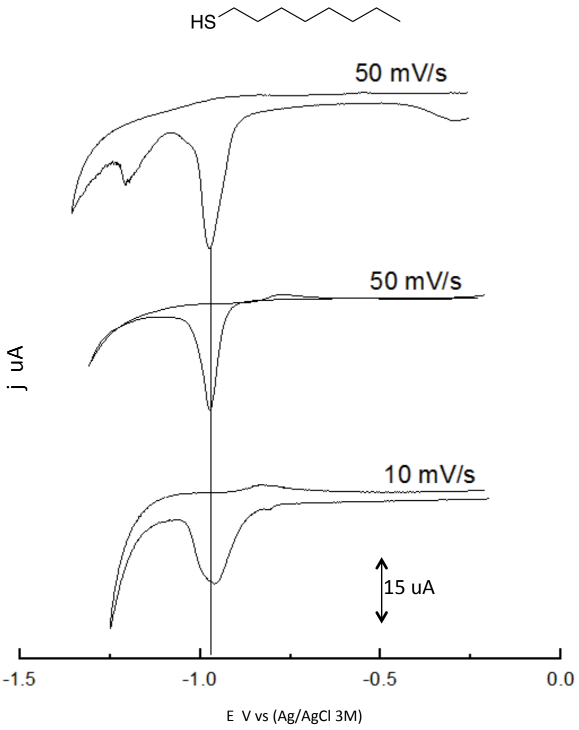

Figure 33. CVs of OT SAM at different scan rates.

The area of the peaks cannot be directly correlated between different measurements, as it is difficult to control with high accuracy the immersed area of each surface. The use of the Au(111) on mica substrates as a working electrode renders us unable measure the exact immersed surface with precision.

The profile of the prepared surfaces will assist in identifying the annealing effect in terms of received phases. Surfaces of same composition, prepared via immersion in the same mother solution of two thiols, are divided and annealed at different times and the received peaks will indicate the changes in morphology and phase separation caused by annealing.

Regarding the non-annealed binary SAMs of this thesis the two peak profiles can be used to calculate the percentage of one peak to another and give an approximate surface ratio of the two ligands. By fitting the peaks and calculating the ratio of the areas of the peak at more positive potentials with the peak at more negative potentials (desorption of OT) the ratio of the CN4T and NB4M can be estimated. Plotting the findings with the ratio of CN4T and NB4M from the XPS results gives as the plot at Figure 34. The almost linear dependence is obvious considering that the XPS values have a **14% error**.

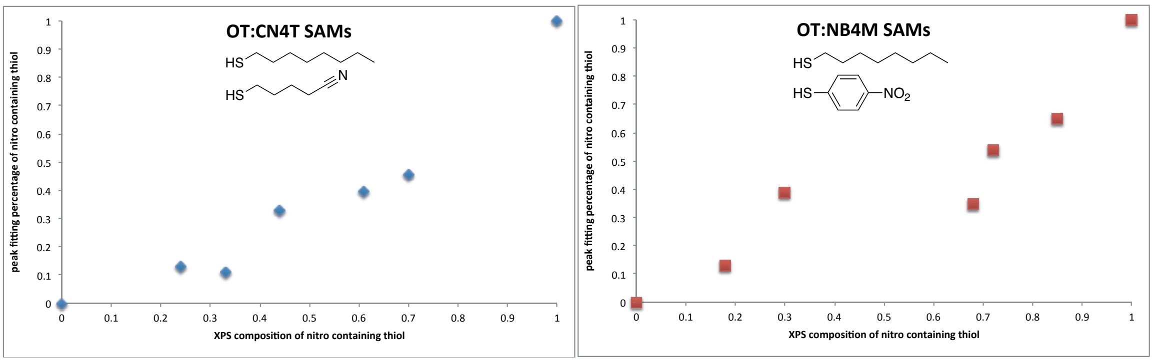

Figure 34. Fraction of CN4T and NB4M according to XPS versus the ratio of CN4T and NB4M to OT from the CVs.

Cyclic Voltammograms (CV) measurements were performed with a Gamry E-600 potentiostat and a 3-electrode cell. A separate compartment for the reference electrode (Ag/AgCl (NaCl 3M)) and a fixed position for the working electrode (clamp for the Au(111) surfaces) and the counter electrode (Pt foil). The 0.1 M KOH electrolyte was thoroughly deoxygenated by sonication and Argon bubbling prior to each experiment. All measurements were made at a sweep rate of 50 mV/s.

STM

The domain formation in terms of shape and size has been studied with the use of STM. The phase separation of two thiols that differ in terms of terminal group and molecular length will give STM contrast during imaging allowing the identification of the domains. The effect of annealing on the domains will be studied according to different compositions and annealing times.

The morphological analysis of the prepared SAMs was performed using STM in air and in liquid (phenyloctane). Unless mentioned otherwise, the scans are performed in positive bias. No differences have been identified between the scans in air and in liquid. The resolution obtained from scans performed in liquid is typically much higher than in scans performed in ambient conditions.

The STM has been calibrated using a clean HOPG surface. The stand up phase of OT on Au(111) has been correctly measured with an average distance of 0.507 nm as seen at Figure 35.

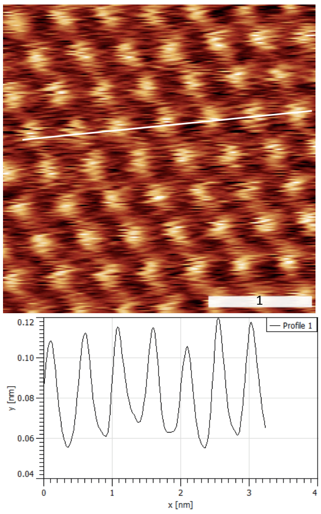

Figure 35. STM image of OT stand up phase. The line profile has measured the distance to be 0.5 nm. Set point current=50 pA and voltage bias=450 mV.

The z-height of the one-atom terrace on the Au(111) modified with OT is measured to be 240pm, in agreement with the Au-Au distance of 233 pm (Figure 36).

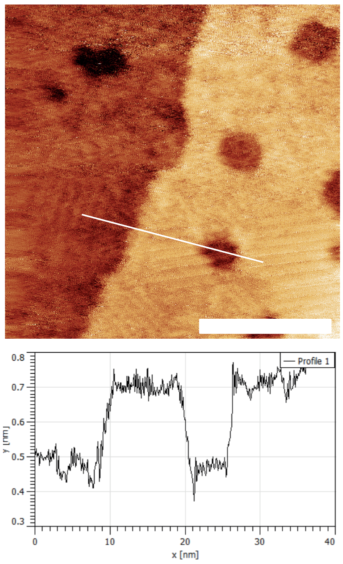

Figure 36. OT SAM. The line profile is measuring the height of the terrace to be 230 pm. scale bar is 20nm. Set point current=55 pA and voltage bias=450 mV

Numerous images have been acquired at different areas of the surface of replicates. The images that are shown in this chapter are representative in terms of surface morphology and characteristics. The table below contains the number of STM images per composition that have been acquired.

	OT%-> 0	10	20	30	40	50	60	70	80	90	100
OT:CN4T	120	200	400	120	300	500	400	155	240	320	150
OT:NB4M	100	800	900	300	260	550	500	130	500	200	150
OT:MPA	32	120	890	120	80	650	160	130	1200	60	150

Figure 37. Number of acquired STM images per sample, per composition

The domains that will be shown in the case of binary SAMs have been carefully studied to exclude any probability of them being an STM imaging artefact. The system was left overnight to stabilize or thermalise in order to minimize thermal drift. Thermal drift is the relative motion between the tip and the sample caused by thermal gradients. The changes in scan angle Figure 38 and zooming-in during the scans can also verify that the observed features are real Figure 39.

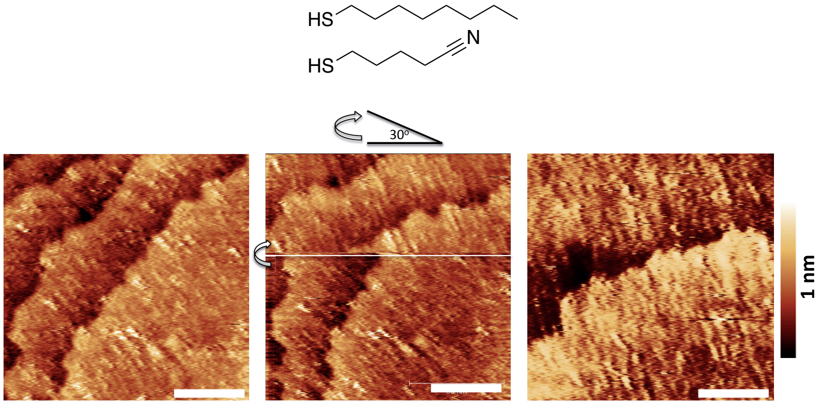

Figure 38. STM images of OT:CN4T binary SAM. The image on the left has been scanned at 0 degrees. The image at the right has been scanned at 30 degrees, clockwise. In the middle, the angle was changed during the scan. The white line indicates when the piezo changed the angle from 0 degrees (bottom half of the image) to 30 degrees (upper half of the image). The domains followed the change. The scale bar is 20nm.

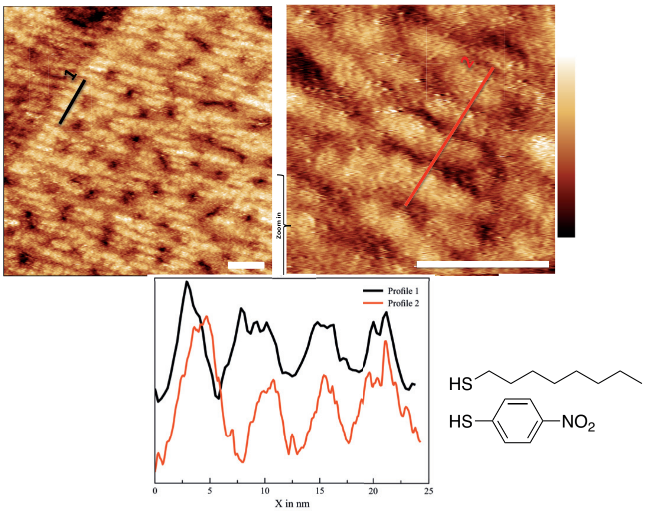

Figure 39. STM image of a OT:NB4M binary SAM (right) and next to it a zoom-in scan. The domains follow the zoom without changes in the dimensions or the shape. The scale bar is 20nm

A great number of samples have been imaged with two different STM instruments. The examples shown below, portrait that the same samples or reproduction of the samples give the same features on the two STMs. The two most important features of a surface science research is reproducibility and to be able to verify the results using more than one technique or one technique in different instruments. As it presented below, the similarity of the features of the same surface (Figure 40) scanned by different instruments indicates that the surface is homogenously patterned with the same domains and that both instruments are reliable for the study. The micelles and the same pits are distinguishable by the contrast of both instruments and no differences can be identified.

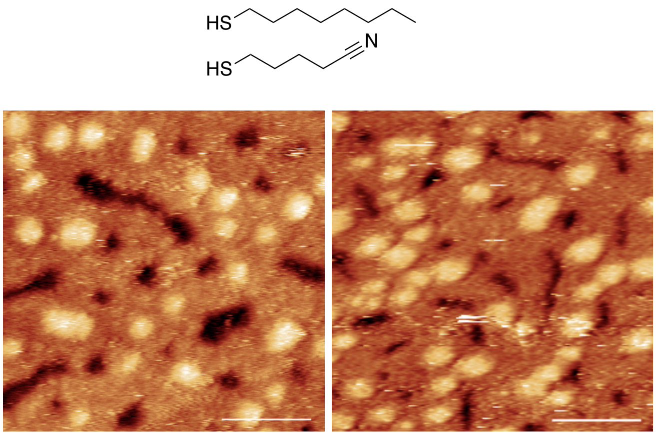

Figure 40. STM images taken by of the Veeco Multimode STM in phenyloctane (left) and Nanosurf easyScan 2 STM in air (right). The two scans were performed by 7 days apart. The sample is OT:CN4T (35%CN4T). The contrast of both instruments show the identical domains. Scale bar is 20nm

At Figure 41 the reproduction of the binary SAM and the analysis of the two samples with the two instruments verify even further the homogeneity of the binary SAM domains but also shows the very good reproducibility of the studied systems. The extended use of the easyScan instrument has been limited due to the above-mentioned reasons. The major disadvantage of the Nanosurf easyScan 2 STM is the inability to perform the analysis in solvent. Using this disadvantage in our favor, the images provide a verification that the in-situ STM at the Veeco Multimode does not cause artefacts since the image at Figure 40 (left) has been imaged in phenyloctane. Molecular resolution with the easyScan instrument is also very difficult to achieve with an imperfect tip.

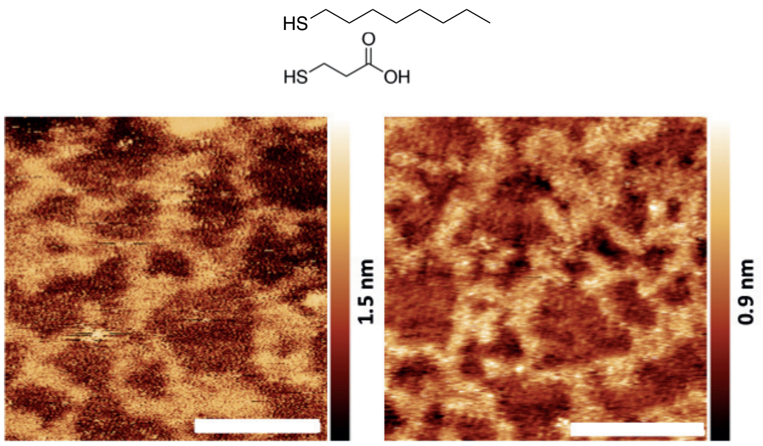

Figure 41. STM images of taken STM images taken by of the Veeco Multimode STM (left) and Nanosurf easyScan 2 STM (right). The two scans were performed on two different, reproduced SAMs. The sample is OT:MPA 20:80. The contrast of both instruments show the identical domains. Scale bar is 20nm

The characteristic length scales and dimensions of the domains identified by the STM can be extracted and measured with horizontal topographical power spectral density (PSD). The PSD analysis is an established method to extract information from the collected STM images and it is operator independent. It has been successfully employed for the determination of the domain sizes in binary-coated Au nanoparticles that have stipe-like domains [109]–[111]. Large sets of images can be compared and the average NP size and domain size can be extracted. PSD analysis has been also employed in morphological analysis of biomolecules, macromolecular films and pattern analysis in forensic science [112], [113].

PSD is the norm squared of the Fourier transform of the STM topography. It is a plot of the contribution of different surface lengths to the topography fluctuations. The characteristic lengths of the features on the whole STM image can be measured with PSD, offering a complete characterization as opposed to the line profiles at specific areas. The orientation or size of the domains can result in a PSD without a prominent peak or change in the slope. The reason lies to the fact that only the distances in the horizontal direction are taken into account, and pits or atomic steps can be considered in the ensemble of averages. The use of radial PSD (azimuthal averaging of the 2D PSD) could offer more useful results.

In the examples presented below, the radial and horizontal PSDs can be used to extract values of the domains dimensions and spacing. The micellar domains of the OT:CN4T binary SAM- annealed for 20 days were measured with line profile to have a diameter of 6-8nm. From the radial PSD a characteristic length at k=0.88 nm^{-1} (red dot) that corresponds to 7.13 nm can be extracted Figure 42.

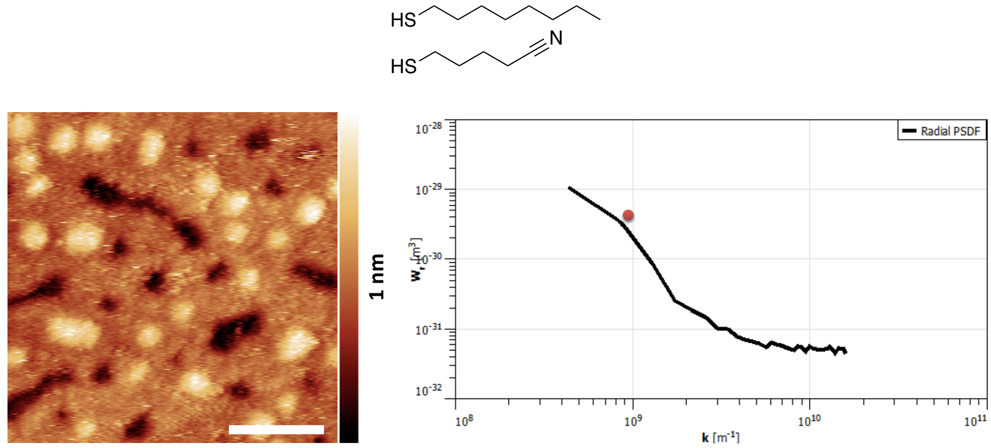

Figure 42.STM image of the OT:CN4T (35% CN4T) binary SAM annealed for 20 days with micellar domains of 6-8nm. The correlation length of 7.13 nm can be identified and extracted from the radial PSD (W/k plot on the left)

The binary SAMs with stripes are presenting good PSD plots. On the example below, the OT:CN4T STM image show stripes of 5 nm width and an average interspace of 14nm. The PSD extracted from the flattened region on the bottom shows a correlation length extracted form the first shoulder of 16.5 nm (blue dot) and a peak at k=1.25 nm^{-1} which corresponds to 4.8 nm attributed to the stipe width Figure 43.

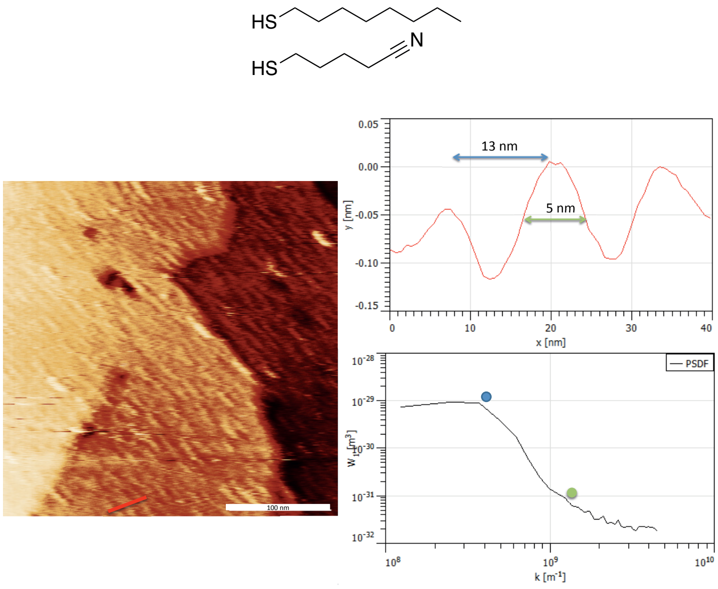

Figure 43. STM image of the OT:CN4T (45% CN4T). The line profile (red line) on the top right measures a distance between the stripes of 14nm (blue line) and a stripe width of ~5nm (green line). Dimensions that can be extracted from horizontal PSD at right bottom. Scale bar is 100nm.

The STM experiments were performed at room temperature using a Veeco Multimode Scanning Probe Microscopy with E scanner in an acoustic chamber sitting on a vibration damping table in air and a Nanosurf easyScan 2 STM. Mechanically cut Platinum-iridium STM tips were used. Set point currents were in the range of 40 pA to 400 pA with a voltage bias of 400-900 mV. Integral gains varied from 0.7 to 0.5 and proportional gains from 0.5 to 0.2. STM in liquid (phenyloctane) was performed only on Veeco multimode. All analysis and images are the result of scanning after allowing the system to stabilise over night in order to avoid drifting phenomena. Image processing of the STM images was performed with the software Gwyddion. The images were flattened.

Contact Angle

The wetting behavior of the modified surfaces is examined via contact angle measurements. The nitro and nitrile-groups been characterised as hydroneutral (and not hydrophilic)[114]. In the case of OT:MPA binary SAMs the hydrophillicity of the surface is more evident due to the carboxyl terminal group.

The hydro-phillicity/phobicity of the modified surfaces will assist in the determination of whether the annealing cause desorption or alters the chemical stability of the SAM.

The non-annealed OT:CN4T surfaces appear to remain hydrophobic when in binary mixtures. On the other hand, the annealing process is making the binary surfaces more hydrophilic reaching the value of the CN4T-only SAM. The transition of the contact angle in the case of the annealed binary SAMs follows well with composition. Comparing the annealed samples at 20 days and 40 days of annealing no differences are found thus the results support the XPS findings that the annealing process does not cause desorption of ligands (Figure 44).

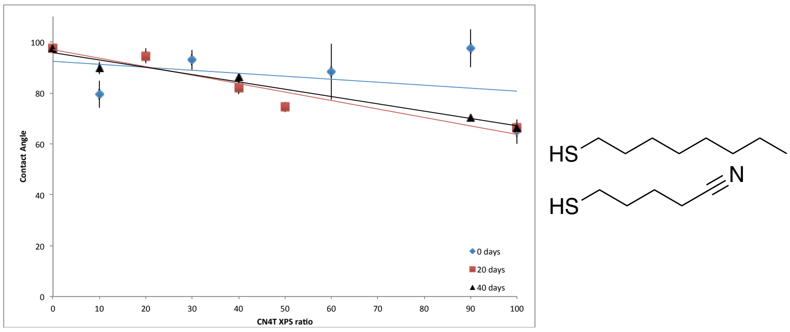

Figure 44. Contact angle measurements of the OT:CN4T binary SAMs on Au(111) at different surface compositions of CN4T and at different annealing times 0, 20 and 40 days

In the OT:MPA binary system, the carboxylic group is giving a more hydrophilic character to the modified surface. The plot below depicts the effect of feed ratio on the surface's hydrophillicity/-phobicity. Focusing on the differences according to the annealing time almost identical values are received for the same OT:MPA feed ratios (Figure 45).

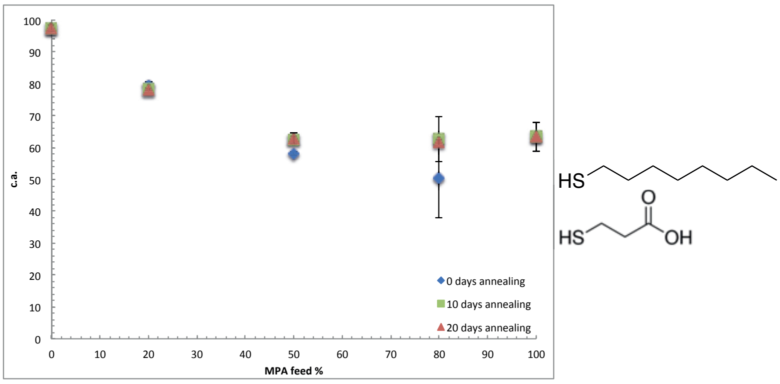

Figure 45. Contact angle measurements of the OT:MPA binary SAMs on Au(111) at different feed ratios of MPA and at different annealing times 0, 10 and 20 days

Static contact angles were measured with OCA 35 from DataPhysics Instruments. Drops were placed on the surface in room temperature. Multiple surfaces were used for the accumulation of the values. The values are an arithmetic mean of at least 15 drops per sample. The error bars at the plot represent plus/minus one standard deviation of the measurements.

Sessile drop contact angles of water were measured on the used Au(111) substrates. The value from 20 drops was found to be 71°. The value coincides with that of other publications. It should be noted that the theoretical value for a perfectly clean gold surface should be 0° but this value is unlikely to be obtained on a surface exposed to ambient conditions and susceptible to random environmental contamination.

4. RESULTS AND DISCUSSION

Chapter outline

Homoligand SAMs on Au (111) surfaces for four different ligands OT, NB4M, CN4T and MPA were studied and used as references for binary SAM functionalized Au (111) surfaces. The high quality binary SAMs of OT and one of the other three molecules, prepared by the co-deposition method, were thermally treated to expedite their transformation into thermodynamically equilibrium states. The transformation was probed by both cyclic voltammetry (CV) and scanning tunneling microscopy (STM) which provide complementary information. The evolution of the binary SAM surfaces under the mild heat treatment in a neat solvent was found to lead to new nanoscale thermodynamic phases that were initially suggested by CV, and then unequivocally identified by STM. The new phases were found to depend on the choice of ligand and the composition, being striped domains or micellar islands that are distinctly different from the phase separated macro domains of the as-prepared binary SAMs. A mechanism to explain the transformation was suggested.

4.1 Homoligand SAMs

The cyclic voltammetry (CV) on one-component SAMs on flat Au (111) surfaces was performed for reference reasons. The single components of the studied binary SAMS were studied first. Their CV curves are presented in Figure 46. A typical voltammogram of a thiolated Au surface is characterised by a single sharp peak at a potential, characteristic of the one-electron desorption process.

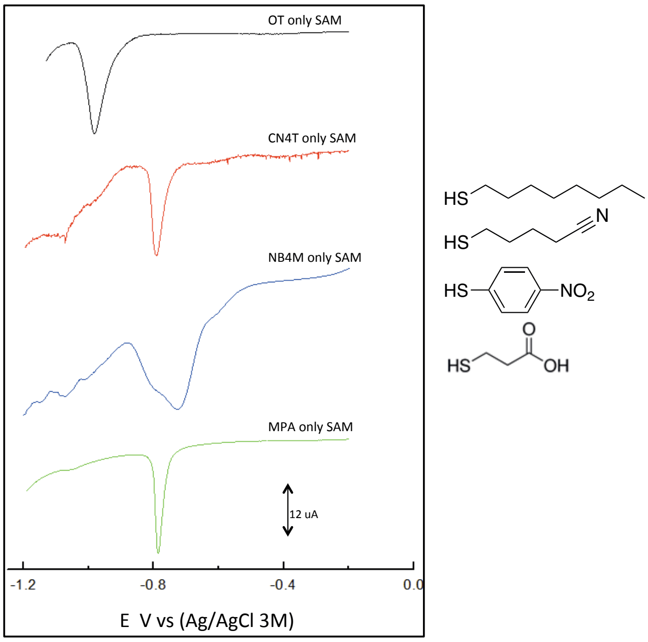

Figure 46. CV peaks of the homoligand SAMs. The small peaks at more negative potentials than -1.1 V are attributed to lost connection while the scan was performed.

The extracted desorption potential values for all the studied thiols can be found in Table 1. The obtained values match closely with those reported in the literature. OT prepared by the same method gave the value of -1 V [98]. MPA was studied documenting the value of MPA desorption at -0.8V [28], for example. The desorption potential of CN4T and NB4M has not been reported so far, but the desorption potential is obtained at the expected range for a thiolated molecule of similar structure.

Table 1. Reductive potential values of homoligand SAMs

	desorption potential V
OT	-0.97
CN4T	-0.79
NB4M	-0.75
MPA	-0.78

These desorption potentials are of great utility to study the quality of the SAMs in a quantitative fashion [52]–[55], [57], [100], [101]. It has been known that the desorption potential is dependent on not only the chemical functionality of the thiol but also the intermolecular interactions. In the case of alkanethiols for instance, it has been reported that a short alkanethiol has a typical reduction potential at about ~ -0.7 V, and this value shifts toward higher potential with greater molecular chain length. Packing defects and different packing structures such as lying-down phases also affect the reduction potential although scarcely reported [98]. In addition, the presence of functional groups also influences greatly this value [54]. The peak shape has been found that it can be used as a diagnostic tool for the homogeneity of the monolayer and can be evaluated by the full-width at half-maximum (fwhm). The studies on the factors that determine the FWHM have been focused on alkanethiol SAMs. It has been found that it narrows with increasing chain length. As it was identified by the received voltammograms in the case of CN4T- and MPA-only SAMs the monolayers were highly ordered. The narrow FWHMs of 40mV and 28mV, respectively, verify the foretold. The OT-only SAMs had a narrow FWHM of 60mV but well in accordance with the literature [93], [115]. In the case of the NB4M, a broader peak was received. The interactions between the adsorbed molecules influence the desorption peak. The broad peak might be attributed due to the pi-pi interactions of the aromatic ligand or the presence of the nitro-terminal group or the existence of two phases of NB4M at the SAM. Focusing on the peak potentials, the CV results indicate that the four chosen thiols are clearly distinguishable. This distinct feature of the four chosen thiols facilitates our studying of binary SAMs by this method.

4.2 Phase separation in non-annealed binary SAMS

The electroreductive desorption of a representative binary SAM of OT and CN4T that has not been thermally treated is employed for the discussion on the phase separation of non-annealled binary SAMs. The efficiency of the technique and the information that can be received on this study classify it as a powerful tool. A typical CV of an OT: CN4T binary SAM on Au (111) with the composition close to 1:1 at zero days was recorded in the same condition as the homoligand-coated surfaces and the result is presented in Figure 47. The two-peak profile is evident compared to that of a single-component SAM. The two peaks were identified as the reduction potentials of the constituting thiols: at -0.97 V for OT, and -0.8 V for CN4T, respectively. The presence of two separate peaks on the CV indicates that each chemisorbed thiol in the binary SAM experiences the same environment as if it were in their own homoligand-coated surface. This means that the Au surface is covered with large domains pure in OT and pure in CN4T. In other words, the voltammogram suggests that the two thiols phase separated on the Au surface into macro domains. In the same manner, Sawaguchi et al. studied the mixtures of decanethiol:MPA and pointed out the link between the macro domains and the appearance of the separate reduction potentials in the CV [116] [117]. Similarly, other studies have also reached the same conclusion based on other systems MPA:hexadecanethiol, MPA:decanethiol, 3-mercapto-1-propanol:Tetradecanethiol and hexadecanethiol:12-

mercaptododecanoicacid. [50], [51], [55], [58]–[60], [101], [118]–[120]. However, the minimum domain area that can lead to the appearance of the two separate peaks is still under debate and should be carefully considered. In the case of 1-hexadecanethiol and 3-mercaptopropionic acid, it is demonstrated that the appearance of the two desorption peaks on the CV are accompanied by the presence of thiol patches in the order of 15 nm^2 or larger [54].

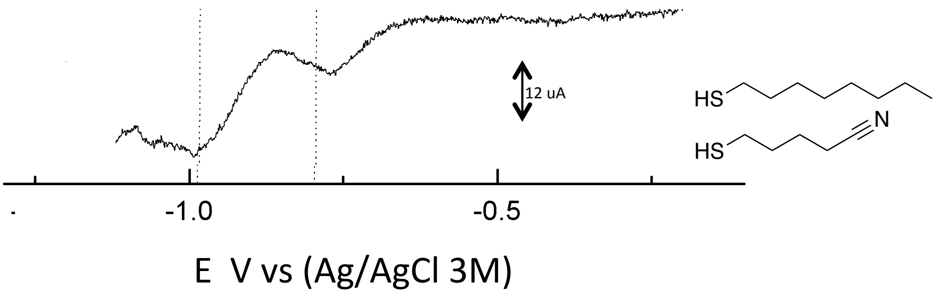

Figure 47 Voltammogram of OT:CN4T binary non-annealed SAM. The vertical lines are indicative of the OT (left) and CN4T (right) homoligand desorption potentials. Electrolyte: 0.1 M KOH. Scan rate 50mV/s

The voltammograms in Appendix C of the non-annealed binary SAMs of OT:CN4T and OT:NB4M show that the same two-peak profiles have been received during the study. STM imaging of the OT:CN4T non-annealed SAMs revealed a contrast during the large scan size image acquisition Figure 48. The observed depressions appear as irregularly shaped patches of a diameter of 25-30 nm. The one-component SAMs and the annealed binary SAMs did not feature these depressions. The contrast is reversed in the case of 87% CN4T binary SAM and islands of an average diameter of 15nm have been observed. The area of the depressions was calculated on an ensemble of 5-10 images per sample with an average size of 350x350nm. The patches' area scales with compositions. As the amount of the CN4T (shorter, in molecular length, ligand) increased, the area covered by the depressions increased as well.

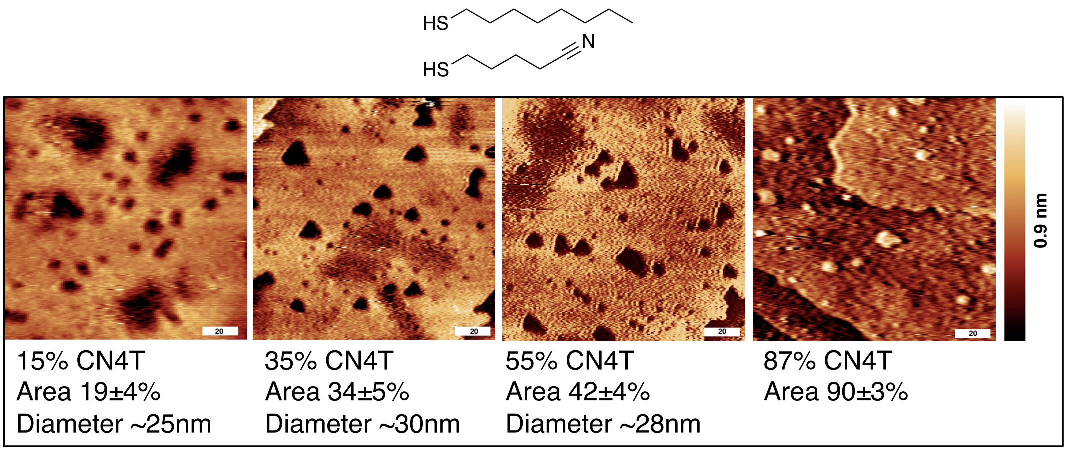

15% CN4T
Area 19±4%
Diameter ~25nm

35% CN4T
Area 34±5%
Diameter ~30nm

55% CN4T
Area 42±4%
Diameter ~28nm

87% CN4T
Area 90±3%

Figure 48. STM images of OT:CN4T non-annealed binary SAMs of different surface composition. The area of the depressions is given in percentage below the CN4T composition. Set point current=50 pA and voltage bias=350 mV. Scale bar is 20nm.

Prior to the results and discussion of the annealed binary SAMs, the reader is urged to study the voltammograms of the non-annealled binary SAMs of OT:CN4T and OT:NB4M at pages 119 and 12, respectively. The two-peak profile on all the samples is evident. The peaks are well separated at the desorption potentials of their constituents. The area of the peaks, as shown in Chapter 3, follows the changes of the ratio of the chemisorbed ligands.

4.3 The phase transformation of binary SAMs by heat treatment (annealing)

The same binary SAM coated Au (111) surface OT:CN4T (1:1) was placed in a pressure-tolerant tube containing degassed toluene. The vial was heated at a controlled temperature of 60°C. The temperature of 60°C was chosen so that the desorption of the thiols is minimal [17], [98], as also being learned from the homoligand reference samples presented in section 3.1. The surface was removed from the solvent, rinsed with toluene and dried with argon after 40days.

The CV study was performed immediately. In Figure 49, the received voltammogram of the OT:CN4T 1:1 is shown. Intriguingly, the two distinct peaks at the desorption potentials of OT (-0.97 V) and CN4T (-0.79 V) became diminished. In stark contrast to the CV of the same composition at zero day, only one peak at a potential between the desorption potentials of pure OT and pure CN4T is present. This interesting result merits further study

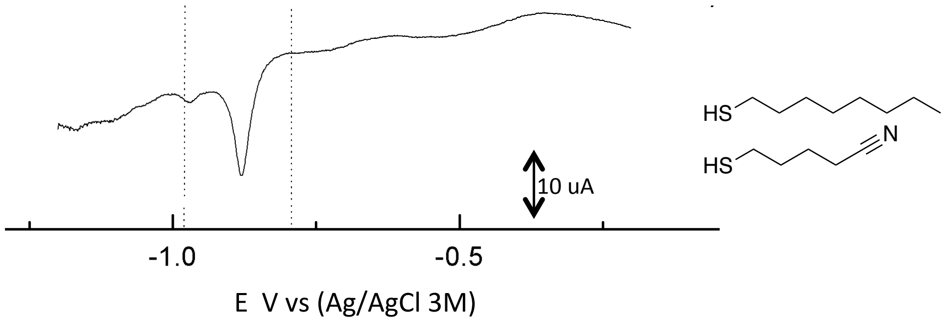

Figure 49.Reductive desorption peak of OT:CN4T binary SAM at 1:1 surface composition annealed for 40 days

In order to understand the CV data, we first investigated the quality of the binary SAMs to know if the annealing deteriorated the monolayer or not and to what extent. The XPS data pointed out that the composition of the annealed SAM was essentially equivalent to that of the non-annealed one. Overall, the XPS data did not suggest any deterioration of the binary SAM under this mild annealing condition. It is also further confirmed by wettability study where it was showed that the contact angles of the annealed films and of the as-prepared film are effectively similar (data available in Chapter 3.3).

The presence of a single peak at the intermediate region in the CV of the binary SAM OT: CN4T 1:1 suggests the change in the morphology of the thiolated surface layer. As the reductive desorption peak carries the information on not only the S-Au bonding but also the adsorbate-adsorbate intermolecular interactions. The role of the latter is especially noticeable in the present study. The reductive desorption peak at the intermediate region in between those of the constituting thiols suggests that the thiols are electrochemically desorbed from a homogenously mixed phase where each and every thiol in the mixture finds the same exact local environment. It can also suggest that the binary SAM has a particular morphological phase such as nano stripes or micellar domains with substantially small dimensions. Besides, the presence of a mixture of all of these phases is not to be excluded. A clear qualitative and quantitative determination of the suggested phases is of great interest, but it is presently beyond the scope of the CV being a spectroscopic technique. We resort to scanning tunneling microscopy (STM) to identify the new phases.

4.4 Identification of the new phase in annealed binary SAMs by STM imaging.

As CV suggests the existence of a new phase on the surface of OT:CN4T 1:1 binary SAM, STM is the most appropriate surface analysis technique to obtain its morphology. Being a microscopic technique with high resolution, it was employed to identify the size and shape of this new phase. Shown in Figure 50 is an STM image—height image—of the binary SAM OT:CN4T 1:1 after 40 days of annealing in toluene. The image has 3 different types of features that mark the locations of OT molecules (brightest contrast), CN4T molecules (intermediate contrast) and etched pits (dark brown contrast) that are unavoidable. This assignment of the molecular contrast is based on the molecular height difference between OT and CN4T, and that etched pits on a thiolated gold surface are located at a fixed depth of n x 230 pm (where n=1,2,3…) [25], [26], [121]–[126].

It is apparent that the surface possesses a morphology composed of striped domains where alternate between bright and dark contrasts appears throughout the scanned area. Manual estimation of the dimension of the phase provides an inter-domain spacing of 2.4 nm which is about 200pm molecular thick and a length of the domains from 5 to 10 nm. A better, fast and objective method based on power spectrum density (PSD) to obtain the dimension,- equivalently in this case the correlation length- of the striped domains was reported by Biscarini et al [127]. The technique is based on 1D FFT of the height image and available in most scanning probe image analysis softwares. The PSD of the STM image is displayed in Figure 50. The correlation length of the striped domains is readily extracted from the first shoulder of the PSD plot, and yields approximately 2.7 nm.

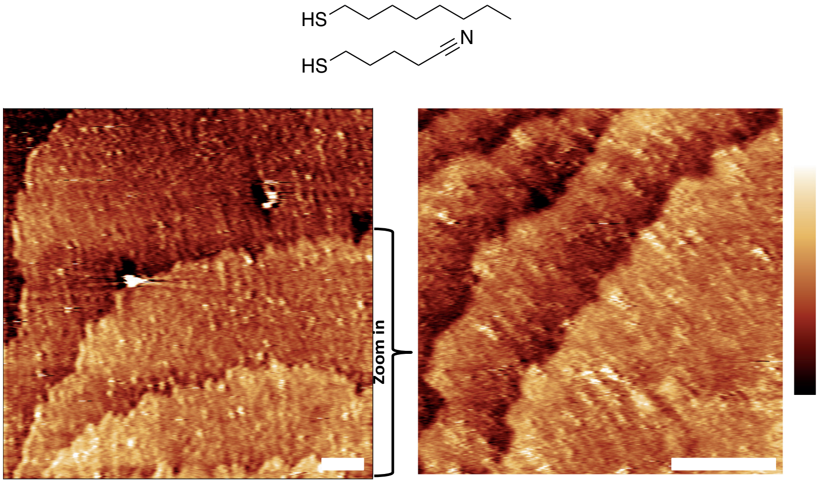

Figure 50. STM images of the OT:CN4T binary SAM annealed for 40 days. On the far right image, the angle was changed during the scan. The white line indicates when the piezo changed the angle from 0 degrees (bottom half of the image) to

30 degrees (upper half of the image). As it can be seen the domains followed the change.Set point current=50 pA and voltage bias=350 mV. Scale bar 20nm.

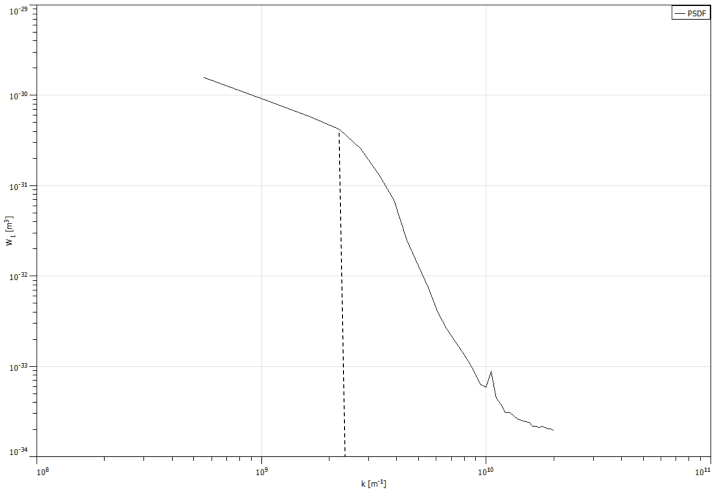

Figure 51. Horizontal Power Spectral Density of the OT:CN4T 1:1 binary SAM image presented above. The logarithmic yy' and xx' axis is helping with the identification of the shoulder, indicated with a vertical line at 2.48 nm^{-1}.

High-resolution, close to molecular scale, imaging by STM of this phase often poses a challenge, as this type of morphology is known to possess complex interfacial domain structures. The molecules at these interfaces usually assume randomly orientated conformation that hinders effective imaging [128], [129] . In Figure 52, a high resolution image of the binary SAM OT:CN4T 1:1 is presented. In this image, the location of CN4T domains is vaguely resolved, although an intermoleculardistance of a regular close-packed thiolated surface about ~0.5 nm is measurable.

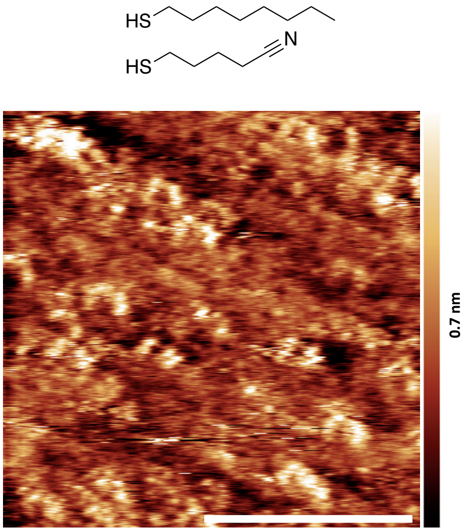

Figure 52. High resolution STM image of the binary SAM OT:CN4T 1:1-40 days. Scale bar is 20nm. The STM was performed in phenyloctane.

4.5 Evolution of morphology in binary SAMs

In order to verify that the new phase is the thermodynamically equilibrium phase of the OT: CN4T 1:1 mixture, a time dependent annealing was performed which was then investigated by CV at different annealing times. The CVs for the binary SAMs at the annealing time of 40 days and 60 days are presented in Figure 53. It is clear that the CV of the two annealed samples became effectively invariable, with only one desorption peak at the intermediate potential. This implies that the binary SAM has reached the equilibrium state within the studied annealing time.

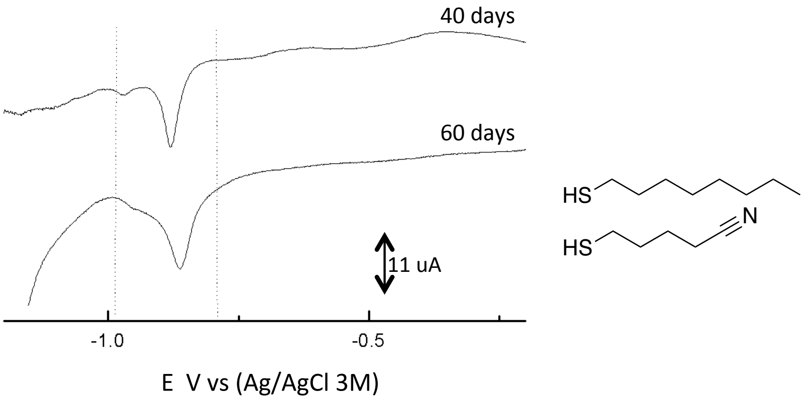

Figure 53. Cyclic voltammograms for reductive desorption of OT:CN4T binary SAMs at 1:1 surface composition annealed at 40 and 60 days. Electrolyte: 0.1M KOH aqueous solution. Scan rate was 50 mV/s.

STM imaging of the annealed SAMs at different times was also followed in order to elucidate the morphology present during the phase evolution, as shown in Figure 54. After 20 days, the surface exhibits micellar domains and a peak at an intermediate potential. The micellar domains evolved into elongated stripe-like domains at 40 days, and these domains remained effectively unaltered. The images at Figure 55 of the OT:CN4T SAM annealed for 60 days at different scan sizes further verify the aligned elongated domains.

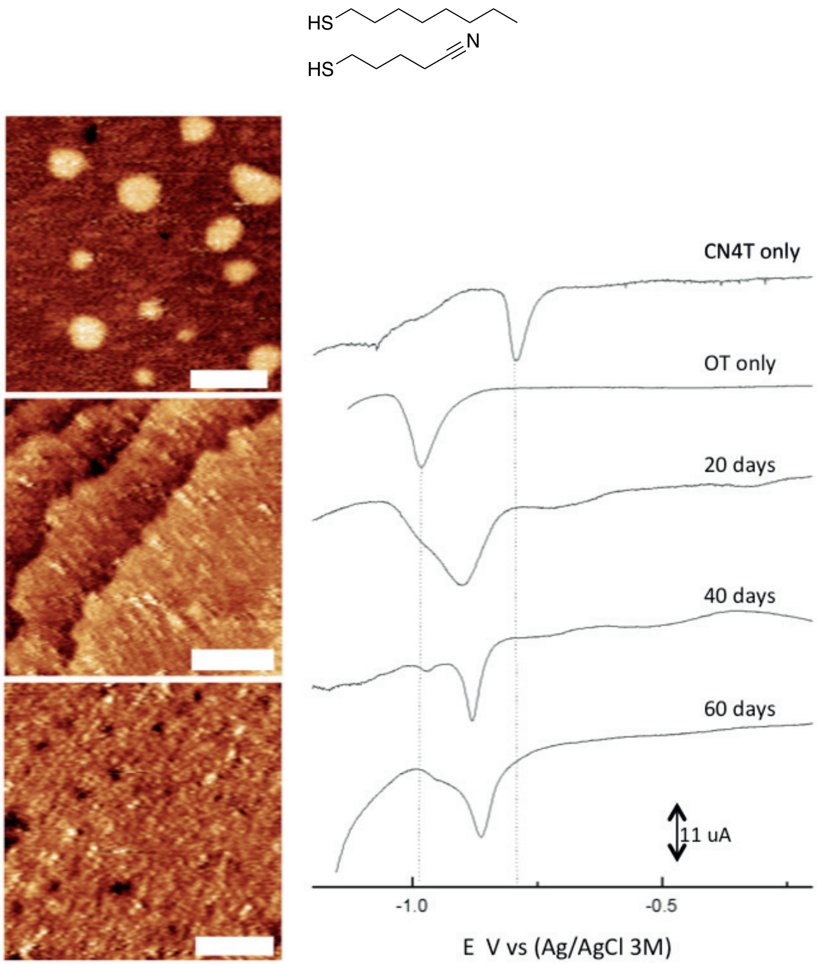

Figure 54. STM images of OT:CN4T binary SAMs at 1:1 composition, at different days of annealing. Set point current=50 pA and voltage bias=350 mV. Scale bar 20nm.

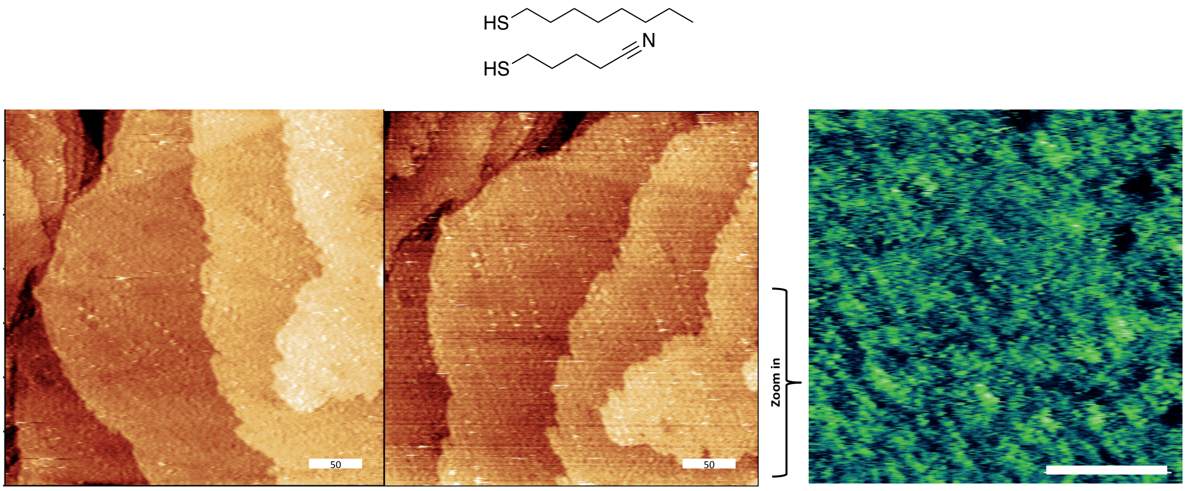

Figure 55. Large area STM images of OT:CN4T binary SAMs at 1:1 composition, at 60 days of annealing. The change of the orientation is allowing the comprehension of the stripe domains Set point current=50 pA and voltage bias=350 mV. Scale bar 20nm.

The evolution of the morphology of binary SAMs from complete phase separation at zero days to the formation of the new phase was also studied in other binary SAMs. In the case of OT:NB4M 1:1, we observed the gradually diminishing desorption peaks of OT and NB4M over the course of annealing, and the appearance and prominence of the immediate peak, as shown in Figure 56.

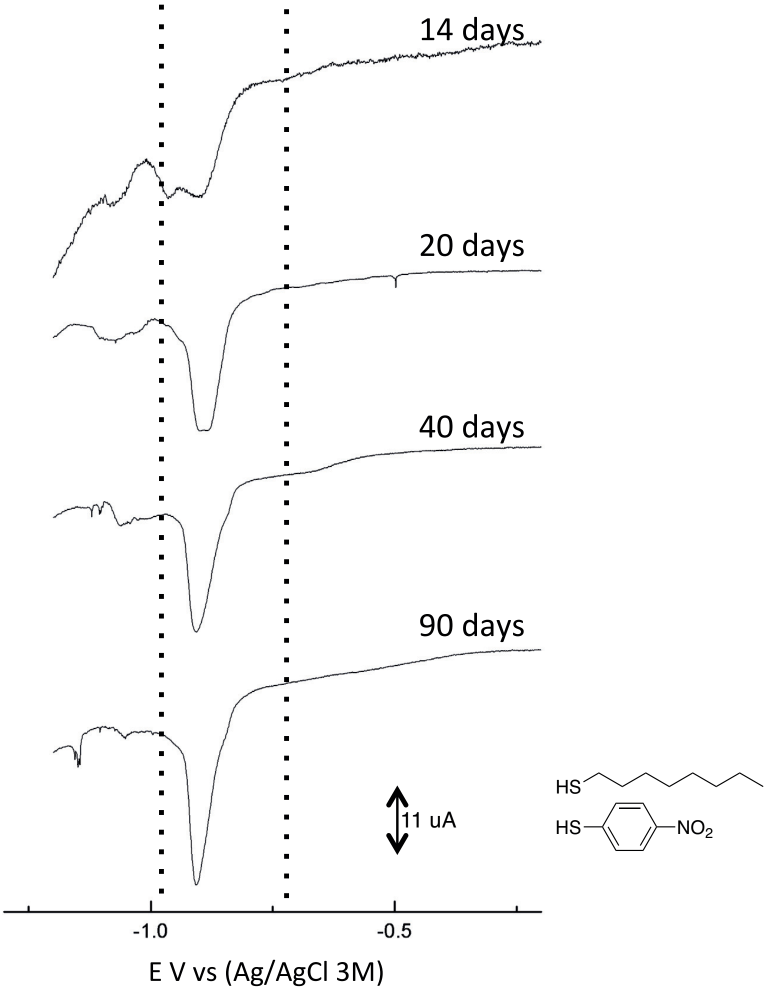

Figure 56. CV of OT:NB4M binary SAM (surface composition 1:1) at different annealing times.. The two lines indicated the reductive potential of the single ligand SAMs. Electrolyte: 0.1 M KOH. Scan rate 50mV/s

STM imaging at intermediate annealing times was also carried out. The result, as can be seen from Figure 57, shows the evolution to the final morphology where stripe-like domains are evident. The binary SAM that was annealed for 14 days presents a three-peak profile. STM images of that intermediate phase depict ragged domain boundaries, suggesting that the new striped phase appears at the expense of the sub-domains. The binary SAM that had been annealed for 90 days resulted in striped domains. The width of the stripes is ~4nm with a spacing of 8nm. The large scan area showed that the orientation of the stripes differs in the different terraces of gold.

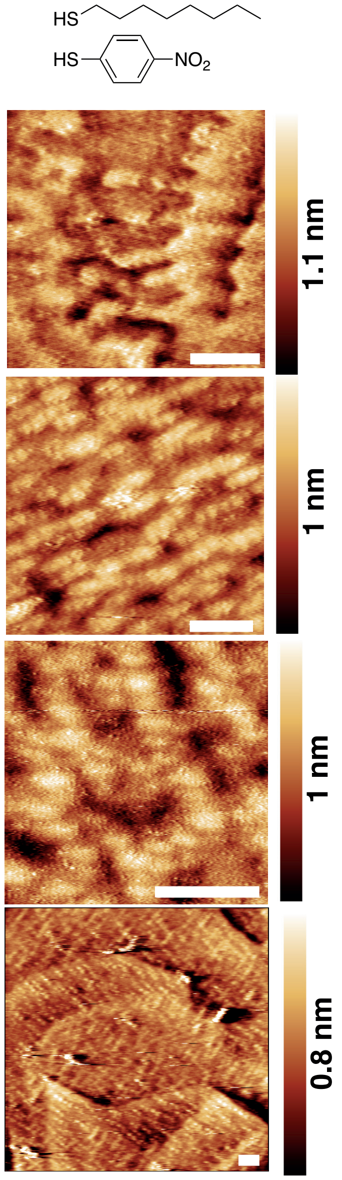

Figure 57. STM images of OT:NB4M binary SAMs at 1:1 surface composition at 14days (top), 20days, 40 days and 90 days (bottom) of annealing. Set point current=50 pA and voltage bias=350 mV. Scale bar 20nm

4.6 Composition dependence of the equilibrium morphology in binary SAMs

We inspected the equilibrium phase of binary SAMs at ratios other than 1:1 by both CV and STM. The one-peak profile is also evident on binary SAMs OT:NB4M, OT:CN4T, and OT:MPA at different composition ratios as presented at Figure 58 - Figure 62. As can be seen, other equilibrium morphologies such as micellar islands can be tuned by changing the composition of the as-prepared SAMs.

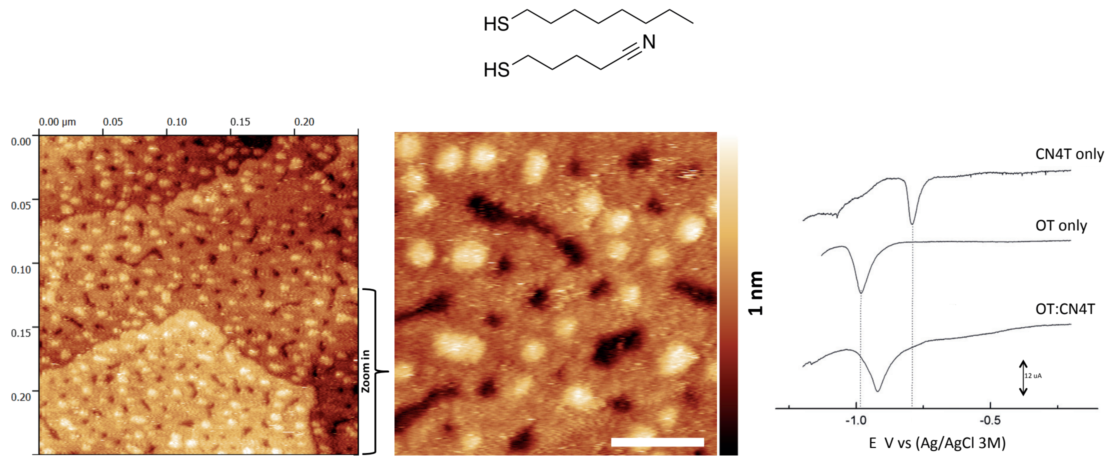

Figure 58. STM image of the binary SAM of 35% CN4T at equilibrium, annealed for 20days. Set point current=50 pA and voltage bias=400 mV. Corresponding CV on the left. Electrolyte: 0.1 M KOH. Scan rate 50mV/s.

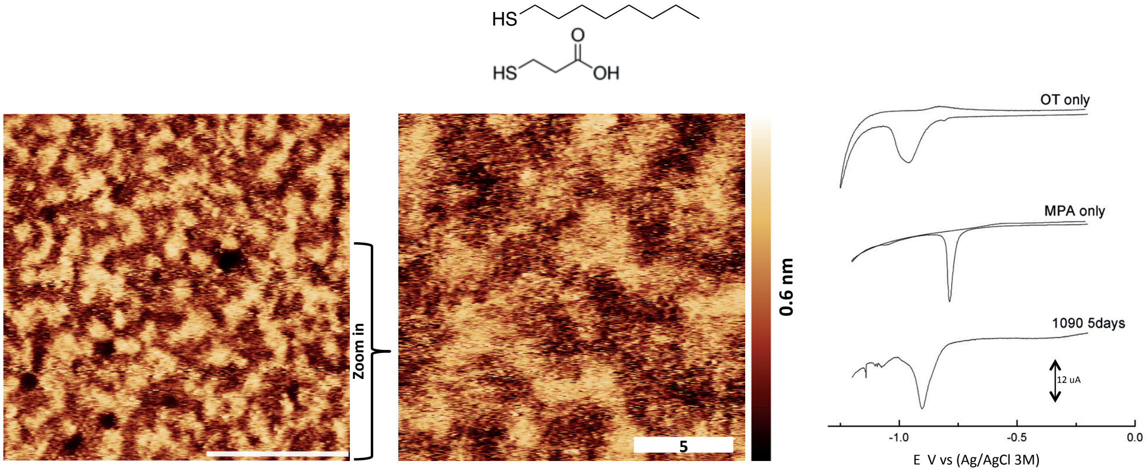

Figure 59. STM image of the OTMPA 1090 binary SAM after 5 days of annealing. Set point current=50 pA and voltage bias=400 mV. Corresponding CV on the left. Electrolyte: 0.1 M KOH. Scan rate 50mV/s.

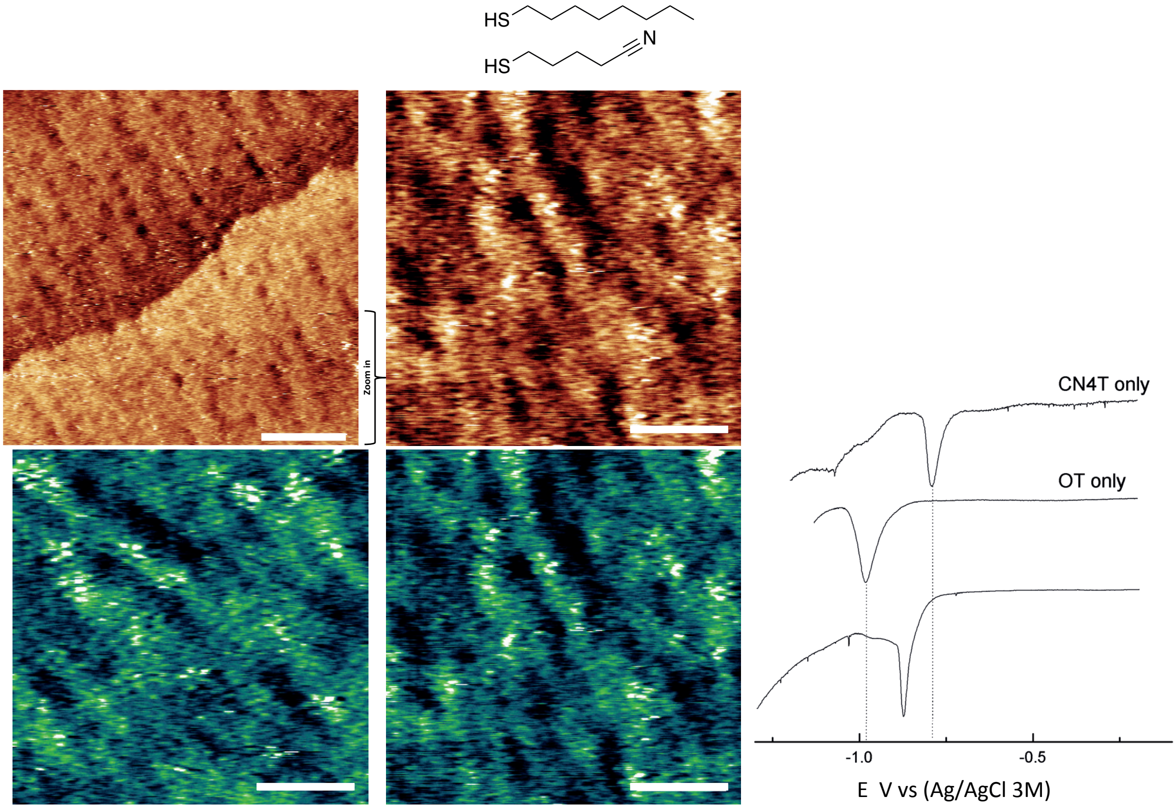

Figure 60. STM image of binary SAM of 35% CN4T at equilibrium, annealed for 60days STM image. Set point current=50 pA and voltage bias=400 mV. scale bar is 20nm. Corresponding CV on the left. Electrolyte: 0.1 M KOH. Scan rate 50mV/s.

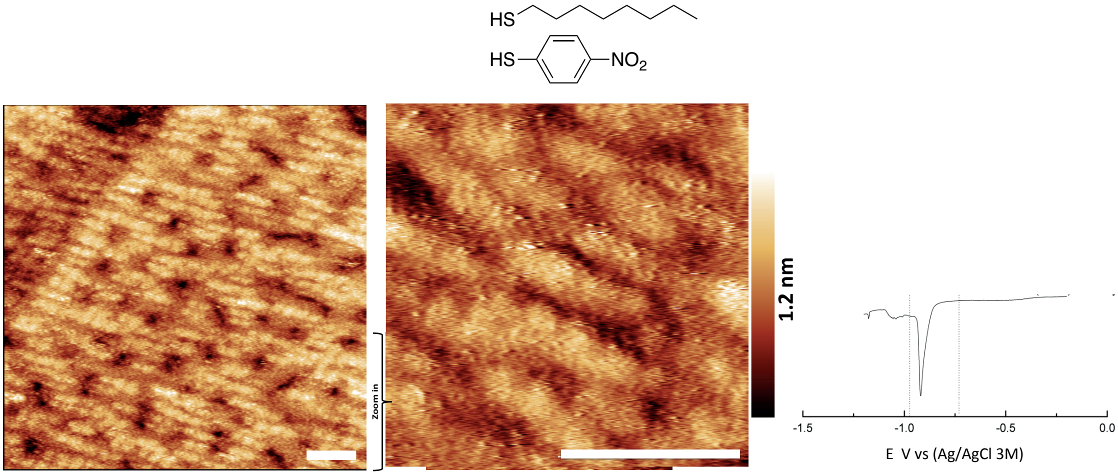

Figure 61. STM image of binary OT:NB4M SAM 30% NB4M at equilibrium, annealed for 40days. Set point current=50 pA and voltage bias=400 mV.

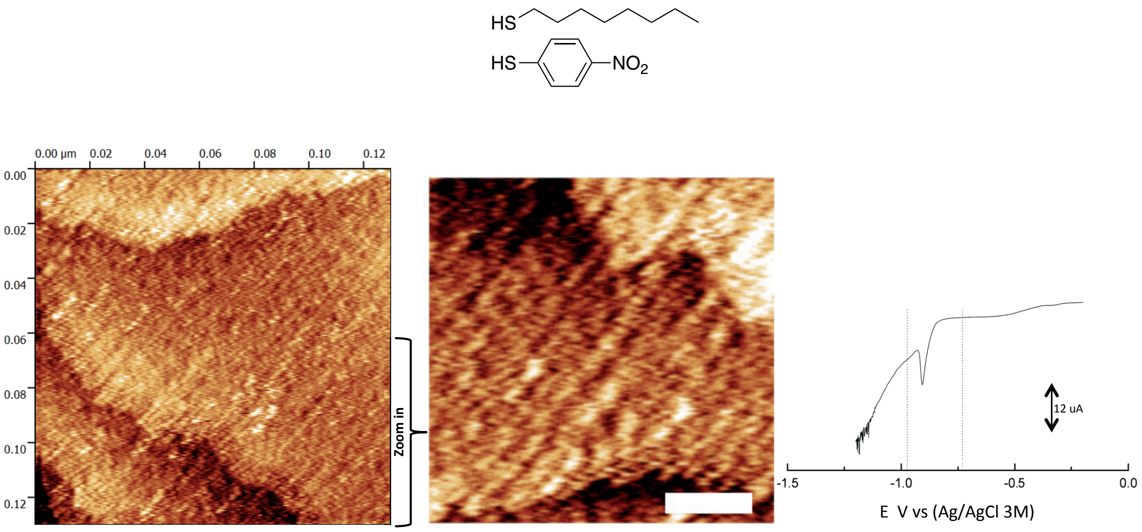

Figure 62. STM of binary SAM 70% NB4M at equilibrium, annealed for 40 days. Set point current=50 pA and voltage bias=400 mV. Corresponding CV on the left. Electrolyte: 0.1 M KOH. Scan rate 50mV/s.

4.7 Mechanism of the phase transformation in binary SAMs

Binary SAMs of thiols on Au(111) can be made by a variety of methods such as co-adsorption or place exchange [48], [49], [51], [52], [55], [57], [58], [130]. The fabrication method influences largely the composition and morphology of the obtained binary SAM. With respect to composition for example, it is often found that composition of the SAMs does not reflect the composition of the solution mixture. It is a consequence of chemical affinity and competitive intermolecular interactions among the thiols of the same species and the thiols of different species. In general, the adsorption of two alkanethiols of different lengths has been known to favor the longer chains over the short ones. In our co-deposition method, we see that the composition of the binary SAMs linearly depends on the solution composition as also reported previously by a number of groups [59]–[61], [131].

The obtained binary SAM is strongly influenced by the solubility of the thiols, the surface diffusion, and the exchange of adsorbates with the thiols in solution. However, it is observed that for any mixtures of any dissimilar thiols, the phase separation occurs by the co-deposition method [107]. Mixtures of alkanethiols having different lengths were investigated and it was shown that the larger length mismatch led to greater macro phase domains [51]. A mixture of molecules of the same chain length but with different head groups was also found to separate into macro domains [52]. In our study, the molecular pair OT:CN4T is distinct in both chemical nature and in length, hence the conclusion is supported by our CV study at zero day that the macro phases are present, as is evident by the sole presence of the two separate desorption peaks -0.97 V for OT, and -0.79 V for CN4T, respectively. Indeed, all three mixtures chosen show a distinct difference in chemical nature of the thiols and length, hence one would expect the phase separation occurs in all of these mixtures at day zero. It is believed that due to the short deposition time and slow mobility of thiols on gold surfaces, the thiols are kinetically trapped in this initial morphology.

The progression of domain formation towards an equilibrium phase is scarcely reported in the literature. In one particular case, Tantakitti et al. reported the progression of binary SAMs of a sugar derived thiol in the form of a synthetic tetrasaccharide-terminated oligo(ethylene glycol) thiol and an OEG-derived thiol having hydroxyl-terminated oligo(ethylene glycol) towards the equilibrium phase [61]. The binary SAMs, made by co-deposition from the aqueous solution of the two thiols, possess the usual patchy domains formed upon adsorption and changed with time in ambient condition toward micellar or island-like at low molar ratios, and worm-like or continuous clustering at high composition. Due to the negligible mobility of the thiols at room temperature, especially when they are in close-packed form on the surface of Au(111), the heat treatment (annealing in neat solvent in our case) would speed up the coarsening process and lead faster to equilibrium.

The annealing of the binary SAM OT:CN4T indeed led to a different phase, as suggested by its CV where a single desorption peak at the intermediate potential was observed. The STM imaging elucidated further that the new phase was striped domains where alternate stripes of OT and CN4T stood next to each other. Analysis of the STM images gave the stripe correlation length of ~3 nm. Other mixtures of OT and CN4T (35% CN4T), and OT:NB4M (30% NB4M) OT:NB4M (70% NB4M) also gave stripe domains as a final phase, while OT:CN4T at 20 days of annealing, OT:MPA 10:90 led to micellar islands in the size range of 4 nm to 8 nm as the thermodynamic phase.

In order to understand how the binary SAM transformed into the final phase, it is worth noting that when a SAM is composed of two or more components, the self-assembly is controlled by intra- and inter- molecular interactions. In general, molecular organization is dictated by weak non-covalent chemical interactions that include van der Waals, π-π, and electrostatic interactions. In addition to such chemical interactions, molecular geometry has a significant impact on the formation and the final morphology of the assembly. For alkanethiols for example, the strength of tail-tail interactions goes in preferred order of long-

long > short-short > short-long. In general, the phase separation into domains reflects differences in chemical properties, length, and bulkiness between the molecular components and their interactions in bulk and at the interface. Several forms of phase separation are illustrated in Figure 63.On the general mechanism that is suggested, the phase segregated domains that give a two-peak profile at the potentials of the SAMs constituents, they start diffusing upon annealing. This movement increases the length of the interface offering a gain in free volume and entropic freedom due to the differences in length and terminal group of the two components. As the diffusion progresses the thermodynamically equilibrium phase is achieved (D and E). The evolution of domains leads to nanoscale thermodynamic phases that are described as micelles (E, left), prestripes (E, middle) or stripes (E, right). It is important to understand how the thiols self-assemble and what structure and function may arise from such self-assembly.

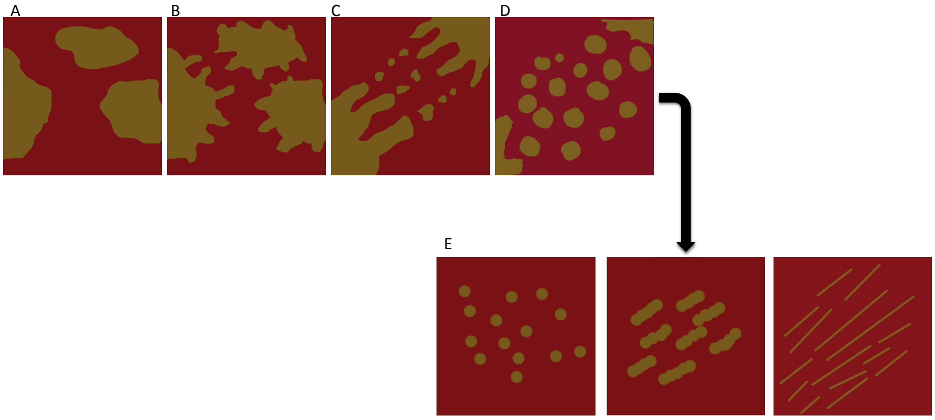

Figure 63. A cartoon of the general mechanism that was derived according to our observations and conclusions form the electroreductive desorption and STM analysis. This cartoons represent a binary SAM onto a flat surface. The two colors represent regions occupied by one type of ligand. The phase segregated phase of the non-annealed surface at (A) which gives a two peak voltammogram at the reduction potentials of the homoligands verifying the presence of pure ligand a and pure ligand b phases. Then by annealing there is a transition as seen at (B) and (C) with a three-peak profile from the CV. The formation of micellar domains that are scattered over the surface or the prestripe or stripe domains that can be received at the next step, where equilibrium has been achieved, at images (E) give a single peak voltammogram with a peak at an intermediate potential. The sizes do not relate to actual dimensions

5. Conclusions and Outlook

Conclusions

Self-assembled monolayers (SAMs) are molecular assemblies formed spontaneously on surfaces by adsorption and are organized into domains. The study of the basic science of SAMs that are composed of binary mixtures of molecules is the aim of this thesis. The surface morphologies and kinetically trapped morphologies are being investigated. The effect of thermal treatment of the SAMs inside degassed neat solvent (annealing) is evaluated. Upon annealing, the evolution of the binary SAM was found to lead to new nanoscale thermodynamic phases as indicated by electroreductive desorption studies. The new phases were morphologically identified and found to depend on the choice of ligand and the composition

Initially high quality single-component SAMs have been produced. The four different thiols (OT, CN4T, NB4M and MPA) have been dissolved in degassed ultra pure toluene and SAMs have been formed via immersion for 24 hours. The same incubation procedure has been meticulously followed for all the prepared SAMs in this work. The extensive rinse with toluene after the incubation, the drying under a flow of argon and the placement of the substrates inside a vacuum desiccator ensured the resulting SAM to be free of physisorbed thiols, solvent traces and other contaminants as verified by AFM imaging.

The resulted modified surfaces have been investigated with XPS, CV contact angle and STM. In the case of all one-component SAMs XPS detected the gold substrate and the C, S, O elements. In the case of the nitrogen containing monolayers the nitrogen has also been detected. STM analysis of the one-component SAMs showed the ordered striped lying-down phase of the alkanethiol SAM (OT). The other three thiols have resulted in non-ordered SAMs (amorphous phase) with a high number of pits. No definitive answer has been given yet concerning the reason of the pits. The most reported conclusion states that surface reconstruction leads to these pits while providing the monolayer with adatoms as it forms. Cyclic voltammetry and linear sweep voltammetry have been employed for the reductive desorption of the bounded thiols. The difference in the peak potentials facilitates our studying of binary SAMs by this method since the qualitative analysis is possible. Although the intermolecular interactions can alter the desorption potential, as it will be mentioned in the next paragraph. The coverage of the thiols can be calculated from the reductive peak. The substrates (Au on mica) posed a difficulty on coverage calculations via CV due to the reason that the immersed area of the working electrode (modified Au on mica) cannot be precisely measured and it is different for each analysis and each sample. The contact angle measurements revealed the hydrophobic character of the OT-only SAM (~98°), the hydrophilic character of the MPA-only SAM (~64°) but no great changes have been observed at the NB4M (~90°) and CN4T-only (~75°) SAMs.

Three different binary SAMs of OT:CN4T, OT:NB4M and OT:MPA at different feed ratios have been produced. The XPS measurements of the N/S atomic percentage concentration versus the feed ratios for the OT:CN4T and OT:NB4M determined the surface composition of the prepared SAMs. The CV showed the two distinct separated peaks of the non-annealed binary SAMs at the reductive potentials of the two constituting thiols, which indicates that each thiol experiences the same environment as if it were in their own homoligand-coated surface. The CV verifies that the two thiols phase separated on the Au surface into macro domains. The relative composition of the thiols from the reductive peaks reveal a linear dependence with the surface composition (ratio) from the XPS results.

A new series of one- and two-components SAMs that have been prepared at the same way as described above, were immersed in a pressure-tolerant vial containing degassed neat toluene. The vial was heated at a controlled temperature of 60°C for a dedicated amount of time. The annealed one-component SAMs have been investigated by XPS, CV and contact angle and verified that no desorption has taken place during the process. The reductive peak at the same potential and the same contact angle has been received for the annealed one-component SAMs. STM imaging of the samples have shown that the SAM is still present on the gold.

Annealing of the binary SAMs caused no noticeable decomposition or desorption of the components. Surface composition via XPS showed no changes between the non-annealed and annealed binary SAMs that have been immersed in the same feed ratio incubation solution. The contact angle also when compared for different annealing times shows no great differences. As hypothesised from simulation studies and seen on some publications, annealing is expected to expedite the transformation of the phase separated domains into thermodynamically equilibrium states. Upon annealing, the evolution of the binary SAM surfaces was found to lead to new nanoscale thermodynamic phases that were initially suggested by CV. The two distinct CV peaks that where received on all non-annealed binary SAMs have indicated the presence of phase segregated phases of the constituents. As the annealing time increases the two-peak profiles are changing to three-peak profiles, with the appearance of a new peak at an intermediate potential. The new peak is at a potential where none of the thiols is expected to desorb and it has never been seen during the homoligand SAMs electrochemical studies. The two peaks at the desorption potentials of the constituents are diminishing as the annealing time increases and a single peak profile is received. At 14 days of annealing for the OT:NB4M the three-peak profile was received at almost all compositions. The three-peak profiles were also received throughout the whole OT:MPA series but the CV study consisted of samples whose annealing period has not exceeded the 20 days. The three peak profiles according to the literature indicated the presence of 3 phases. The two pure phases of the components and one mixed phase of the two. After 20 days of annealing the CV profiles of the annealed binary SAMs presented on almost all the OT:CN4T and OT:NB4M SAMs a single peak at an intermediate potential, which suggests the change in the morphology of the thiolated surface layer. The CV profiles remain unaltered (one peak at an intermediate potential) upon further annealing of binary SAMs with the same composition. The new phase is therefore the thermodynamically equilibrium phase.

The verification of the new equilibrium phase has been identified by STM. The new phases were found to depend on the choice of ligand and the composition. In the case of OT:NB4M near the 1:1 surface composition the equilibrium domains that have been received since day 20 of annealing, are caracterised as prestripes with an average of 5nm width and 20nm length. At higher NB4M compositions the equilibrium domains are stripes with smaller width. The OT:CN4T equilibrium domains at 20 days of annealing are characterised as micellar. The evolution of the micellar domains at higher annealing times leads to stripes with an average width of 3 nm.

The findings of this thesis are remarkable. Different pairs of thiols have proven that can be lead to equilibrium phases via annealing. The process does not have any negative effect on the SAM. The differences in length and terminal group are key factors that should be taken into account in future binary SAMs studies. What is the most important finding is that the transition to a new phase can be easily identified via CV. The new phase can be morphologically identified in three types of nano-domains, for our three examined systems.

As the annealing increases the nano-domains continue to evolve, in an effort to increase the interface between the two chemisorbed thiols leading to elongated aligned domains.

Outlook

The work presented in this thesis has shown how nanostructured surfaces with a variety of domains can be achieved. The established, in this thesis, framework will help surface scientists to produce various surface patterns in binary SAMs. The next steps in binary SAMs research could include the use of other pairs of thiols, following the same procedure as presented here, in order to enrich the components list that self-assemble and result in nano-domains.

The ultimate purpose of the researchers should be focused on constructing an experimental phase diagram. Similar to the case of block-copolymers, an experimental phase diagram will be a powerful tool in surface science. From the experience gained during my thesis, the composition and annealing time are the key factors that lead to ordered nano-domains when dissimilar thiols self-assemble onto a flat surface. A phase diagram will allow the production of a variety of patterned surfaces with various thiols in order to ascribe new properties on a solid surface. Special attention should be given to the fact that the type of the solvent and the quality of the substrate must be taken into consideration since they are very important elements in SAM formation. An improper solvent could affect the physisorption process and might cause the selective desorption of a ligand during the annealing. A gold surface that is polycrystalline will affect the thiol coverage and a flat Au111 surface without large terraces and a great number of atomic steps will disrupt the evolution of domains, affecting the verification of the equilibrium morphologies.

Future studies on the same or similar systems can include Tip-enhanced raman scattering (TERS) and STM-TERS since I believe it is a powerful technique that would offer further understanding of the morphological changes that annealing is inflicting upon. The chemical information from the nanodomains will allow the mapping of the surface and the distinction between the phases. One last recommended future step is the study of binary SAMs that instead of annealing, we apply small amounts of pressure. This approach might also speed up the thiol diffusion and lead to nanodomain formation.

The use of electrochemistry has proven to be a very powerful tool in phase separated SAMs. The method can be applicable on thiolated coated gold nanoparticles as well. Publications and preliminary results form our lab on non-water soluble binary NPs indicate that the quantitative analysis of thiols is possible with electrochemistry. The future goal would be to study whether it is possible to extract information on the domain sizes on binary NPs due to phase separation as a complementary technique to STM and SANs. One weakness of the CV setup that is employed here is that the water-soluble nanoparticles diffuse form the working electrode (HOPG) making them impossible to measure. A solution might lie on the construction of new electrochemical cell and the study of the electroreductive desorption of the water soluble single or binary NPs dispersed in the electrolyte.

The terminal groups of the ligands used in this work serve as an excellent group for further addition reactions. Initiators, conductive molecules and molecules that will bind to an analyte can be added on the already patterned surface. As an SPM analyst I have the need for available substrates that will immobilise the biomolecule or nanoparticle in such way that I can perform better quality scans. The nano patterned binary SAMs of this thesis can be employed for this purpose. Either by entrapment of the nanoparticle between the patchy or striped geometries or by using binary SAM that can interact with the analyte forming a permanent of temporary bond.

The alignment that has been observed in the case of stripes can serve as an excellent modified substrate for molecular electronics. The attachment of a conductive molecule, selectively at one of the chemisorbed thiols can create a molecular wire or an array of molecular wires that will follow the pattern that we have. A very rough representation can be found at Figure 64.

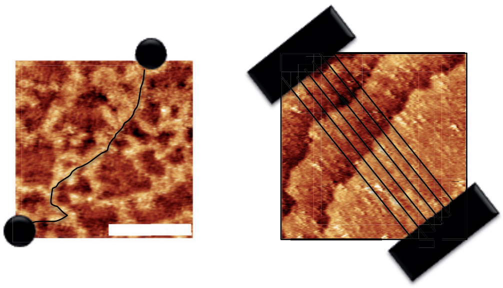

Figure 64. As indicated by the black line, a continuous path of the binary SAMs can serve as a surface for molecular electronics applications.

The homogeneity of the dimensions and spacing on the micellar or pre-stripes morphology can enhance the binding abilities of the surface of a biomolecule or other analytes producing more efficient sensors. A patterned binary surface versus an amorphous one offers better sensitivity and selectivity, repelling unwanted species of different geometries. Electrochemical Impedance Spectroscopy and cyclic voltammetry are widely used to verify and calculate the binding. Future efforts should first establish the domain sizes that can be received or altered upon annealing of a binary SAM and then study the binding. The main difficulty in the utilisation of thiol-gold systems as sensors lies to the deterioration of the monolayer upon continuous exposure to aggressive bioactive media. The avoidance of acidic or oxidative media is advised but the advancements on binary SAMs research will soon enable the quick and massive production of patterned surfaces with controllable nano domains that will solve the surface destruction issue.

Tailoring a surface with domains of specific sizes and terminal groups that provide bonding or different wetting properties on the binary SAM could imitate the structure of proteins that bind specific hormones. The surface now can be characterised as a biomimetic surface. The ability to bind to hormones such as cortisol can be used for the early detection of Cushing syndrome or liver cancer. The plethora of choices that are available by this biomimetc approach are innumerable and the better control that we can now have over binary SAMs (as discussed in this thesis) can assist more in the exploration of options.

Surface immobilized initiator or even better two types of initiators can be added in one surface via bond formation and allow the formation of binary polymer brushes. The surface-initiated controlled radical polymerisation has been significantly advanced over the last years. The application of photo-mask and Y-shaped initiators has given the ability to scientists to create binary polymer brushes but the use of binary SAMs and surface-initiated polymerization could lead to brushes of various polymer thicknesses according to the domain sizes.

A lot of researchers have done amazing things in surface science, but according to my opinion the field lacks some basic understanding of key-points and mechanisms that denies them absolute control over the potential morphologies or properties a binary or tertiary-component coated surface can offer. This thesis has given us some control over nanostructured surfaces. Greater things are coming.

BIBLIOGRAPHY

[1] Chuanzhen Zhou, and Gabriella Nagy, and A. V. Walker*, “Toward Molecular Electronic Circuitry: Selective Deposition of Metals on Patterned Self-Assembled Monolayer Surfaces,” 2005.

[2] S. Ramachandran, B.-L. Tsai, M. Blanco, H. Chen, Y. Tang, and W. A. Goddard, “Self-Assembled Monolayer Mechanism for Corrosion Inhibition of Iron by Imidazolines,” *Langmuir*, vol. 12, no. 26, pp. 6419–6428, 1996.

[3] W. Senaratne, L. Andruzzi, and C. K. Ober, “Self-assembled monolayers and polymer brushes in biotechnology: Current applications and future perspectives,” *Biomacromolecules*, vol. 6, no. 5. American Chemical Society, pp. 2427–2448, 2005.

[4] † Nirmalya Ballav, † Andrey Shaporenko, ‡ Simone Krakert, ‡ and Andreas Terfort, and † Michael Zharnikov*, “Tuning the Exchange Reaction between a Self-assembled Monolayer and Potential Substituents by Electron Irradiation,” 2007.

[5] A. Ferrario, M. Scaramuzza, E. Pasqualotto, A. De Toni, and A. Paccagnella, “Coadsorption optimization of DNA in binary self-assembled monolayer on gold electrode for electrochemical detection of oligonucleotide sequences,” *J. Electroanal. Chem.*, vol. 689, pp. 57–62, 2013.

[6] A. Ulman, “Formation and Structure of Self-Assembled Monolayers.,” *Chem. Rev.*, vol. 96, no. 4, pp. 1533–1554, Jun. 1996.

[7] A. Ulman, *An introduction to ultrathin organic films : from Langmuir-Blodgett to self-assembly*. .

[8] A. D. Q. Li, *Molecular self-assembly : advances and applications*. Pan Stanford Pub, 2013.

[9] A. M. Turing, “The chemical basis of morphogenesis,” *Bull. Math. Biol.*, vol. 52, no. 1–2, pp. 153–197, 1990.

[10] J. Petitot, “Complexity and self-organization in Turing,” Feb. 2015.

[11] G. M. Whitesides and B. Grzybowski, “Self-assembly at all scales.,” *Science*, vol. 295, no. 5564, pp. 2418–21, Mar. 2002.

[12] R. C. Desai and R. Kapral, *Dynamics of self-organized and self-assembled structures*. Cambridge University Press, 2009.

[13] S. Zhang, *Handbook of nanostructured thin films and coatings*. CRC Press, 2010.

[14] J. L. Mueller, D. R. Ripoll, C. F. Aquadro, and M. F. Wolfner, “Comparative structural modeling and inference of conserved protein classes in Drosophila seminal fluid,” *Proc.*

Natl. Acad. Sci., vol. 101, no. 37, pp. 13542–13547, Sep. 2004.

[15] M. E. Furman and F. P. Gallo, *The neurophysics of human behavior.* CRC Press, 2000.

[16] E. B. Troughton, C. D. Bain, G. M. Whitesides, R. G. Nuzzo, D. L. Allara, and M. D. Porter, "Monolayer Films Prepared by the Spontaneous Self -Assembly of Symmetrical and Unsymmetrical Dialkyl Sulfides from Solution onto Gold Substrates : Structure , Properties , and Reactivity of Constituent Functional Groups '," no. 10, pp. 365–385, 1988.

[17] E. Paul, R. G. Nuzzo, and G. M. Whitesides, "Structure of Monolayers Formed," pp. 5097–5105, 1992.

[18] L. Kankate, A. Turchanin, and A. Gölzhäuser, "On the release of hydrogen from the S-H groups in the formation of self-assembled monolayers of thiols," *Langmuir*, vol. 25, no. 18, pp. 10435–10438, 2009.

[19] C. Vericat, M. E. Vela, G. Benitez, P. Carro, and R. C. Salvarezza, "Self-assembled monolayers of thiols and dithiols on gold : new challenges for a well-known system," pp. 1805–1834, 2010.

[20] A. Ulman, "Formation and Structure of Self-Assembled Monolayers.," *Chem. Rev.*, vol. 96, no. 4, pp. 1533–1554, Jun. 1996.

[21] M. G. Roper, M. P. Skegg, C. J. Fisher, J. J. Lee, V. R. Dhanak, D. P. Woodruff, and R. G. Jones, "Atop adsorption site of sulphur head groups in gold-thiolate self-assembled monolayers," *Chem. Phys. Lett.*, vol. 389, no. 1–3, pp. 87–91, 2004.

[22] A. Chaudhuri, T. J. Lerotholi, D. C. Jackson, D. P. Woodruff, and V. R. Dhanak, "The local adsorption structure of methylthiolate and butylthiolate on Au(1 1 1): A photoemission core-level shift investigation," *Surf. Sci.*, vol. 604, no. 2, pp. 227–234, 2010.

[23] G. D. Barmparis, K. Honkala, and I. N. Remediakis, "Thiolate adsorption on Au(hkl) and equilibrium shape of large thiolate-covered gold nanoparticles," *J. Chem. Phys.*, vol. 138, no. 6, p. 64702, Feb. 2013.

[24] A. Cossaro, R. Mazzarello, R. Rousseau, L. Casalis, A. Verdini, A. Kohlmeyer, L. Floreano, S. Scandolo, A. Morgante, M. L. Klein, and G. Scoles, "X-ray Diffraction and Computation Yield the Structure of Alkanethiols on Gold(111)," *Science (80-.).*, vol. 321, no. 5891, pp. 943–946, 2008.

[25] P. Maksymovych, D. C. Sorescu, and J. T. Yates, "Gold-Adatom-Mediated Bonding in Self-Assembled Short-Chain Alkanethiolate Species on the Au(111) Surface," *Phys. Rev. Lett.*, vol. 97, no. 14, p. 146103, Oct. 2006.

[26] P. Maksymovych and J. T. Yates, "Au adatoms in self-assembly of benzenethiol on the

Au(111) surface.," *J. Am. Chem. Soc.*, vol. 130, no. 24, pp. 7518–9, Jun. 2008.

[27] O. Azzaroni, M. E. Vela, H. Martin, A. Herna, and R. C. Salvarezza, "Electrodesorption Kinetics and Molecular Interactions at Negatively Charged Self-Assembled Thiol Monolayers in Electrolyte Solutions," no. 20, pp. 6647–6654, 2001.

[28] T. Sawaguchi, Y. Sato, and F. Mizutani, "In situ scanning tunneling microscopy observation of self-assembled monolayers of 3-mercaptopropionic acid on Au(111) in perchloric acid solution," *J. Electroanal. Chem.*, vol. 507, no. 1–2, pp. 256–262, Jul. 2001.

[29] C. Dubois and F. Stellacci, "Self-Assembled Monolayer of Short Carboxyl-Terminated Molecules Investigated with ex Situ Scanning Tunneling Microscopy," *J. Phys. Chem. C*, vol. 112, no. 19, pp. 7431–7435, May 2008.

[30] M. Sun, Z. Zhang, H. Zheng, and H. Xu, "In-situ plasmon-driven chemical reactions revealed by high vacuum tip-enhanced Raman spectroscopy," *Sci. Rep.*, vol. 2, no. 1, p. 647, 2012.

[31] O. A. Stasyuk, H. Szatylowicz, T. M. Krygowski, and C. Fonseca Guerra, "How amino and nitro substituents direct electrophilic aromatic substitution in benzene: an explanation with Kohn–Sham molecular orbital theory and Voronoi deformation density analysis," *Phys. Chem. Chem. Phys.*, vol. 18, no. 17, pp. 11624–11633, 2016.

[32] X. Ren, E. Tan, X. Lang, T. You, L. Jiang, H. Zhang, P. Yin, and L. Guo, "Observing reduction of 4-nitrobenzenthiol on gold nanoparticles in situ using surface-enhanced Raman spectroscopy.," *Phys. Chem. Chem. Phys.*, vol. 15, no. 34, pp. 14196–201, 2013.

[33] Q. He, Y. Tian, A. Kueller, M. Grunze, A. Goelzhaeuser, and J. Li, "Self-assembled molecular pattern by chemical lithography and interfacial chemical reactions," *J. Nanosci. Nanotechnol.*, vol. 6, no. 6, pp. 1838–1841, 2006.

[34] J. U. Nielsen, M. J. Esplandiu, and D. M. Kolb, "4-nitrothiophenol SAM on Au(111) investigated by in situ STM, electrochemistry, and XPS," *Langmuir*, vol. 17, no. 11, pp. 3454–3459, 2001.

[35] H. Y. Weng, Q. H. Guo, X. R. Wang, M. M. Xu, Y. X. Yuan, R. A. Gu, and J. L. Yao, "Inhibiting plasmon catalyzed conversion of para-nitrothiophenol on monolayer film of Au nanoparticles probed by surface enhanced Raman spectroscopy," *Spectrochim. Acta - Part A Mol. Biomol. Spectrosc.*, vol. 150, no. 1, pp. 331–338, 2015.

[36] T. Zhu, H. Z. Yu, Y. C. Wang, and Z. F. Liu, "Irreversible Adsorption and Reduction of p - Nitrothio-Phenol Monolayers on Gold: Electrochemical in Situ Surface Enhanced Raman Spectroscopy," *Mol. Cryst. Liq. Cryst. Sci. Technol. Sect. A. Mol. Cryst. Liq. Cryst.*, vol. 337, no. 1, pp. 241–244, 1999.

[37] Z. Suo, Y. F. Gao, and G. Scoles, "Nanoscale Domain Stability in Organic Monolayers on Metals," *J. Appl. Mech.*, vol. 71, no. 1, p. 24, 2004.

[38] R. A. L. (Richard A. L. Jones, *Soft condensed matter*. Oxford University Press, 2002.

[39] Y. Mai and A. Eisenberg, "Self-assembly of block copolymers.," *Chem. Soc. Rev.*, vol. 41, no. 18, pp. 5969–5985, Sep. 2012.

[40] Z. Wu, B. Li, Q. Jin, D. Ding, and A.-C. Shi, "Phase Behavior of Binary Blends of Diblock Copolymers," *J. Phys. Chem. B*, vol. 114, no. 48, pp. 15789–15798, Dec. 2010.

[41] R. a. Segalman, "Patterning with block copolymer thin films," *Mater. Sci. Eng. R Reports*, vol. 48, no. 6, pp. 191–226, Feb. 2005.

[42] M. Melli, G. Scoles, and M. Lazzarino, "Fast detection of biomolecules in diffusion-limited regime using micromechanical pillars.," *ACS Nano*, vol. 5, no. 10, pp. 7928–7935, Oct. 2011.

[43] A. Napoli, D. Sebk, A. Senti, and W. Meier, "Block Copolymer Vesicles," in *Block Copolymers in Nanoscience*, Weinheim, Germany: Wiley-VCH Verlag GmbH & Co. KGaA, pp. 39–71.

[44] S. C. Greer, "Living polymers," *Comput. Mater. Sci.*, vol. 4, no. 4, pp. 334–338, 1995.

[45] S. O. Kim, H. H. Solak, M. P. Stoykovich, N. J. Ferrier, J. J. De Pablo, and P. F. Nealey, "Epitaxial self-assembly of block copolymers on lithographically defined nanopatterned substrates.," *Nature*, vol. 424, no. 6947, pp. 411–4, Jul. 2003.

[46] F. S. Bates and G. H. Fredrickson, "Block Copolymers—Designer Soft Materials," *Phys. Today*, vol. 52, no. 2, p. 32, 1999.

[47] M. W. Matsen and F. S. Bates, "Unifying Weak- and Strong-Segregation Block Copolymer Theories," *Macromolecules*, vol. 29, no. 4, pp. 1091–1098, Jan. 1996.

[48] Y. K. Kim, J. P. Koo, C. J. Huh, J. S. Ha, U. H. Pi, S. Y. Choi, and J. H. Kim, "Adsorption behavior of binary mixed alkanethiol molecules on Au: Scanning tunneling microscope and linear-scan voltammetry investigation," *Appl. Surf. Sci.*, vol. 252, no. 14, pp. 4951–4956, 2006.

[49] D. M. Fitzgerald, E. K. Krisanda, C. G. Szypko, and L. Gaby Avila-Bront, "Ambient STM study of sequentially adsorbed octanethiol and biphenylthiol monolayers on Au(111)," *Surf. Sci.*, vol. 662, no. March, pp. 102–112, 2017.

[50] B. Lüssem, L. Müller-Meskamp, S. Karthäuser, R. Waser, M. Homberger, and U. Simon, "STM study of mixed alkanethiol/biphenylthiol self-assembled monolayers on Au(111)," *Langmuir*, vol. 22, no. 7, pp. 3021–3027, 2006.

[51] T. Ichii, T. Fukuma, K. Kobayashi, H. Yamada, and K. Matsushige, "Surface potential

measurements of phase-separated alkanethiol self-assembled monolayers by non-contact atomic force microscopy," *Nanotechnology*, vol. 15, no. 2, p. 30, 2004.

[52] A. R. Puente Santiago, T. Pineda, M. Blázquez, and R. Madueño, "Formation of 2-D Crystalline Intermixed Domains at the Molecular Level in Binary Self-Assembled Monolayers from a Lyotropic Mixture," *J. Phys. Chem. C*, vol. 120, no. 16, pp. 8595–8606, 2016.

[53] T. Kakiuchi, M. Iida, N. Gon, D. Hobara, S. Imabayashi, and K. Niki, "Miscibility of Adsorbed 1-Undecanethiol and 11-Mercaptoundecanoic Acid Species in Binary Self-Assembled Monolayers on Au(111)," *Langmuir*, vol. 17, no. 5, pp. 1599–1603, Mar. 2001.

[54] D. Hobara, M. Ota, S. Imabayashi, K. Niki, and T. Kakiuchi, "Phase separation of binary self-assembled thiol monolayers composed of 1-hexadecanethiol and 3-mercaptopropionic acid on Au(111) studied by scanning tunneling microscopy and cyclic voltammetry," *J. Electroanal. Chem.*, vol. 444, no. 1, pp. 113–119, 1998.

[55] H. Munakata, S. Kuwabata, Y. Ohko, and H. Yoneyama, "Spatial distribution of domains in binary self-assembled monolayers of thiols having different lengths," *J. Electroanal. Chem.*, vol. 496, no. 1–2, pp. 29–36, Jan. 2001.

[56] N. J. Brewer and G. J. Leggett, "Chemical force microscopy of mixed self-assembled monolayers of alkanethiols on gold: Evidence for phase separation," *Langmuir*, vol. 20, no. 10, pp. 4109–4115, 2004.

[57] H. Schönherr, G. J. Vancso, B.-H. Huisman, F. C. J. M. van Veggel, and D. N. Reinhoudt, "An Atomic Force Microscopy Study of Self-Assembled Monolafyers of Calix[4]resorcinarene Adsorbates on Au(111)," *Langmuir*, vol. 13, no. 6, pp. 1567–1570, 1997.

[58] S. J. Stranick, a. N. Parikh, Y.-T. Tao, D. L. Allara, and P. S. Weiss, "Phase Separation of Mixed-Composition Self-Assembled Monolayers into Nanometer Scale Molecular Domains," *J. Phys. Chem.*, vol. 98, no. 31, pp. 7636–7646, Aug. 1994.

[59] P. A. Lewis, R. K. Smith, K. F. Kelly, L. A. Bumm, S. M. Reed, R. S. Clegg, J. D. Gunderson, J. E. Hutchison, and P. S. Weiss, "The role of buried hydrogen bonds in self-assembled mixed composition thiols on Au{111}," *J. Phys. Chem. B*, vol. 105, no. 43, pp. 10630–10636, 2001.

[60] R. K. Smith, S. M. Reed, P. A. Lewis, J. D. Monnell, R. S. Clegg, K. F. Kelly, L. A. Bumm, J. E. Hutchison, and P. S. Weiss, "Phase separation within a binary self-assembled monolayer on Au{111} driven by an amide-containing alkanethiol," *J. Phys. Chem. B*, vol. 105, no. 6,

pp. 1119–1122, 2001.

[61] F. Tantakitti, J. Burk-Rafel, F. Cheng, R. Egnatchik, T. Owen, M. Hoffman, D. N. Weiss, and D. M. Ratner, "Nanoscale clustering of carbohydrate thiols in mixed self-assembled monolayers on gold," *Langmuir*, vol. 28, no. 17, pp. 6950–6959, 2012.

[62] W. A. Hayes, H. Kim, X. H. Yue, S. S. Perry, and C. Shannon, "Nanometer-scale patterning of surfaces using self-assembly chemistry .2. Preparation, characterization, and electrochemical behavior of two-component organothiol monolayers on gold surfaces," *Langmuir*, vol. 13, no. 9, pp. 2511–2518, 1997.

[63] K. Tamada, M. Hara, H. Sasabe, and W. Knoll, "Surface Phase Behavior of n-Alkanethiol Self-Assembled Monolayers Adsorbed on Au(111): An Atomic Force Microscope Study," *Langmuir*, vol. 13, no. 6, pp. 1558–1566, 1997.

[64] S. Chen, L. Li, C. L. Boozer, and S. Jiang, "Controlled chemical and structural properties of mixed self-assembled monolayers of alkanethiols on Au(111)," *Langmuir*, vol. 16, no. 24, pp. 9287–9293, 2000.

[65] S. Imabayashi, D. Hobara, and T. Kakiuchi, "Voltammetric Detection of the Surface Diffusion of Adsorbed Thiolate Molecules in Artificially Phase-Separated Binary Self-Assembled Monolayers on a Au (111) Surface," no. 14, pp. 2560–2563, 2001.

[66] F. Terán Arce, M. E. Vela, and R. C. Salvarezza, and A. J. Arvia*, "Complex Structural Dynamics at Adsorbed Alkanethiol Layers at Au(111) Single-Crystal Domains," 1998.

[67] P. Español and P. Warren, "Statistical Mechanics of Dissipative Particle Dynamics," *Europhys. Lett.*, vol. 30, no. 4, pp. 191–196, May 1995.

[68] C. Singh, "Computational Studies of Surfactant Self-Assembly on Nanostructured Surfaces.," 2010.

[69] S. C. Glotzer, E. A. Di Marzio, and M. Muthukumar, "Ical review letters," vol. 74, no. 11, 1995.

[70] S. C. Glotzer and A. Coniglio, "Self-consistent solution of phase separation with competing interactions," *Phys. Rev. E*, vol. 50, no. 5, pp. 4241–4244, Nov. 1994.

[71] W. Lu and Z. Suo, "Symmetry breaking in self-assembled monolayers on solid surfaces: Anisotropic surface stress," *Phys. Rev. B*, vol. 65, no. 8, p. 85401, Jan. 2002.

[72] D. Hobara, M. Ota, S. Imabayashi, K. Niki, and T. Kakiuchi, "Phase separation of binary self-assembled thiol monolayers composed of 1-hexadecanethiol and 3-mercaptopropionic acid on Au(111) studied by scanning tunneling microscopy and cyclic voltammetry," *J. Electroanal. Chem.*, vol. 444, no. 1, pp. 113–119, 1998.

[73] K. Aoki, "Theory of phase separation of binary self-assembled films," *J. Electroanal.*

Chem., vol. 513, no. 1, pp. 1–7, 2001.

[74] W. Mizutani, T. Ishida, and H. Tokumoto, “Monte Carlo simulation of phase-separated self-assembled films,” *Appl. Surf. Sci.*, vol. 130–132, pp. 792–796, 1998.

[75] A. V. Shevade, J. Zhou, M. T. Zin, and S. Jiang, “Phase behavior of mixed self-assembled monolayers of alkanethiols on Au(111): A configurational-bias Monte Carlo simulation study,” *Langmuir*, vol. 17, no. 24, pp. 7566–7572, 2001.

[76] W. L. Miller, B. Bozorgui, K. Klymko, and A. Cacciuto, “Free energy of alternating two-component polymer brushes on cylindrical templates,” *J. Chem. Phys.*, vol. 135, no. 24, 2011.

[77] S. A. Egorov, “Microphase separation of mixed polymer brushes physisorbed on cylindrical surfaces,” *Soft Matter*, vol. 8, no. 14, p. 3971, 2012.

[78] S. N. Yaliraki, G. Longo, E. Gale, I. Szleifer, and M. a Ratner, “Stability and phase separation in mixed self-assembled monolayers.,” *J. Chem. Phys.*, vol. 125, no. 7, p. 74708, 2006.

[79] D. Nassoko, M. Seydou, C. Goldmann, C. Chanéac, C. Sanchez, D. Portehault, and F. Tielens, “Rationalizing the formation of binary mixed thiol self-assembled monolayers,” *Mater. Today Chem.*, vol. 5, pp. 34–42, 2017.

[80] J. I. Siepmann and I. R. McDonald, “Monte Carlo simulations of mixed monolayers,” *Mol. Phys.*, vol. 75, no. 2, pp. 255–259, 1992.

[81] L. A. Bumm, J. J. Arnold, L. F. Charles, T. D. Dunbar, D. L. Allara, and P. S. Weiss, “Directed self-assembly to create molecular terraces with molecularly sharp boundaries in organic monolayers,” *J. Am. Chem. Soc.*, vol. 121, no. 35, pp. 8017–8021, 1999.

[82] “A review of atomic force microscopy imaging systems: application to molecular metrology and biological sciences,” *Mechatronics*, vol. 14, no. 8, pp. 907–945, Oct. 2004.

[83] C. J. Chen, “Introduction to Scanning Tunneling Microscopy Second Edition,” *Oxford Univ. Press*, p. (2008), 2008.

[84] G. Binnig and H. Rohrer, “Scanning Tunneling Microscopy—from Birth to Adolescence (Nobel Lecture),” *Angew. Chemie Int. Ed. English*, vol. 26, no. 7, pp. 606–614, 1987.

[85] P. M. Williams, M. S. Cheema, M. C. Davies, D. E. Jackson, and S. J. B. Tendler, “Biological Applications of Scanning Tunneling Microscopy,” in *Microscopy, Optical Spectroscopy, and Macroscopic Techniques*, C. Jones, B. Mulloy, and A. H. Thomas, Eds. Totowa, NJ: Humana Press, 1994, pp. 25–37.

[86] P. A. Christensen, “Electrochemical Aspects of STM and Related Techniques.”

[87] L. A. Bumm, J. J. Arnold, T. D. Dunbar, D. L. ALLARA, and P. S. Weiss, “Electron transfer

through organic molecules," *J. Phys. Chem. B*, vol. 103, no. 38, pp. 8122–8127, 1999.

[88] L. A. Bumm, J. J. Arnold, M. T. Cygan, T. D. Dunbar, T. P. Burgin, P. S. Weiss, J. M. Tour, D. L. Allara, and L. J. II, "Are Single Molecular Wires Conducting?," *Science (80-.).*, vol. 271, no. 20, pp. 1705–1707, 1996.

[89] H. Bloom, *Electrochemistry : the past thirty and the next thirty years.* Springer, 2012.

[90] M. D. Porter, T. B. Bright, D. L. Allara, and C. E. Chidsey, "Spontaneously Organized Molecular Assemblies. 4. Structural Characterization of n-Alkyl Thiol Monolayers on Gold by Optical Ellipsometry, Infrared Spectroscopy, and Electrochemistry," *J. Am. Chem. Soc.*, vol. 109, no. 12, pp. 3559–3568, 1987.

[91] C. A. Widrig, C. Chung, and M. D. Porter, "The electrochemical desorption of n-alkanethiol monolayers from polycrystalline Au and Ag electrodes," *J. Electroanal. Chem.*, vol. 310, no. 1–2, pp. 335–359, 1991.

[92] M. Walczak, D. D. Popenoe, R. S. Deinhammer, B. D. Lamp, C. Chung, and M. D. Porter, "Reductive Desorption of Alkanethiolate Monolayers at Gold: A Measure of Surface Coverage," *Langmuir*, vol. 7, pp. 2687–2693, 1991.

[93] T. Kakiuchi, H. Usui, D. Hobara, and M. Yamamoto, "Voltammetric properties of the reductive desorption of alkanethiol self-assembled monolayers from a metal surface," *Langmuir*, vol. 18, no. 13, pp. 5231–5238, 2002.

[94] "The electrochemical desorption of n-alkanethiol monolayers from polycrystalline Au and Ag electrodes," *J. Electroanal. Chem. Interfacial Electrochem.*, vol. 310, no. 1–2, pp. 335–359, 1991.

[95] F. P. Cometto, V. A. Macagno, P. Paredes-Olivera, E. M. Patrito, H. Ascolani, and G. Zampieri, "Decomposition of Methylthiolate Monolayers on Au(111) Prepared from Dimethyl Disulfide in Solution Phase," *J. Phys. Chem. C*, vol. 114, no. 22, pp. 10183–10194, Jun. 2010.

[96] P. G. Lustemberg, C. Vericat, G. A. Benitez, M. E. Vela, N. Tognalli, A. Fainstein, M. L. Martiarena, and R. C. Salvarezza, "Spontaneously Formed Sulfur Adlayers on Gold in Electrolyte Solutions: Adsorbed Sulfur or Gold Sulfide?," 2008.

[97] F. P. Cometto, C. a. Calderón, M. Berdakin, P. Paredes-Olivera, V. a. Macagno, and E. M. Patrito, "Electrochemical detection of the thermal stability of n-alkanethiolate monolayers on Au(111)," *Electrochim. Acta*, vol. 61, pp. 132–139, Feb. 2012.

[98] F. P. Cometto, C. a. Calderón, M. Berdakin, P. Paredes-Olivera, V. a. Macagno, and E. M. Patrito, "Electrochemical detection of the thermal stability of n-alkanethiolate monolayers on Au(111)," *Electrochim. Acta*, vol. 61, pp. 132–139, Feb. 2012.

[99] Z. Wang, Y.-L. Shi, and H.-L. Li, “Investigation of two-component mixed self-assembled monolayers on gold,” *Can. J. Chem.*, vol. 79, no. 3, pp. 328–336, 2001.

[100] Z. Gonzlez-Granados, G. Sanchez-Obrero, R. Madue??o, J. M. Sevilla, M. Bl??zquez, and T. Pineda, “Formation of mixed monolayers from 11-mercaptoundecanoic acid and octanethiol on Au(111) single crystal electrode under electrochemical control,” *J. Phys. Chem. C*, vol. 117, no. 46, pp. 24307–24316, Nov. 2013.

[101] M. Nishizawa, T. Sunagawa, and H. Yoneyama, “Selective desorption of 3-mercaptopropionic acid from a mixed monolayer with hexadecanethiol assembled on a gold electrode,” *J. Electroanal. Chem.*, vol. 436, no. 1–2, pp. 213–218, 1997.

[102] M. L. Carot, V. A. Macagno, P. Paredes-Olivera, and E. M. Patrito, “Structure of mixed carboxylic acid terminated self-assembled monolayers: Experimental and theoretical investigation,” *J. Phys. Chem. C*, vol. 111, no. 11, pp. 4294–4304, 2007.

[103] C. D. Bain, H. A. Biebuyck, and M. George, “Comparison of Self-Assembled Monolayers on Gold : Coadsorption of Thiols and Disulfidesr,” pp. 2–6, 1989.

[104] J. Heeg, U. Schubert, and F. Küchenmeister, “Mixed self-assembled monolayers of terminally functionalized thiols at gold surfaces characterized by angle resolved X-ray photoelectron spectroscopy (ARXPS) studies,” *Fresenius. J. Anal. Chem.*, vol. 365, no. 1–3, pp. 272–276, 1999.

[105] S. Frey, A. Shaporenko, M. Zharnikov, P. Harder, and D. L. ALLARA, “Self-assembled monolayers of nitrile-functionalized alkanethiols on gold and silver substrates,” *J. Phys. Chem. B*, vol. 107, no. 31, pp. 7716–7725, 2003.

[106] * M. Zharnikov, S. Frey, and K. Heister, and M. Grunze, “Modification of Alkanethiolate Monolayers by Low Energy Electron Irradiation: Dependence on the Substrate Material and on the Length and Isotopic Composition of the Alkyl Chains,” 2000.

[107] Z. González-Granados, G. Sánchez-Obrero, R. Madueño, J. M. Sevilla, M. Blázquez, and T. Pineda, “Formation of Mixed Monolayers from 11-Mercaptoundecanoic Acid and Octanethiol on Au(111) Single Crystal Electrode under Electrochemical Control,” *J. Phys. Chem. C*, vol. 117, no. 46, pp. 24307–24316, Nov. 2013.

[108] * Takashi Kakiuchi, Hideyuki Usui, and Daisuke Hobara, and M. Yamamoto, “Voltammetric Properties of the Reductive Desorption of Alkanethiol Self-Assembled Monolayers from a Metal Surface,” 2002.

[109] F. Biscarini, Q. K. Ong, C. Albonetti, F. Liscio, M. Longobardi, K. S. Mali, A. Ciesielski, J. Reguera, C. Renner, S. De Feyter, P. Samorì, and F. Stellacci, “Quantitative analysis of scanning tunneling microscopy images of mixed-ligand-functionalized nanoparticles.,”

Langmuir, vol. 29, no. 45, pp. 13723–34, Nov. 2013.

[110] Q. K. Ong, S. Zhao, J. Reguera, F. Biscarini, and F. Stellacci, “Comparative STM studies of mixed ligand monolayers on gold nanoparticles in air and in 1-phenyloctane,” *Chem. Commun.*, vol. 50, no. 72, pp. 10456–10459, 2014.

[111] Q. K. Ong, J. Reguera, P. J. Silva, M. Moglianetti, K. Harkness, M. Longobardi, K. S. Mali, C. Renner, S. De Feyter, and F. Stellacci, “High-Resolution Scanning Tunneling Microscopy Characterization of Mixed Monolayer Protected Gold Nanoparticles,” *ACS Nano*, vol. 7, no. 10, pp. 8529–8539, Oct. 2013.

[112] F. Dinelli, M. Murgia, P. Levy, M. Cavallini, F. Biscarini, and D. M. De Leeuw, “Spatially Correlated Charge Transport in Organic Thin Film Transistors,” *Phys. Rev. Lett.*, vol. 92, no. 11, pp. 116801–116802, 2004.

[113] F. Valle, M. Bianchi, S. Tortorella, G. Pierini, F. Biscarini, and M. D’Elia, “Nanotechnology for forensic sciences: Analysis of PDMS replica of the case head of spent cartridges by optical microscopy, SEM and AFM for the ballistic identification of individual characteristic features of firearms,” *Forensic Sci. Int.*, vol. 222, no. 1–3, pp. 288–297, 2012.

[114] N. Sagawa and T. Shikata, “Are all polar molecules hydrophilic? Hydration numbers of nitro compounds and nitriles in aqueous solution.,” *Phys. Chem. Chem. Phys.*, vol. 16, no. 26, pp. 13262–70, Jul. 2014.

[115] A. L. Eckermann, D. J. Feld, J. A. Shaw, and T. J. Meade, “Electrochemistry of redox-active self-assembled monolayers.,” *Coord. Chem. Rev.*, vol. 254, no. 15–16, pp. 1769–1802, Aug. 2010.

[116] T. Sawaguchi, Y. Sato, and F. Mizutani, “In situ STM imaging of individual molecules in two-component self-assembled monolayers of 3-mercaptopropionic acid and 1-decanethiol on Au(111),” *J. Electroanal. Chem.*, vol. 496, no. 1–2, pp. 50–60, Jan. 2001.

[117] R. Smith and S. Reed, “Phase separation within a binary self-assembled monolayer on Au {111} driven by an amide-containing alkanethiol,” *J. Phys. Chem.*, vol. 105, no. 6, pp. 1119–1122, 2001.

[118] K. Aoki, “Theory of phase separation of binary self-assembled films,” *J. Electroanal. Chem.*, vol. 513, pp. 1–7, 2001.

[119] D. Hobara and T. Kakiuchi, “Domain structure of binary self-assembled monolayers composed of 3-mercapto-1-propanol and 1-tetradecanethiol on Au(111) prepared by coadsorption,” *Electrochem. commun.*, vol. 3, no. 3, pp. 154–157, Mar. 2001.

[120] T. Kakiuchi, K. Sato, M. Iida, D. Hobara, S. I. Imabayashi, and K. Niki, “Phase separation of

alkanethiol self-assembled monolayers during the replacement of adsorbed thiolates on Au(111) with thiols in solution," *Langmuir*, vol. 16, no. 18, pp. 7238–7244, 2000.

[121] G. Poirier and E. Pylant, "The Self-Assembly Mechanism of Alkanethiols on Au(111)," *Science*, vol. 272, no. 5265, pp. 1145–8, May 1996.

[122] G. E. Poirier, "Characterization of Organosulfur Molecular Monolayers on Au(111) using Scanning Tunneling Microscopy," 1997.

[123] J.-P. Bucher, L. Santesson, and K. Kern, "Thermal Healing of Self-Assembled Organic Monolayers: Hexane- and Octadecanethiol on Au(111) and Ag(111)," *Langmuir*, vol. 10, no. 4, pp. 979–983, Apr. 1994.

[124] F. P. Cometto, P. Paredes-Olivera, V. A. Macagno, and E. M. Patrito, "Density functional theory study of the adsorption of alkanethiols on Cu(111), Ag(111), and Au(111) in the Low and High Coverage Regimes," *J. Phys. Chem. B*, vol. 109, no. 46, pp. 21737–21748, 2005.

[125] S. Engel, E.-C. Fritz, and B. J. Ravoo, "New trends in the functionalization of metallic gold: from organosulfur ligands to N-heterocyclic carbenes," *Chem. Soc. Rev.*, vol. 46, no. 8, pp. 2057–2075, 2017.

[126] J. a. M. Sondag-Huethorst, C. Schonenberger, and L. G. J. Fokkink, "Formation of Holes in Alkanethiol Monolayers on Gold," *J. Phys. Chem.*, vol. 98, no. 27, pp. 6826–6834, Jul. 1994.

[127] F. Biscarini, Q. K. Ong, C. Albonetti, F. Liscio, M. Longobardi, K. S. Mali, A. Ciesielski, J. Reguera, C. Renner, S. De Feyter, P. Samorì, and F. Stellacci, "Quantitative analysis of scanning tunneling microscopy images of mixed-ligand-functionalized nanoparticles," *Langmuir*, vol. 29, no. 45, pp. 13723–13734, 2013.

[128] M. Moglianetti, Q. K. Ong, J. Reguera, K. M. Harkness, M. Mameli, A. Radulescu, J. Kohlbrecher, C. Jud, D. I. Svergun, and F. Stellacci, "Scanning tunneling microscopy and small angle neutron scattering study of mixed monolayer protected gold nanoparticles in organic solvents," *Chem. Sci.*, vol. 5, no. 3, p. 1232, 2014.

[129] Q. Ong, Z. Luo, and F. Stellacci, "Characterization of Ligand Shell for Mixed-Ligand Coated Gold Nanoparticles," *Acc. Chem. Res.*, vol. 50, no. 8, pp. 1911–1919, Aug. 2017.

[130] L. Li, S. Chen, J. Zheng, B. D. Ratner, and S. Jiang, "Protein Adsorption on Oligo (ethylene glycol) -Terminated Alkanethiolate Self-Assembled Monolayers : The Molecular Basis for Nonfouling Behavior," pp. 2934–2941, 2005.

[131] T. Kakiuchi, M. Iida, N. Gon, D. Hobara, S. I. Imabayashi, and K. Niki, "Miscibility of adsorbed 1-undecanethiol and 11-mercaptoundecanoic acid species in binary self-

assembled monolayers on Au(111)," *Langmuir*, vol. 17, no. 5, pp. 1599–1603, 2001.

Appendix A

Reagents and Materials

All chemicals were purchased form Sigma-Aldrich (St.Louis, MO) and Acros Organics (West Chester, PA) in the highest available purity and used without further purification. Anhydrous toluene 99.8% from Sigma-Aldrich was used after purging with Argon gas for at least 1 hour.

The Au (111) surfaces were purchased from Phasis (Geneva). Gatalog # : 20020015, size: 8 x 4 mm^2 , The gold foil (200 nm thickness) is on top of high grade freshly cleaved mica without the use of adhesives. The surfaces are ready to use, without any cleaning or flame annealing.

2. STM

The STM experiments were performed at room temperature using two different STM instruments. i) a Veeco Multimode Scanning Probe Microscopy with E scanner in an acoustic chamber sitting on a vibration damping table in air and ii) a Nanosurf easyScan 2 STM sitting on a vibration damping table. Mechanically cut Platinum-iridium STM tips were used. Set point currents were in the range of 40 pA to 400 pA with a voltage bias of 400-900 mV. Integral gains varied from 0.7 to 0.5 and proportional gains from 0.5 to 0.2. STM in liquid (phenyloctane) was performed only on Veeco multimode. All analysis and images are the result of scanning after allowing the system to stabilise over night in order to avoid drifting phenomena.

Image processing of the STM images was performed with the software Gwyddion. The images were flattened and the height profiles were obtained by drawing line profiles using Gwyddion.

3. Electrochemistry

Cyclic Voltammograms (CV) measurements were performed with a Gamry-600 potentionstat and a 3-electrode cell. A separate compartment for the reference electrode (Ag/AgCl (NaCl 3M)) and a fixed position for the working electrode (clamp for the Au(111) surfaces) and the counter electrode (Pt foil). The 0.1 M KOH electrolyte was thoroughly deoxygenated by sonication and Argon bubbling prior to each experiment. All measurements were made at a sweep rate of 50 mV/s.

4. XPS

Analysis was performed using a monochromatic Al Kα X-ray source of 25.3 W power with a beam size of 100 μm. The spherical capacitor analyser was set at 45° take-off angle with respect to the sample surface. The pass energy was 46.95-90 eV. Curve fitting was performed using the PHI Multipak software. The binding energies are corrected by C(1s) at 284.6eV. Sensitivity factors extracted from the MultiPak software are: Au4f=Area:6.805/Height:3.849, C1s=Area:0.314/Height:0.314, O1s=Area:0.733/Height:0.733, N1s=Area:0.499/Height:0.499, S2p=Area:0.717/Height:0.650

5. Contact angle

Static contact angles were measured with OCA 35 from DataPhysics Instruments. Drops were placed on the surface in room temperature. Multiple surfaces were used for the accumulation of the values. The values are an arithmetic mean of at least 15 drops per sample. The error bars at the plot come from the standard deviation of the measuments.

Sessile drop contact angles of water were measured on the used Au(111) substrates. The value from 20 drops was found to be 71°. The value coincides that of other publications. It should be noted that the theoretical value for a perfectly clean gold surface should be 0° but this value has not been obtained

Appendix B - additional STM images

#Large scans are presented with a ruler, smaller scan size images have a scale bar. Scale bar corresponds to 20 nm, unless indicated otherwise with a number on the scale bar. The images are categorized by thiol pair and at increasing annealing times.

OT:CN4T

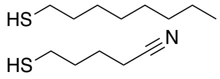

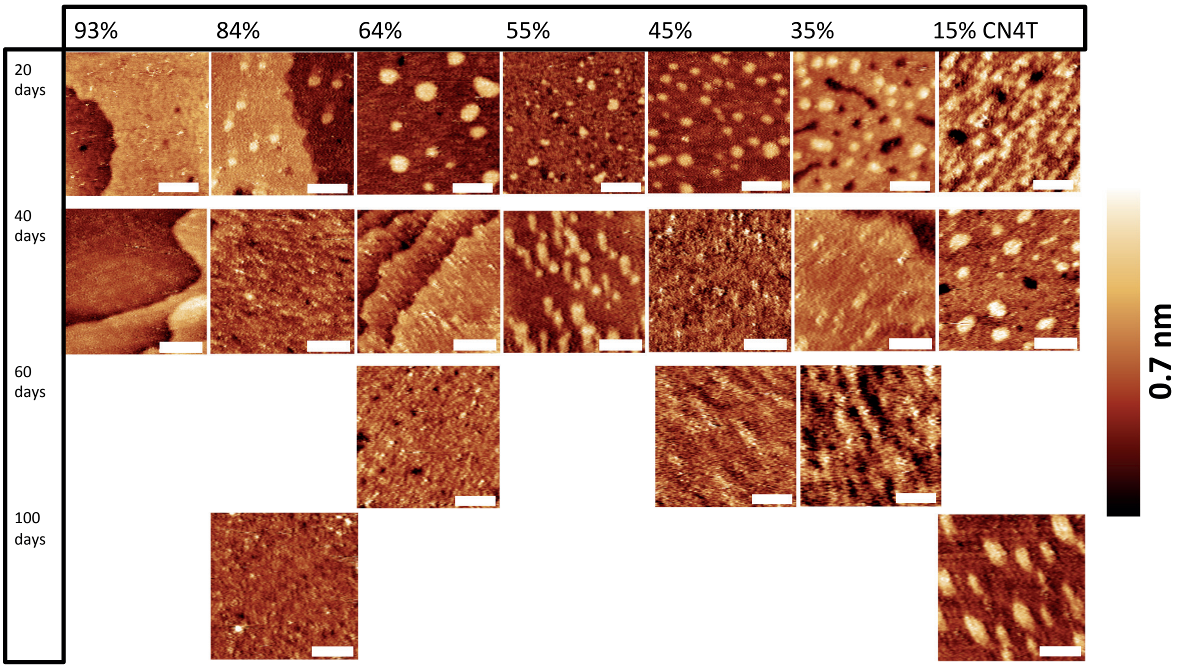

ApB-Fig 1. STM images of OT:CN4T binary SAMs at different surface compositions (indicated at the top of the images) and different annealing times (indicated at the left) taken from Chapter 3. The annealing times are indicated on the left side panel. Set point current=50 pA and voltage bias=350 mV. Scale bar=20nm.

OT:CN4T 20 days of annealing

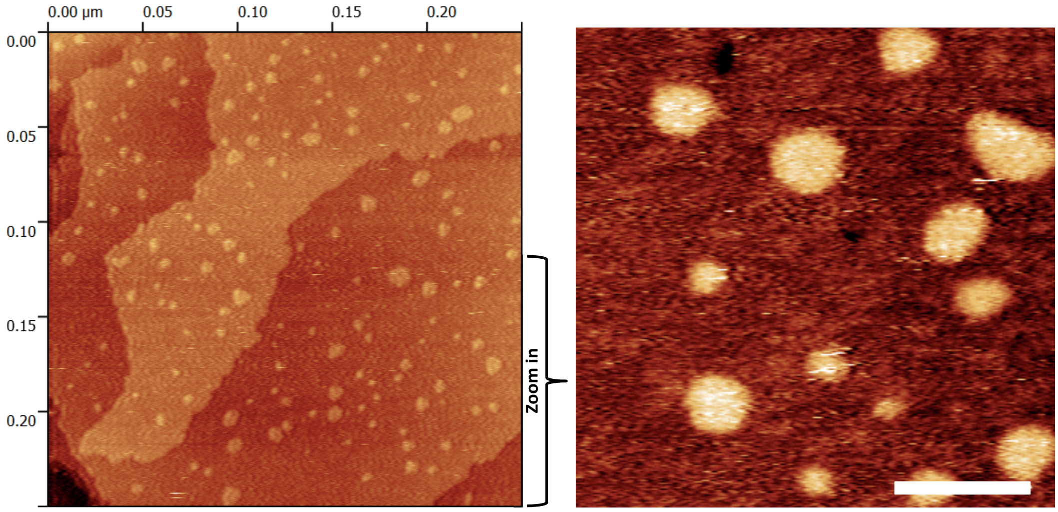

ApB-Fig 2. 64% CN4T - 20days STM image. Set point current=50 pA and voltage bias=400 mV

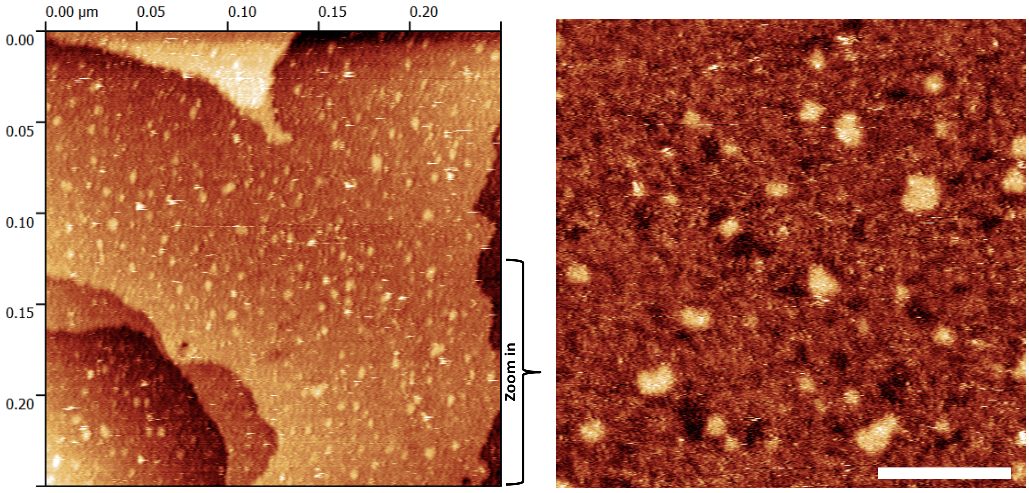

ApB-Fig 3. 55% CN4T - 20days STM image. Set point current=50 pA and voltage bias=400 mV

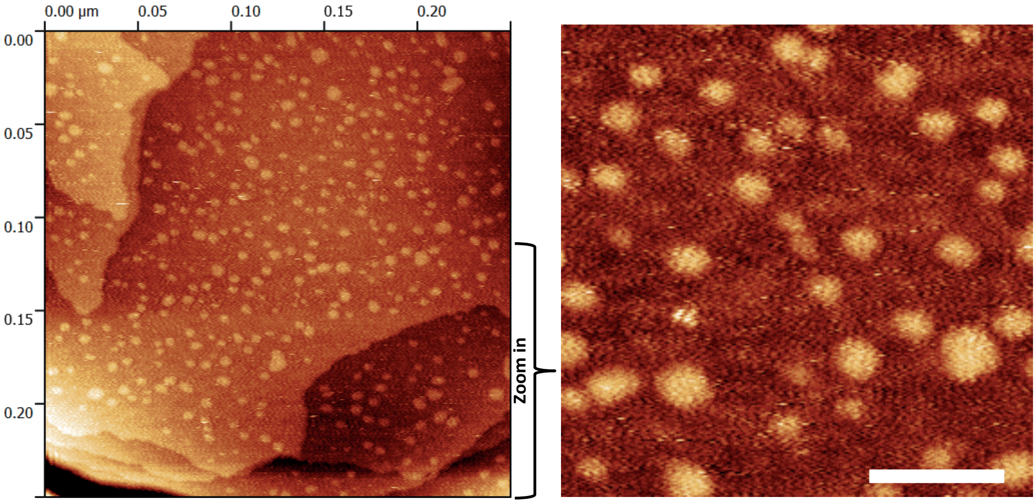

ApB-Fig 4. 45% CN4T - 20days STM image. Set point current=50 pA and voltage bias=400 mV

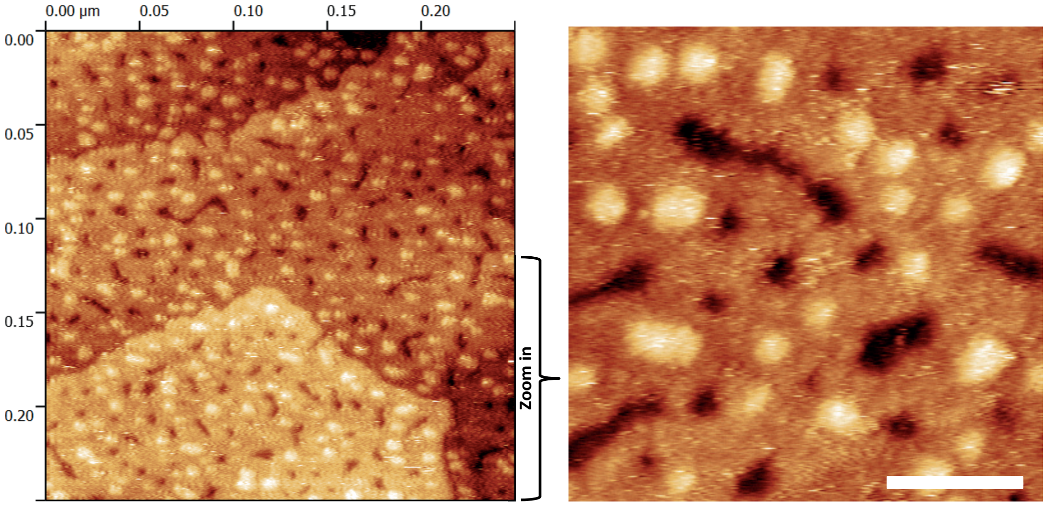

ApB-Fig 5. 35% CN4T - 20days STM image. Set point current=50 pA and voltage bias=400 mV

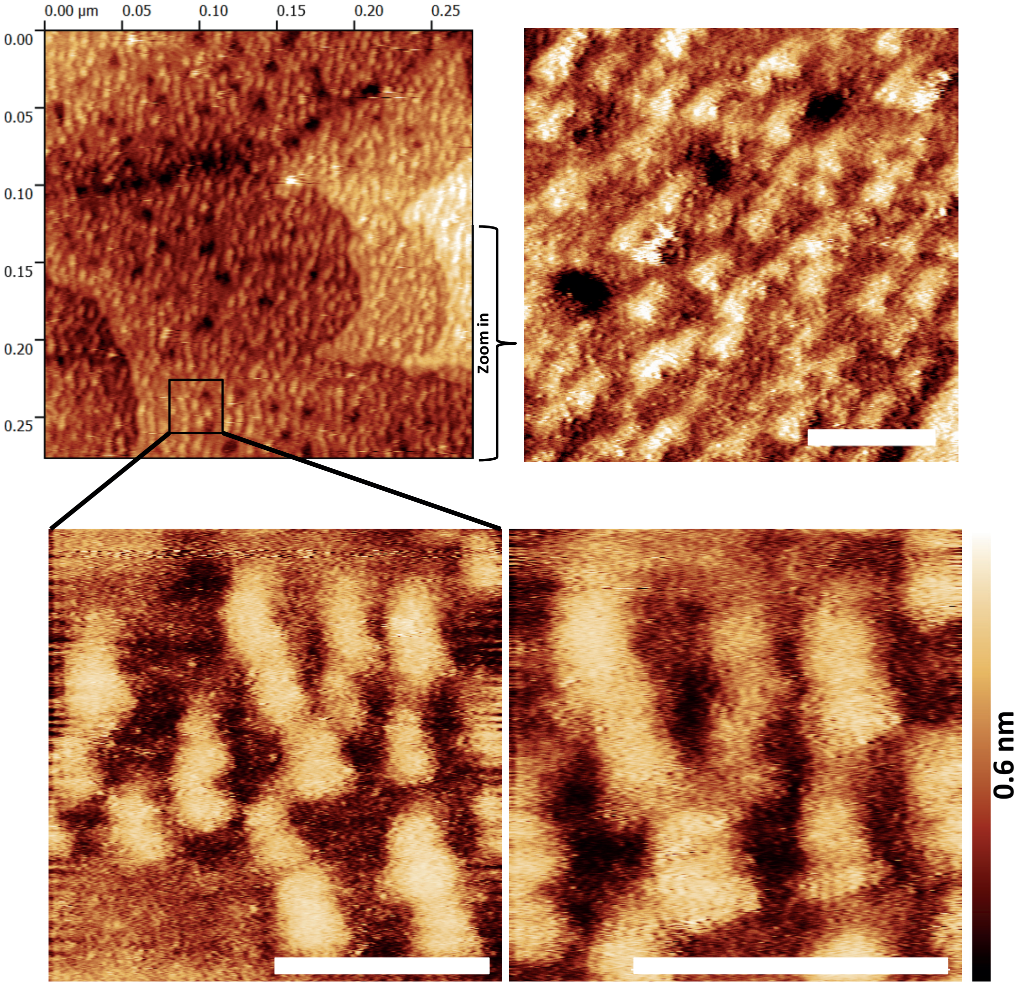

ApB-Fig 6. 15% CN4T - 20days STM image. Set point current=50 pA and voltage bias=400 mV

OT:CN4T 40 days of annealing

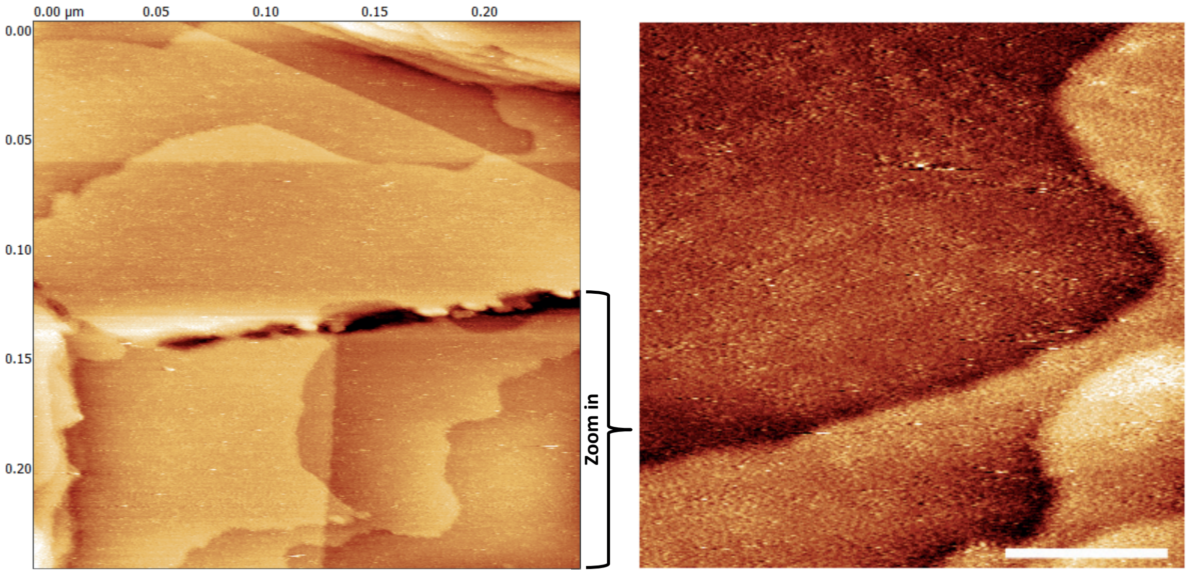

ApB-Fig 7. 93% CN4T - 40days STM image. Set point current=50 pA and voltage bias=400 mV

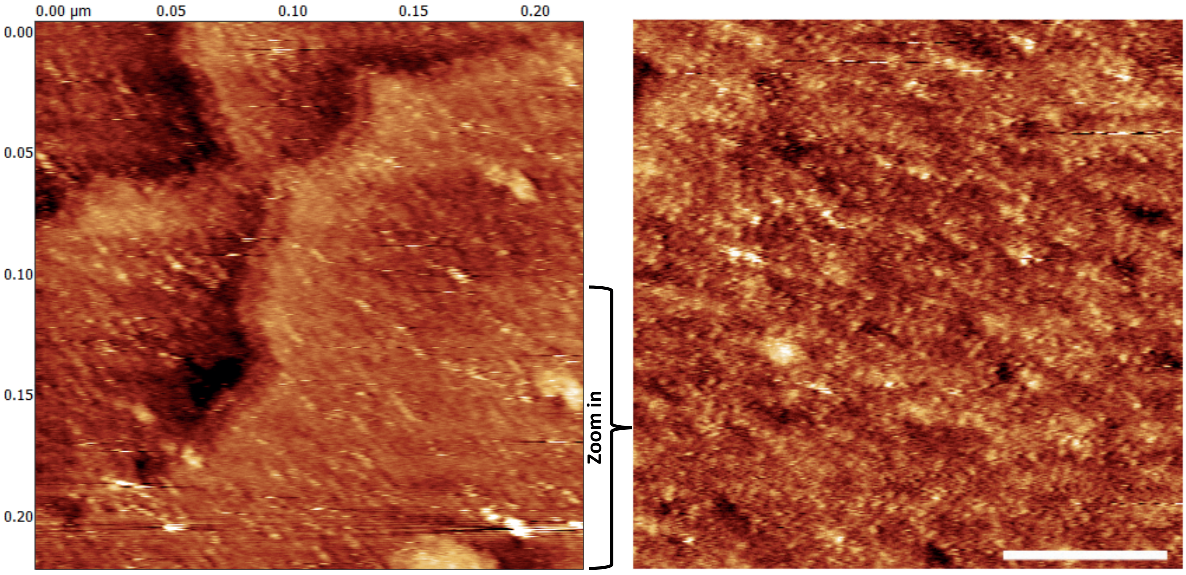

ApB-Fig 8. 84% CN4T - 40days STM image. Set point current=50 pA and voltage bias=400 mV

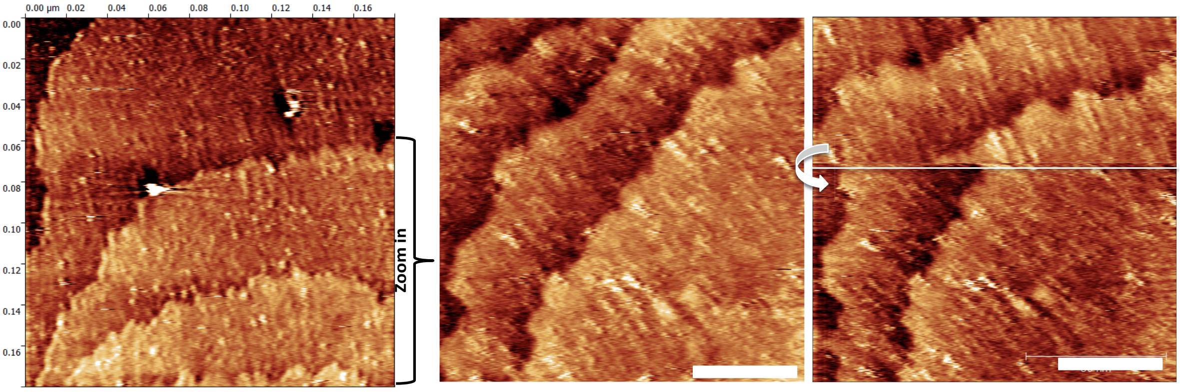

ApB-Fig 9. 64% CN4T - 40days STM image. The arrow indicates the moment of angle change (30O) during one scan to show that the orientation of the stripes followed the change Set point current=50 pA and voltage bias=400 mV

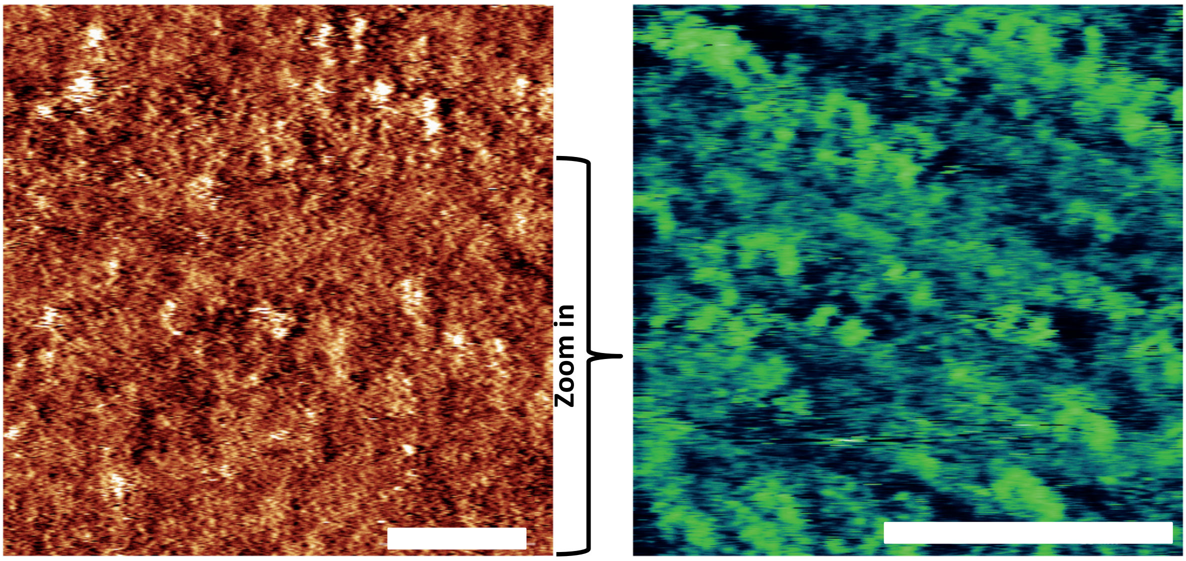

ApB-Fig 10. 45% CN4T - 40days STM image. Set point current=50 pA and voltage bias=400 mV

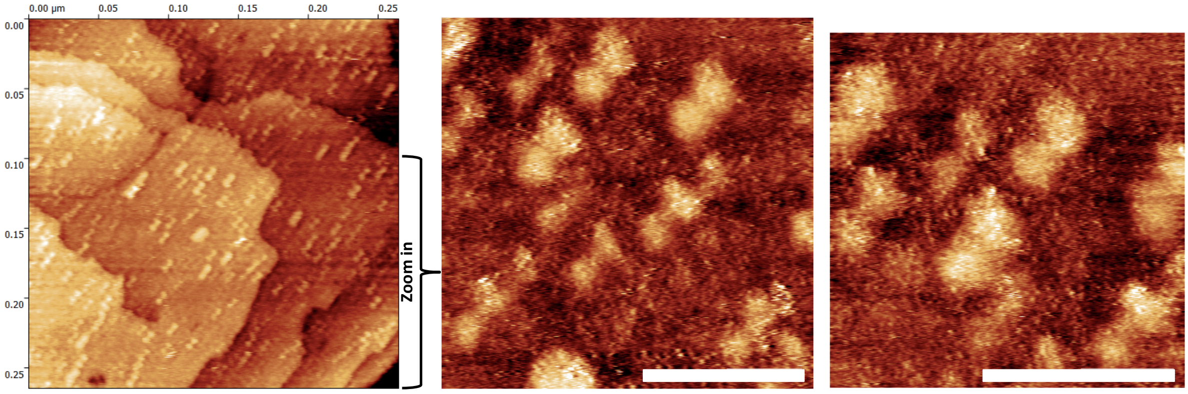

ApB-Fig 11. 35% CN4T - 40days STM image. Set point current=50 pA and voltage bias=400 mV

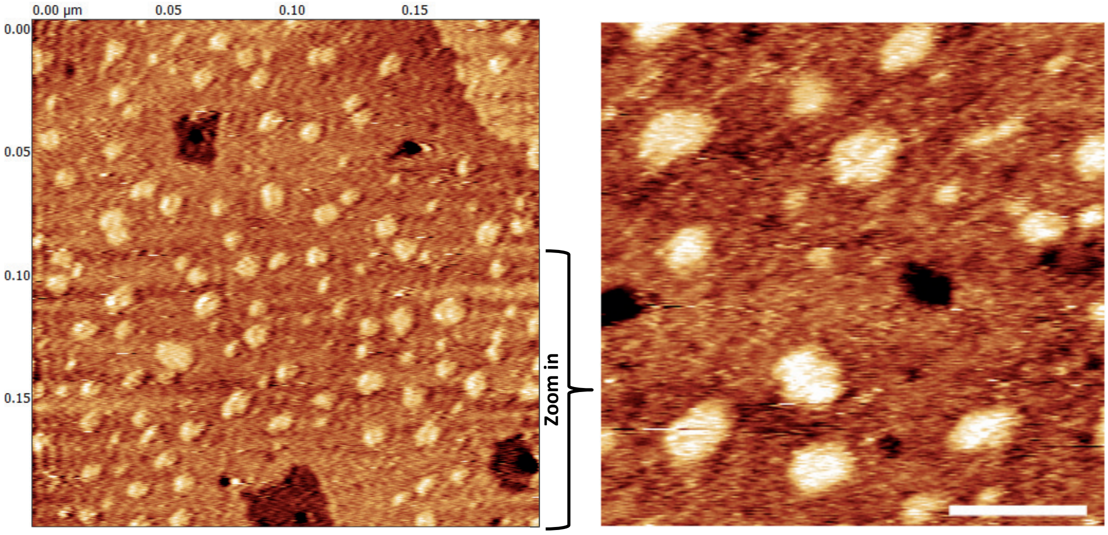

ApB-Fig 12. 15% CN4T - 40days STM image. Set point current=50 pA and voltage bias=400 mV

OT:CN4T 60 days of annealing

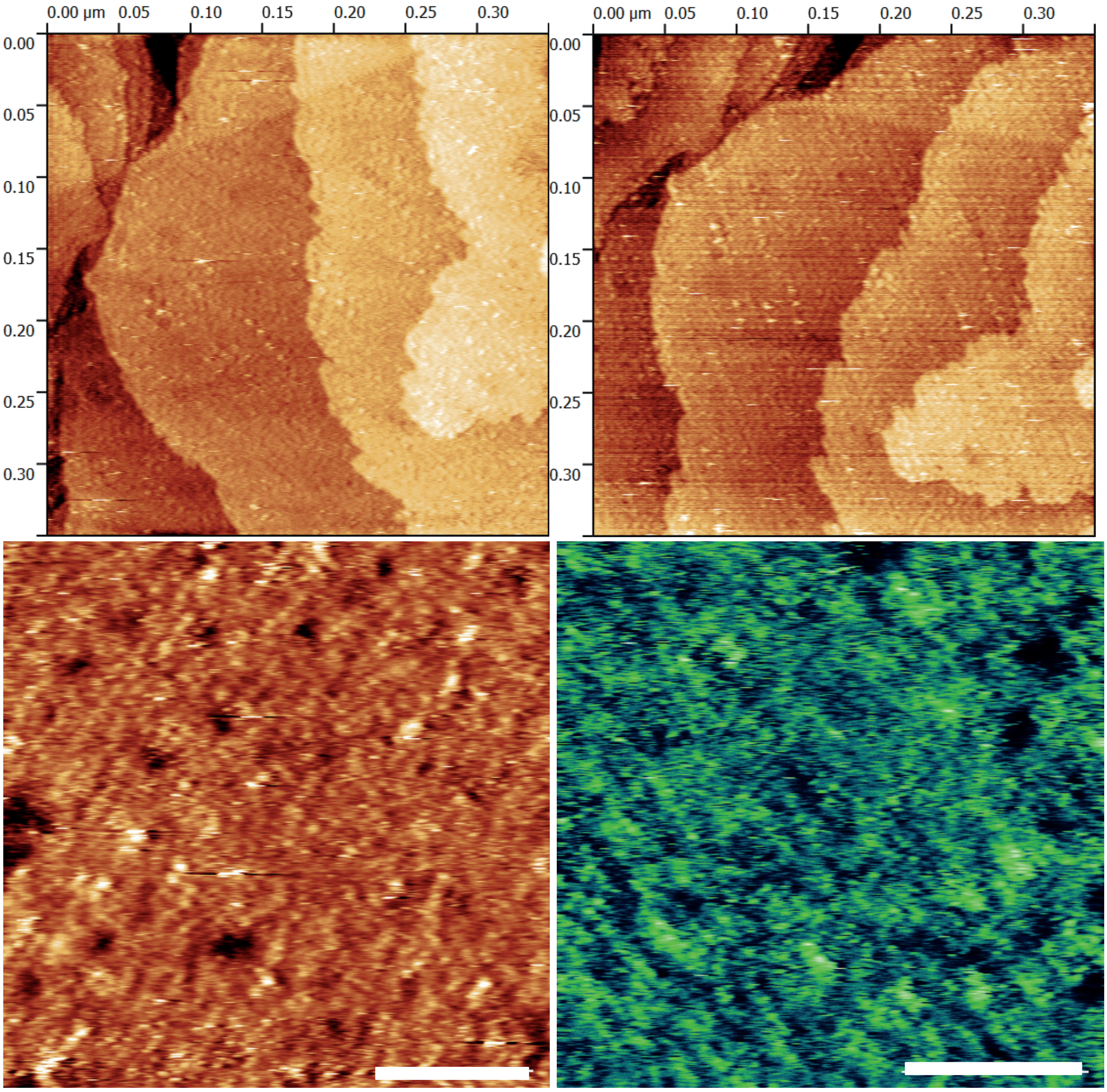

ApB-Fig 13. 64% CN4T - 60days STM image. Set point current=50 pA and voltage bias=400 mV

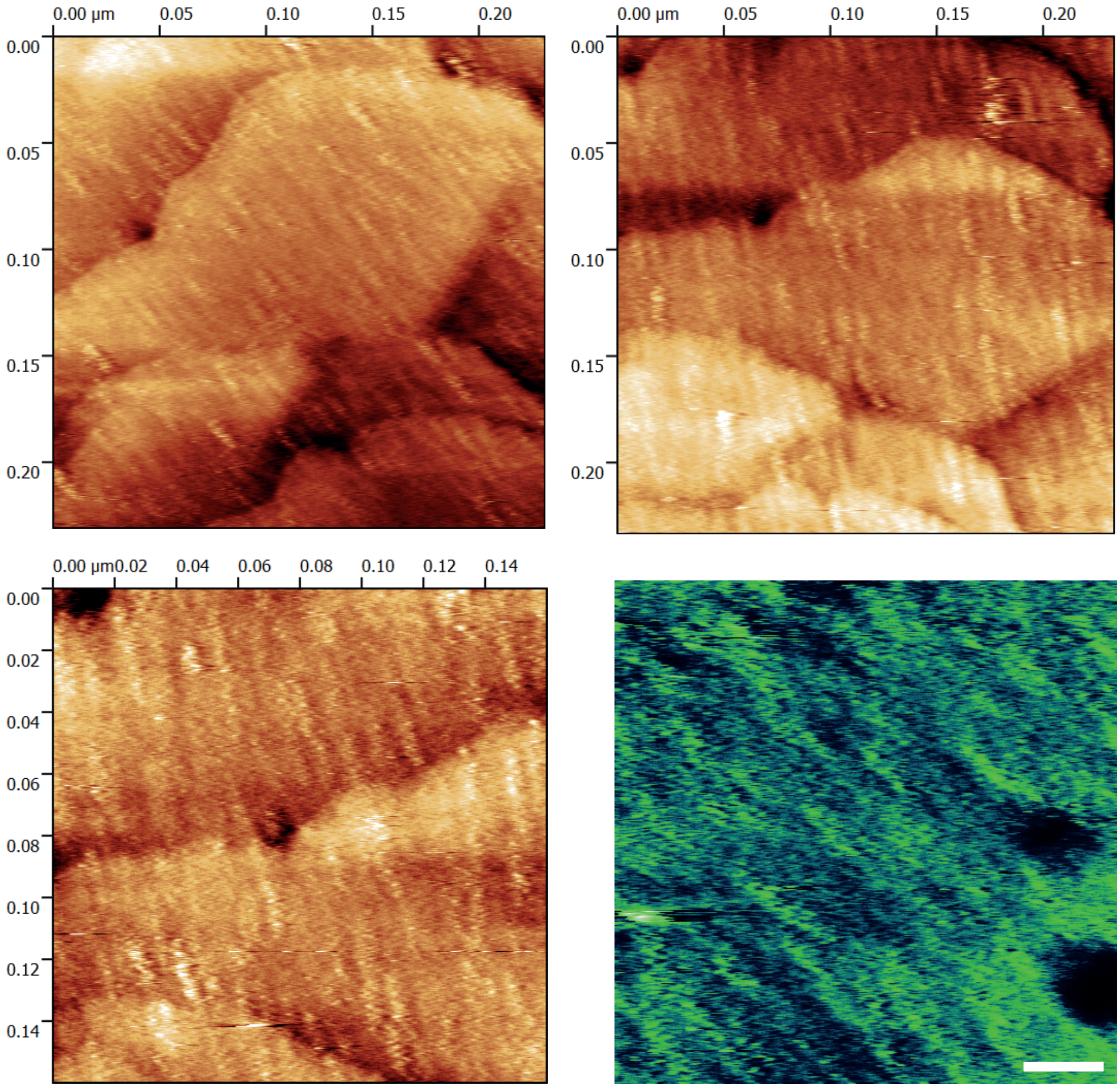

ApB-Fig 14. 45% CN4T - 60days STM image. Set point current=50 pA and voltage bias=400 mV

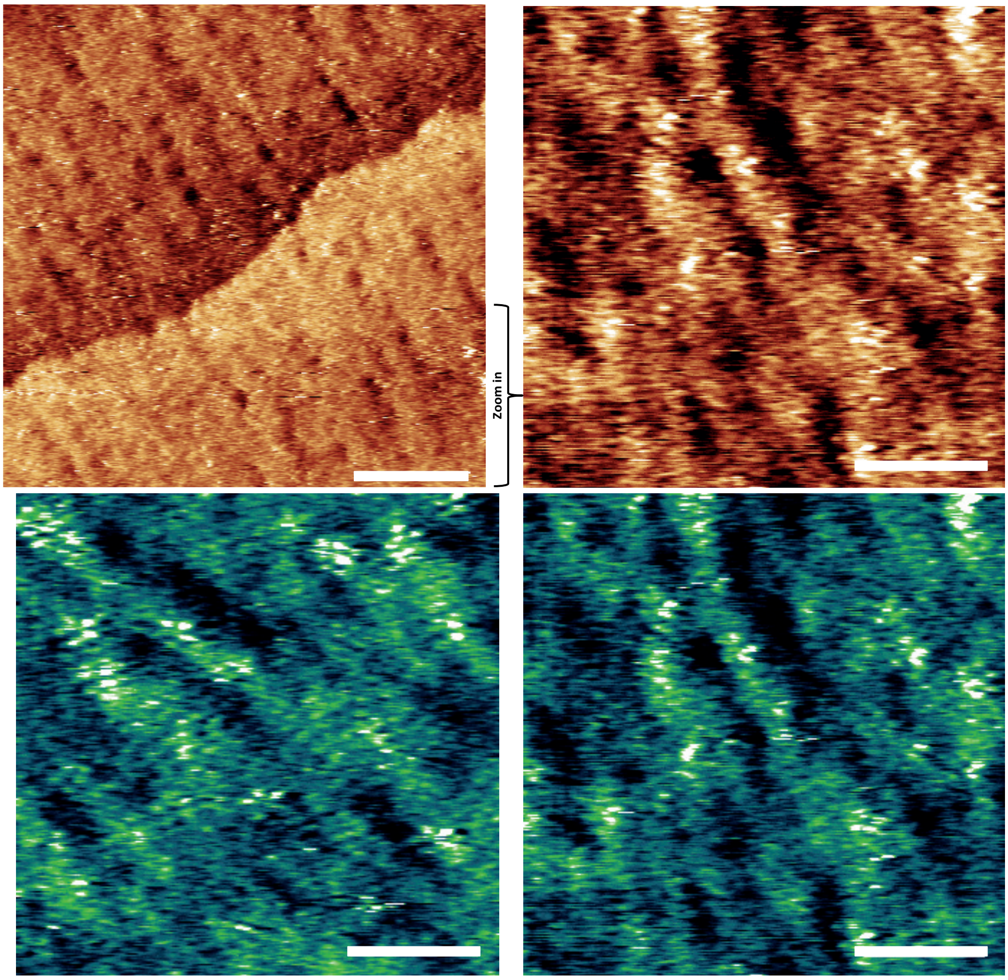

ApB-Fig 15. 35% CN4T - 60days STM image. Set point current=50 pA and voltage bias=400 mV

OT:CN4T 100 days of annealing

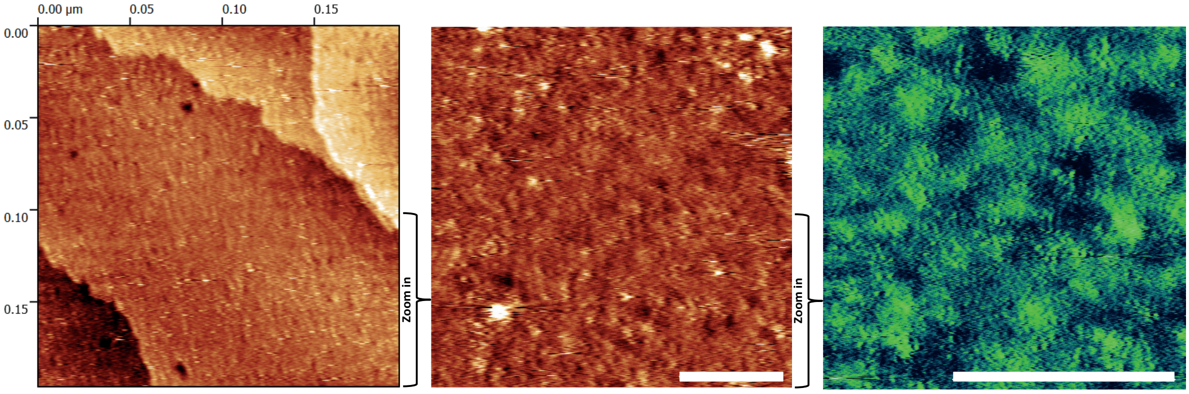

ApB-Fig 16. 85% CN4T - 100days STM image. Set point current=50 pA and voltage bias=400 mV

OT:MPA

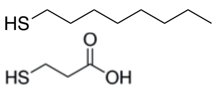

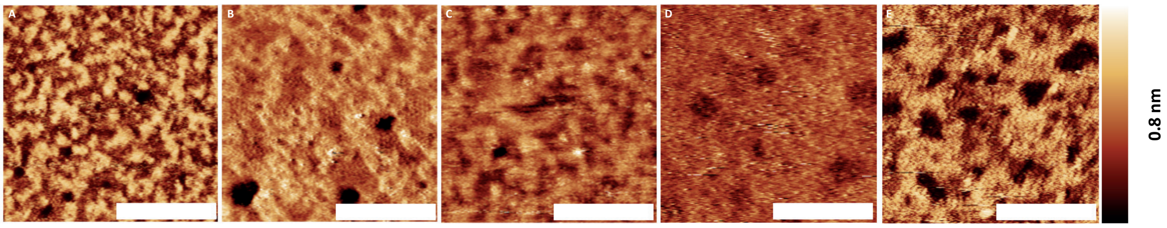

ApB-Fig 17. STM images of binary OT:MPA SAMs annealed for 5 days. The feed ratio of the mother solution during the incubation for the presented sample was: A=1090, B=2080, C=5050, D=8020, E=9010 %. Set point current=50 pA and voltage bias=450 mV. The scale bar is 20nm, unless specified otherwise.

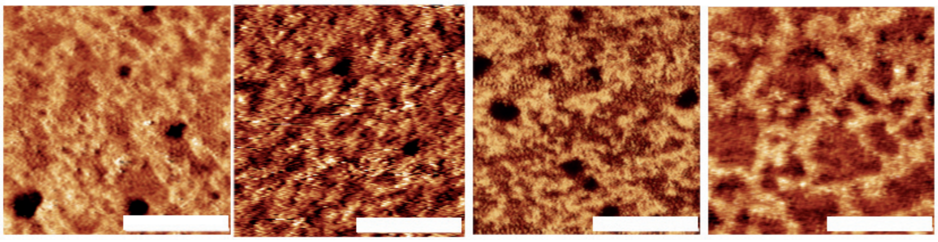

ApB-Fig 18. STM image of the OT:MPA 20:80 binary SAMs at different annealing times: 5days, 10 days, 20 days and 70 days

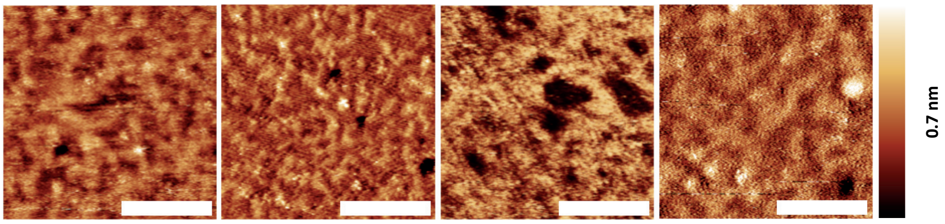

ApB-Fig 19. STM image of the OT:MPA 50:50 binary SAMs at different annealing times: 5days, 7 days, 10 days, 30 days.

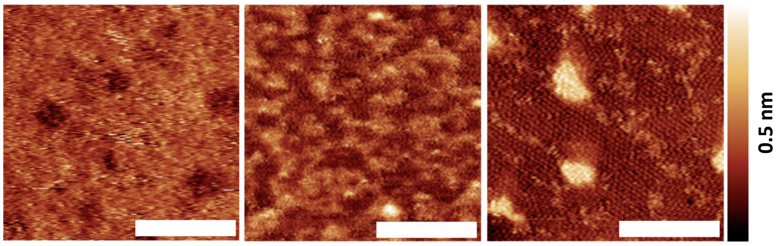

ApB-Fig 20. STM image of the OT:MPA 80:20 binary SAMs at different annealing times: 5 days, 10 days, 20 days

OT:MPA 10:90

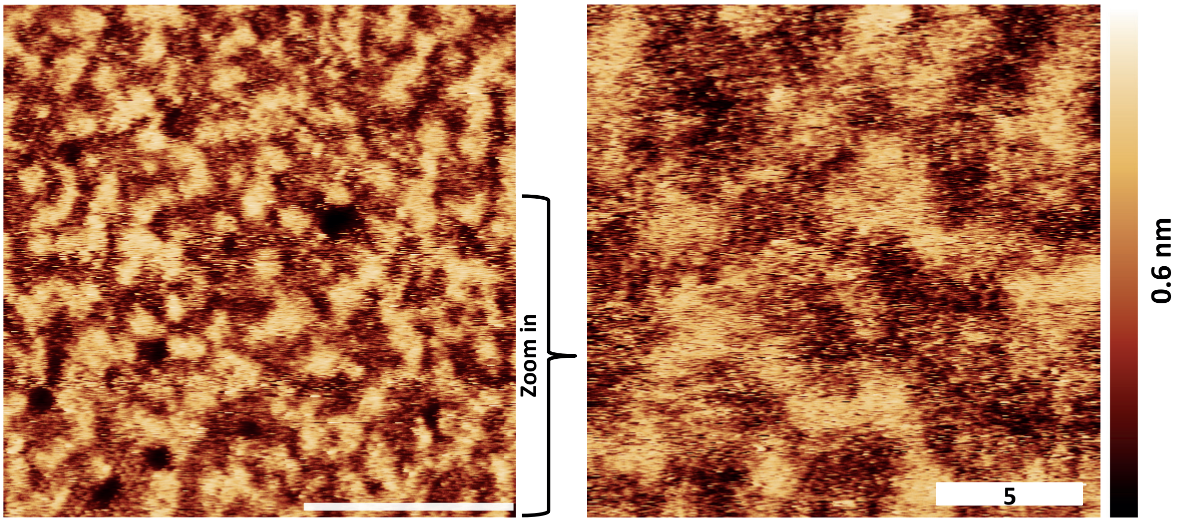

ApB-Fig 21. OT:MPA 1090- 5 days STM image. Set point current=60 pA and voltage bias=500 mV

OT:MPA 20:80

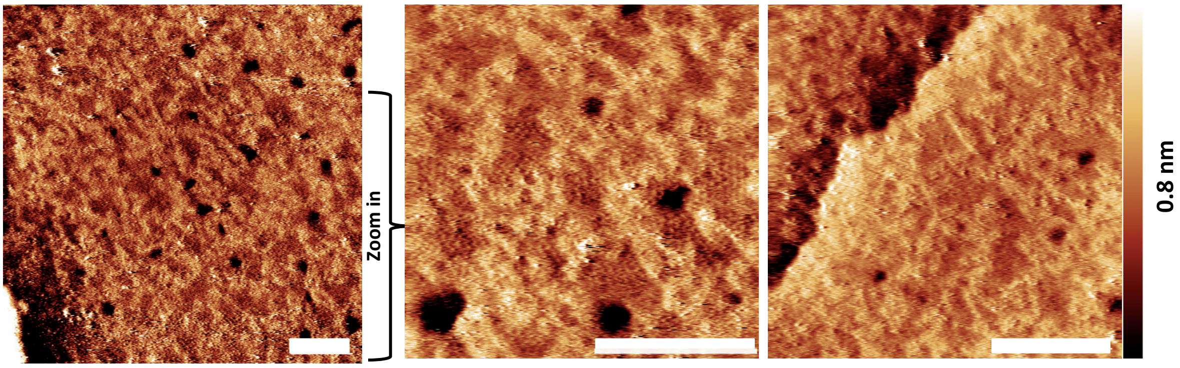

ApB-Fig 22. OT:MPA 2080- 5 days STM image. Set point current=60 pA and voltage bias=500 mV

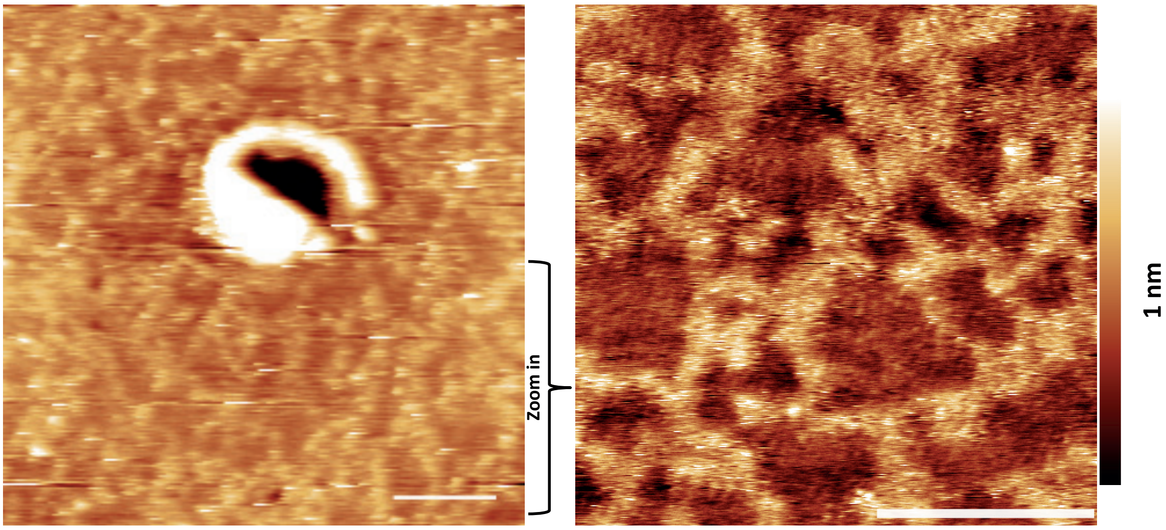

ApB-Fig 23. OT:MPA 2080- 70 days STM image. Set point current=60 pA and voltage bias=500 mV

OT:MPA 50:50

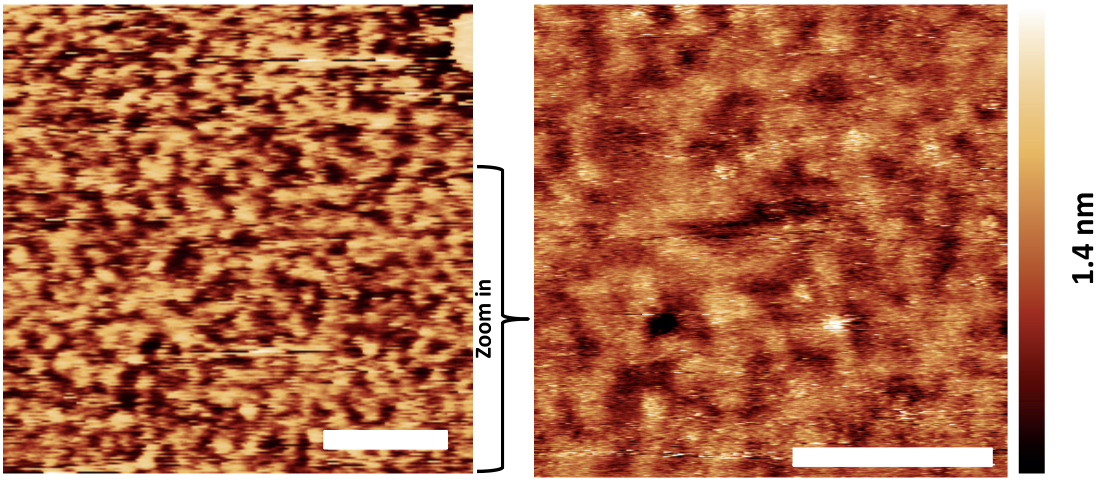

ApB-Fig 24. OT:MPA 5050- 5 days STM image. Set point current=60 pA and voltage bias=500 mV

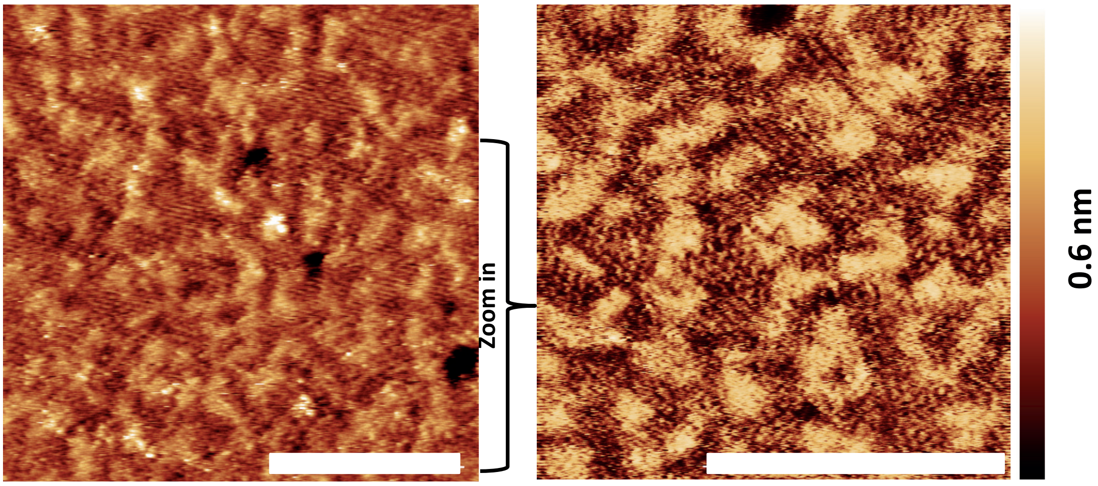

ApB-Fig 25. OT:MPA 5050- 7 days STM image. Set point current=60 pA and voltage bias=500 mV

OT:MPA 80:20

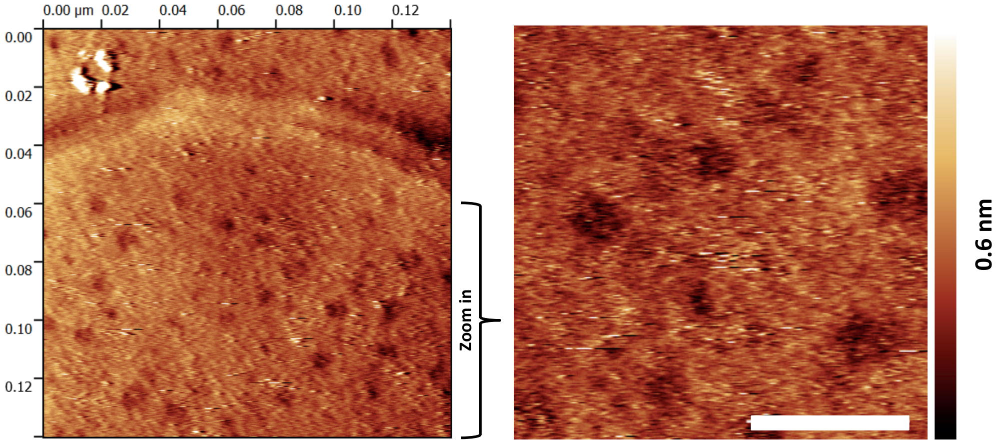

ApB-Fig 26. OT:MPA 8020- 5 days STM image. Set point current=60 pA and voltage bias=500 mV

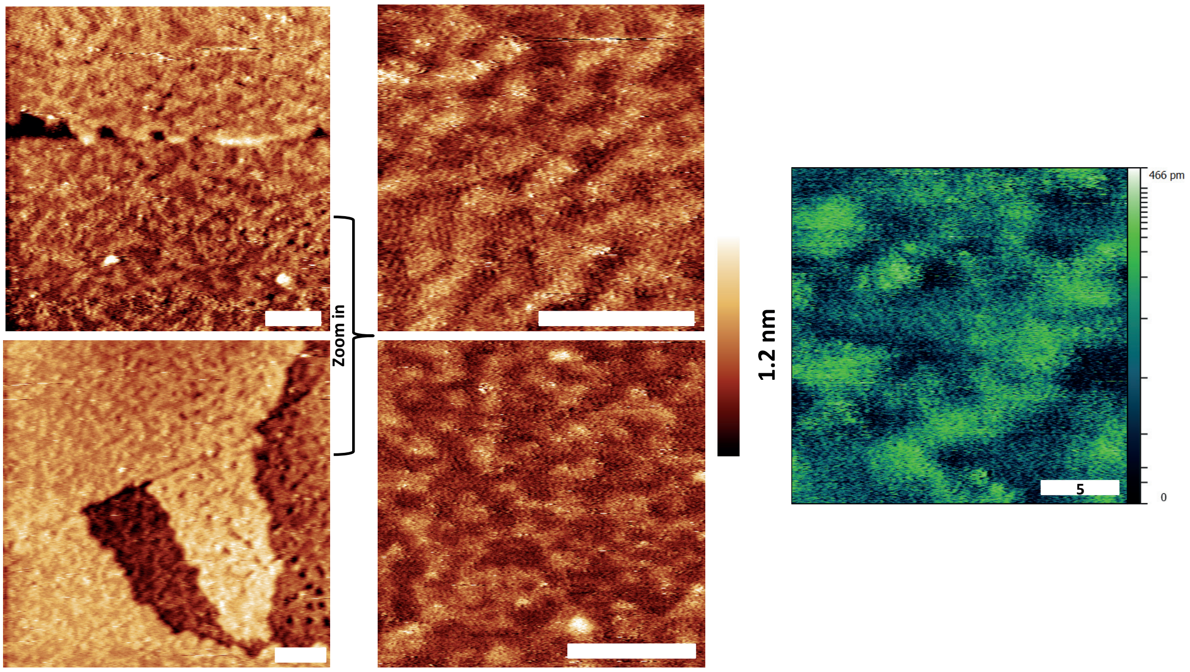

ApB-Fig 27. OT:MPA 8020- 10 days STM image. Set point current=60 pA and voltage bias=500 mV

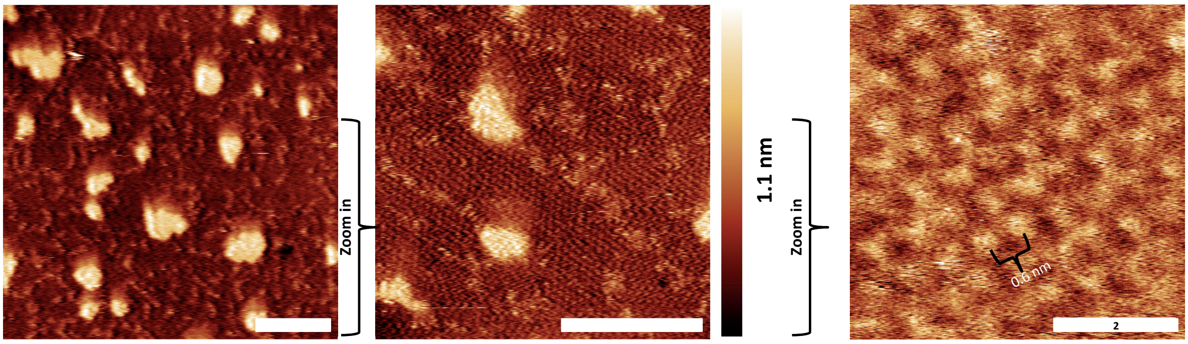

ApB-Fig 28. OT:MPA 8020- 20 days STM image. Set point current=60 pA and voltage bias=500 mV

OT:MPA 90:10

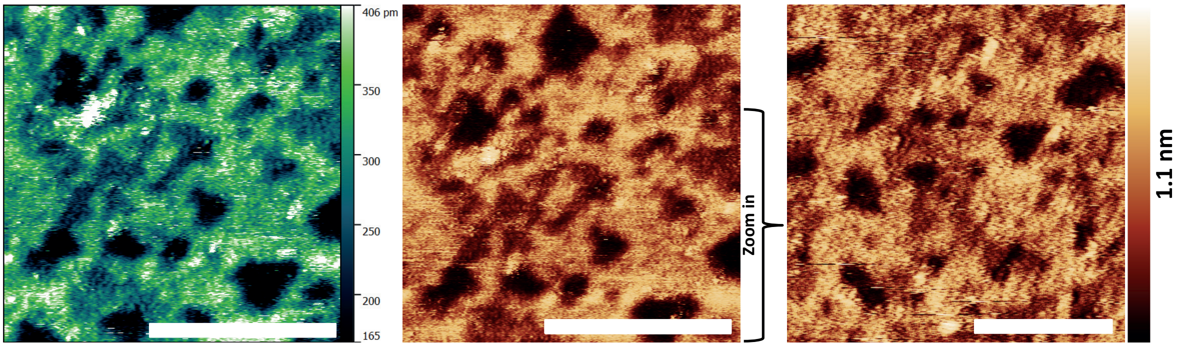

ApB-Fig 29. OT:MPA 9010- 5 days STM image. Set point current=60 pA and voltage bias=500 mV

OT:NB4M

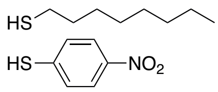

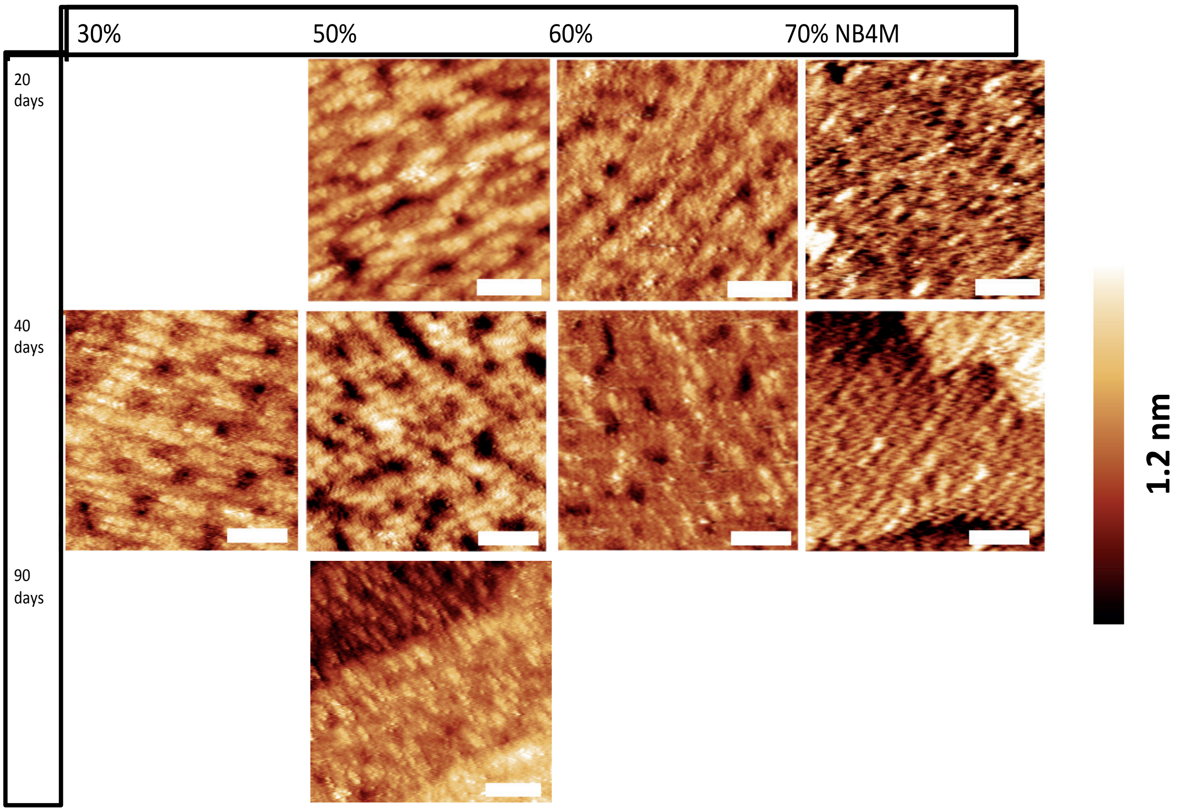

ApB-Fig 30. STM images of the annealed binary SAMs of OT:NB4M from chapter 4 (the surface ratio of NB4M is indicated on the top rectangular). The annealing times are indicated on the left side panel. Set point current=50 pA and voltage bias=350 mV. Scale bar=20nm.

Additional images of the OT:NB4M binary SAMs are presented below, in order to assist with the discussion and the conclusive results.

OT:NB4M 20 days of annealing

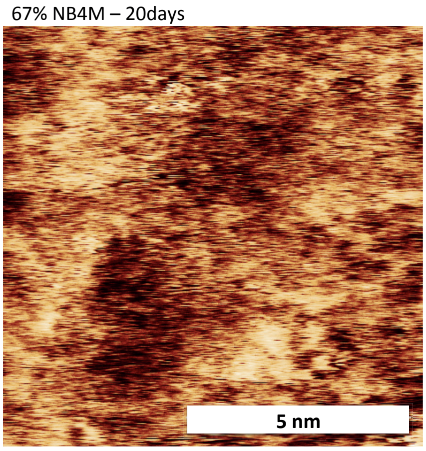

ApB-Fig 31.67% NB4M - 20days STM image. Set point current=50 pA and voltage bias=400 mV

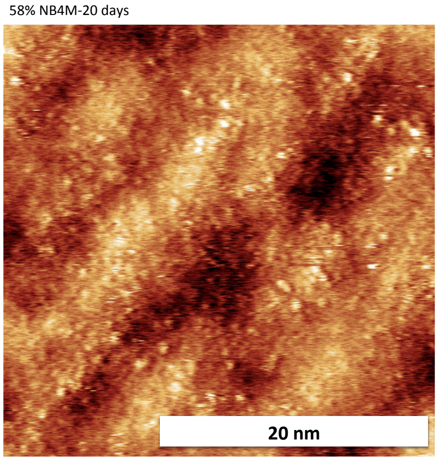

ApB-Fig 32. 58% NB4M - 20days STM image. Set point current=50 pA and voltage bias=400 mV

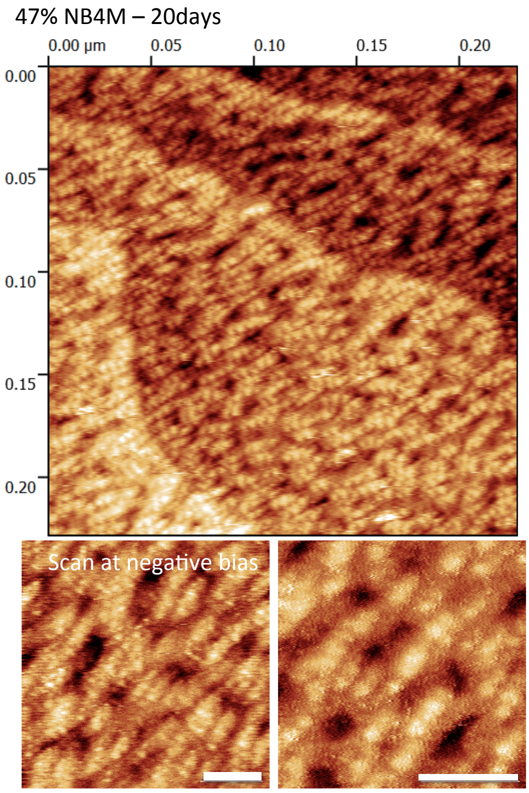

ApB-Fig 33. 47% NB4M-20days STM image. Set point current=50 pA and voltage bias=400 mV

OT:NB4M 40 days of annealing

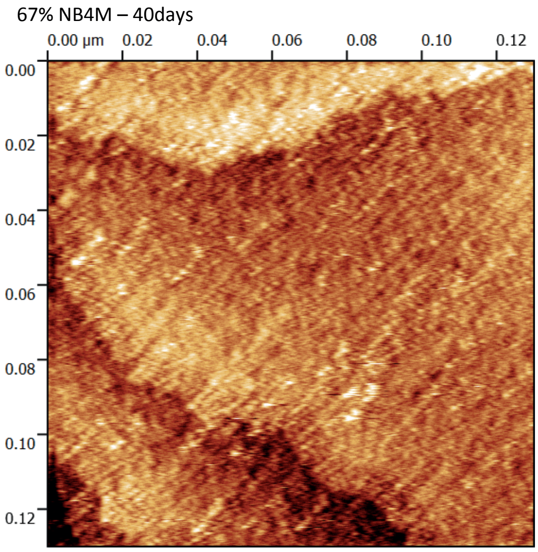

ApB-Fig 34. 67% NB4M-40days STM image. Set point current=50 pA and voltage bias=400 mV

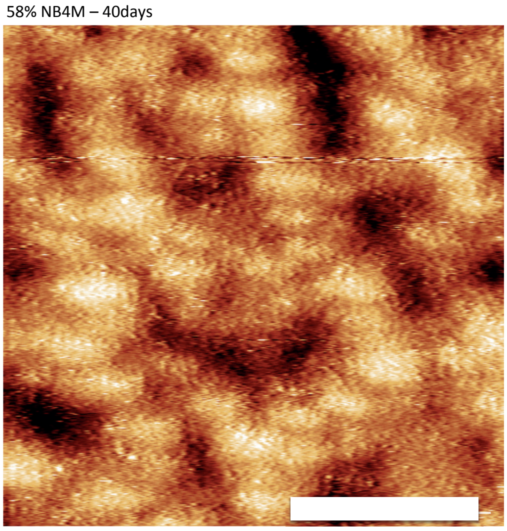

ApB-Fig 35. 58% NB4M-40days STM image. Set point current=50 pA and voltage bias=400 mV

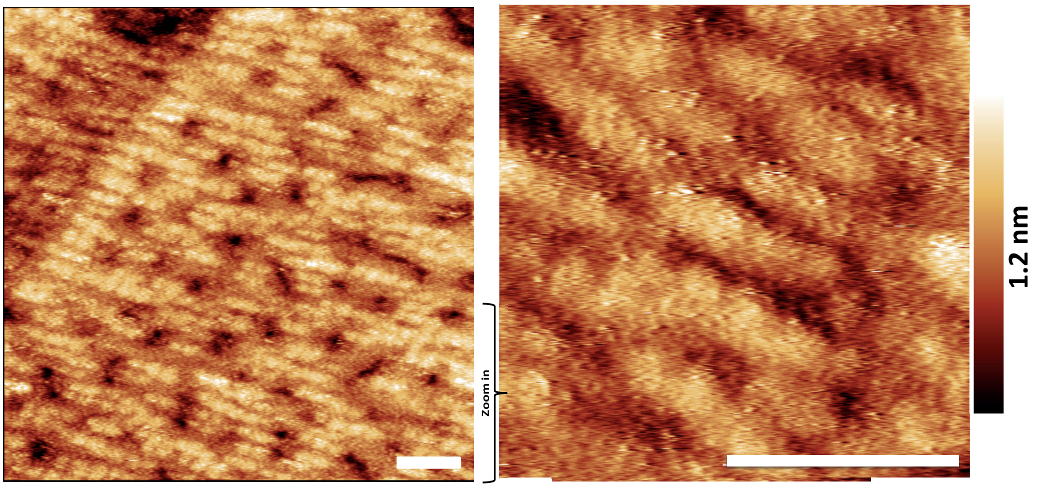

ApB-Fig 36. 30% NB4M-40days STM image. Set point current=50 pA and voltage bias=400 mV

OT:NB4M 90 days of annealing

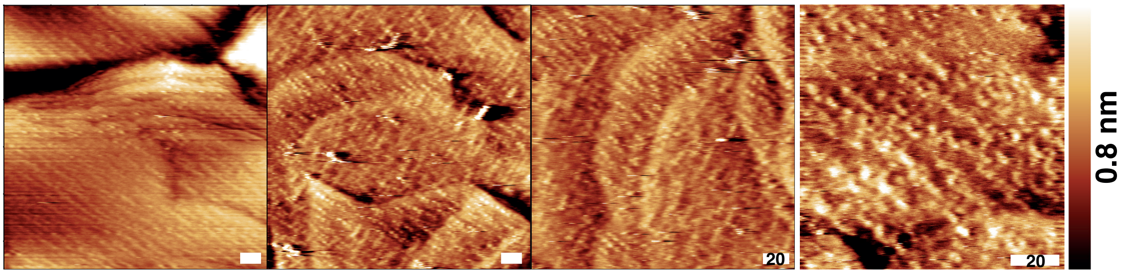

ApB-Fig 37. 47% -90days STM image. Set point current=50 pA and voltage bias=400 mV

Appendix C

Electroreductive desorption voltammograms of OT:CN4T binary SAMs.

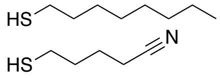

Plots of peak potential as a function of CN4T percentage in the SAM, at different annealing times

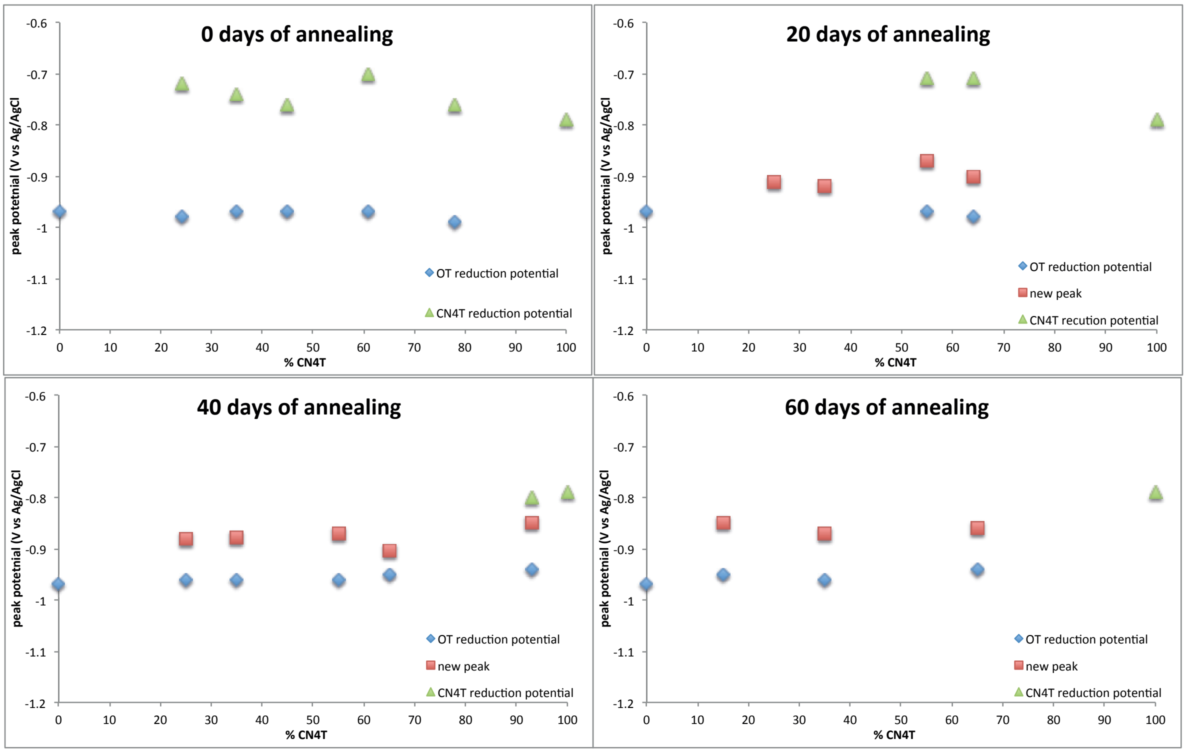

ApndxC Figure 1. Dependence of the peak potentials on the surface composition divided in 4 plots according to the annealing time.

Table 2. FWHM of the OT:CN4T binary SAMs

OT CN4T			OT CN4T	
0 days	fwhm OT (mV)	fwhm CN4T (mV)	20 days	fwhm new phase(mV)
78%	140	90	65%	88
60%	80	76	55%	52
44%	120	100	35%	44
35%	112	70	25%	80
24%	120	84		
OT CN4T			OT CN4T	
40 days	fwhm new phase(mV)		60 days	fwhm new phase(mV)
93%	52		65%	60
55%	41		35%	50
35%	50		15%	60
25%	42			

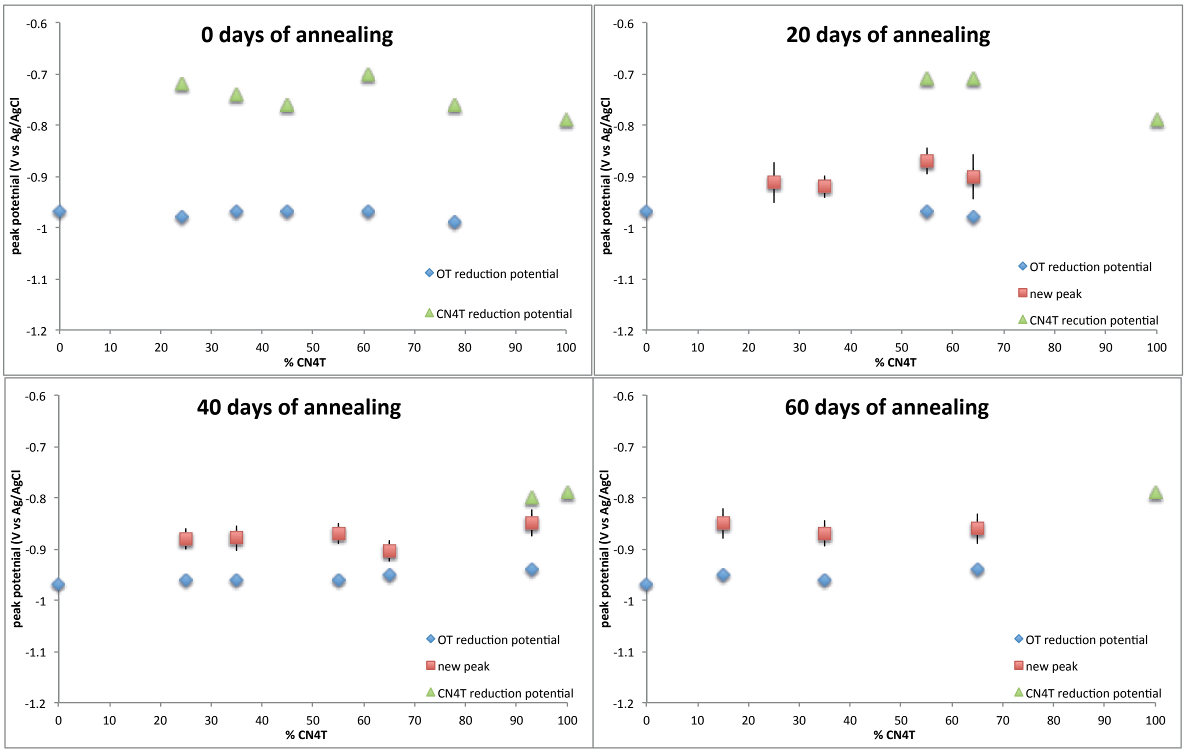

ApndxC Figure 2. Dependence of the peak potentials on the surface composition divided in 4 plots according to the annealing time. The error bars represent the +/-HWHM of the peak at the intermediate potential (new phase) according to the calculated values of FWHM after Gaussian fitting.

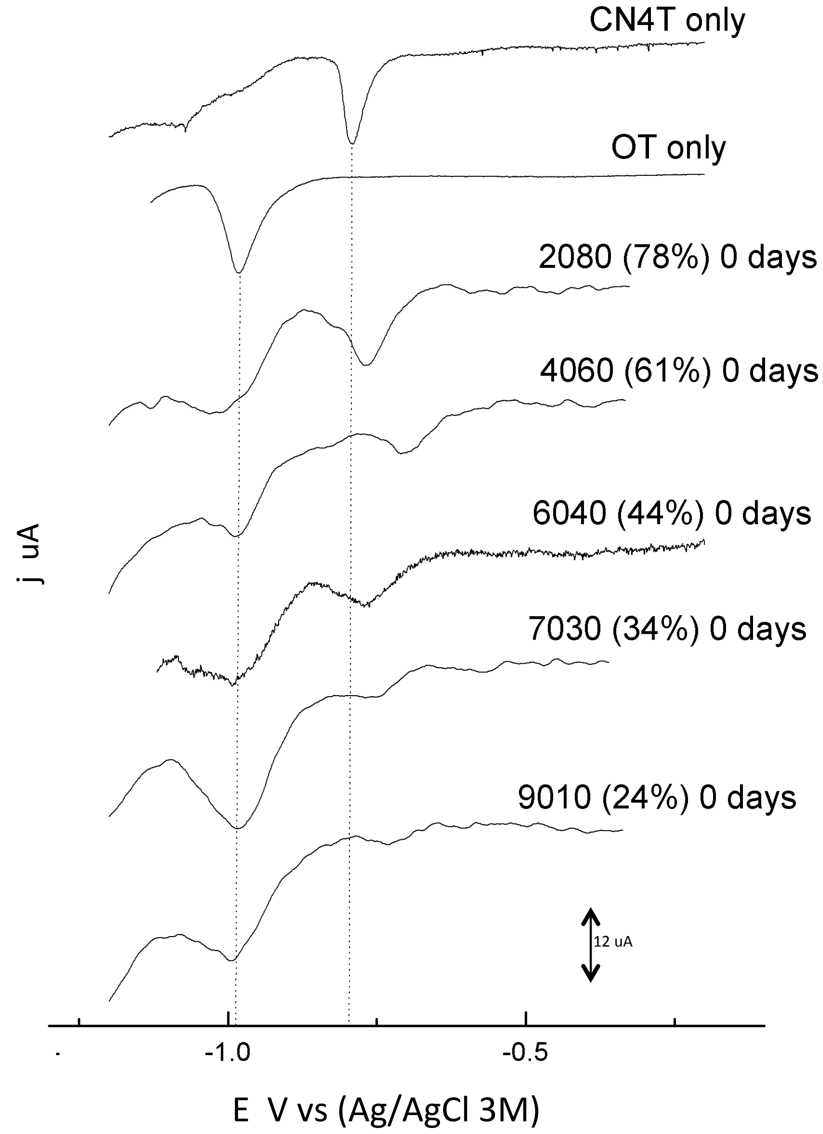

ApndxC Figure 3. voltammograms of the OT:CN4T binary SAMs, different surface compositions non-annealed. Analysis in 0.1 KOH degassed electrolyte. Scan rate 50mV/s.

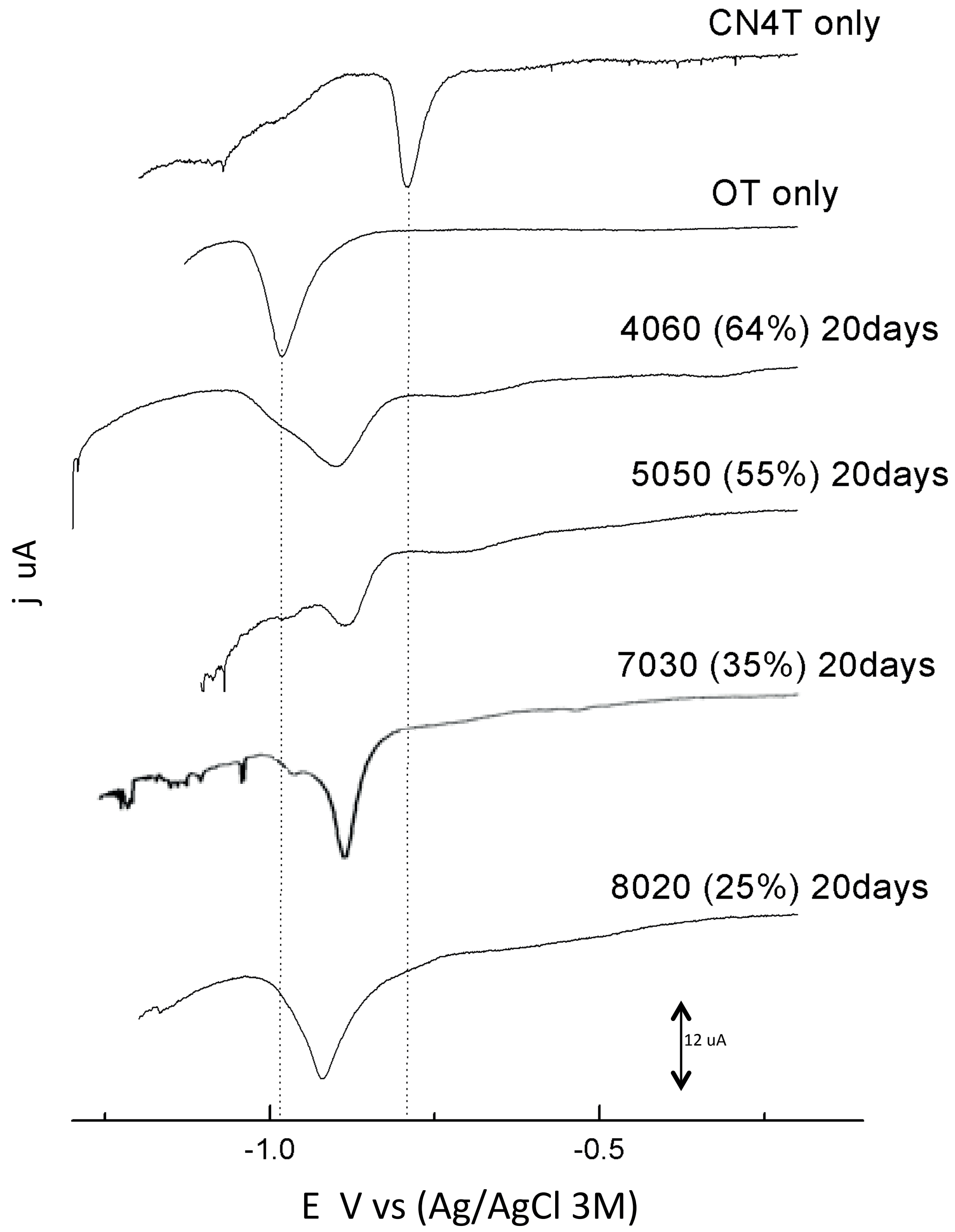

ApndxC Figure 4. Voltammograms of the OT:CN4T binary SAMs, different surface compositions annealed for 20 days. Analysis in 0.1 KOH degassed electrolyte. Scan rate 50mV/s.

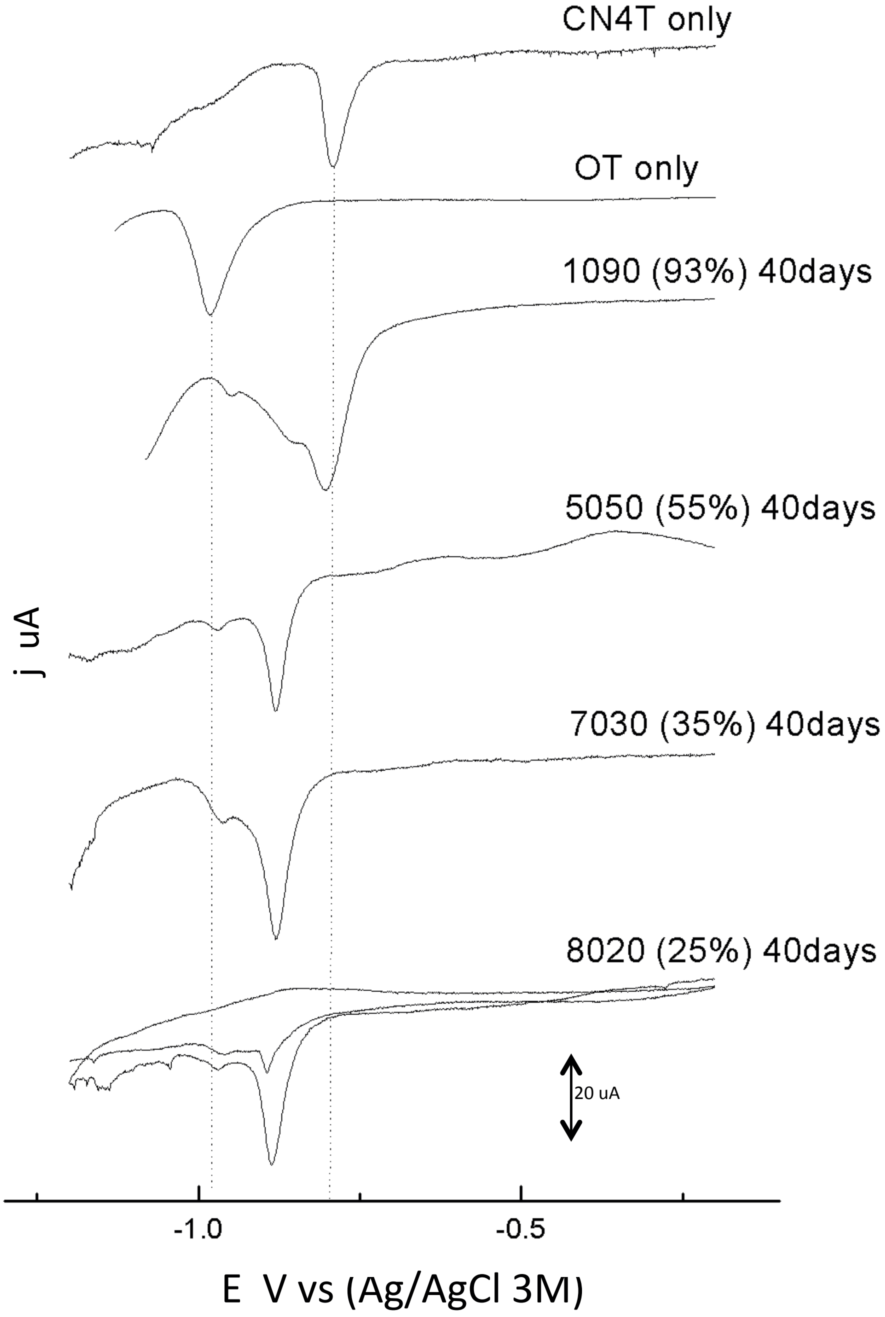

ApndxC Figure 5. Voltammograms of the OT:CN4T binary SAMs, different surface compositions annealed for 40 days. Analysis in 0.1 KOH degassed electrolyte. Scan rate 50mV/s.

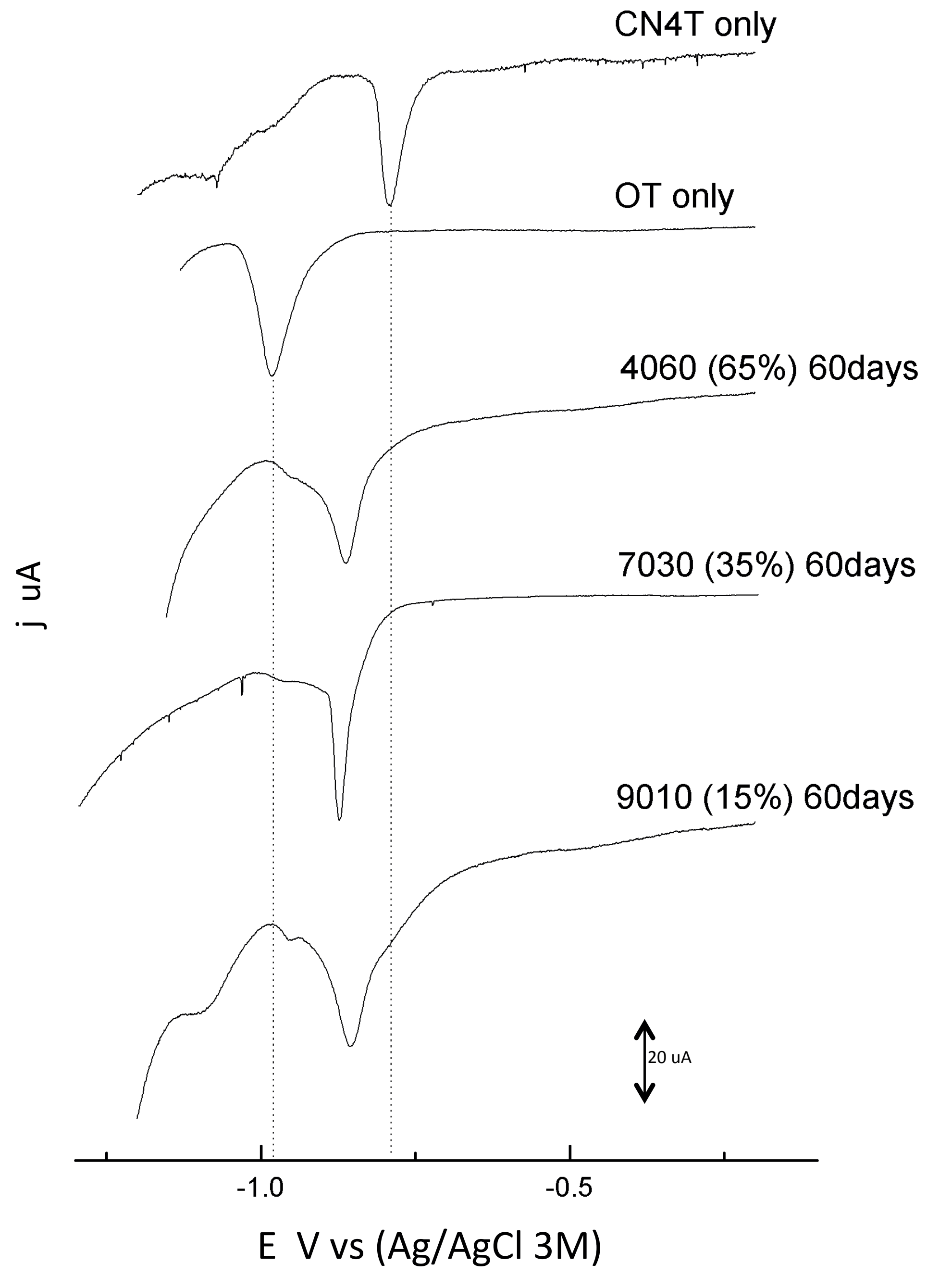

ApndxC Figure 6. Voltammograms of the OT:CN4T binary SAMs, different surface compositions annealed for 60 days. Analysis in 0.1 KOH degassed electrolyte. Scan rate 50mV/s.

Electroreductive desorption voltammograms of OT:NB4M binary SAMs.

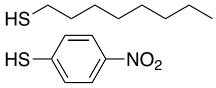

Plots of peak potential as a function of NB4M percentage in the SAM, at different annealing times

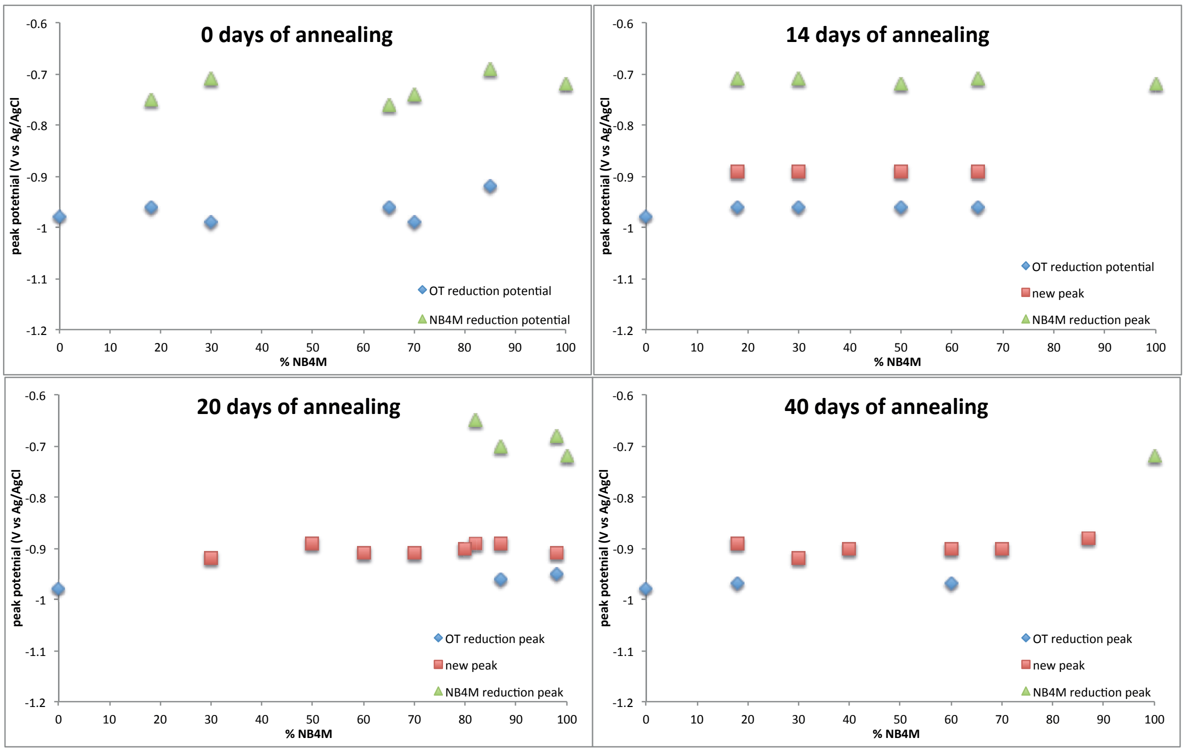

ApndxC Figure 7. Dependence of the peak potentials on the surface composition divided in 4 plots according to the annealing time.

Table 3. FWHM of desorption peaks of OT:NB4M binary SAMs

OT NB4M			OT NB4M	
0 days	fwhm OT(mV)	fwhm NB4M(mV)	15 days	fwhm new phase(mV)
87%	108	140	68%	78
72%	82	broad	48%	74
68%	120	200	30%	74
30%	98	190	18%	80
18%	125	122		
OT NB4M			OT NB4M	
20 days	fwhm new phase(mV)		40 days	fwhm new phase(mV)
97%	60		87%	52
87%	80		72%	50
82%	76		60%	52
80%	56		40%	49
72%	58		30%	36
60%	55		18%	50
48%	66			
30%	52			

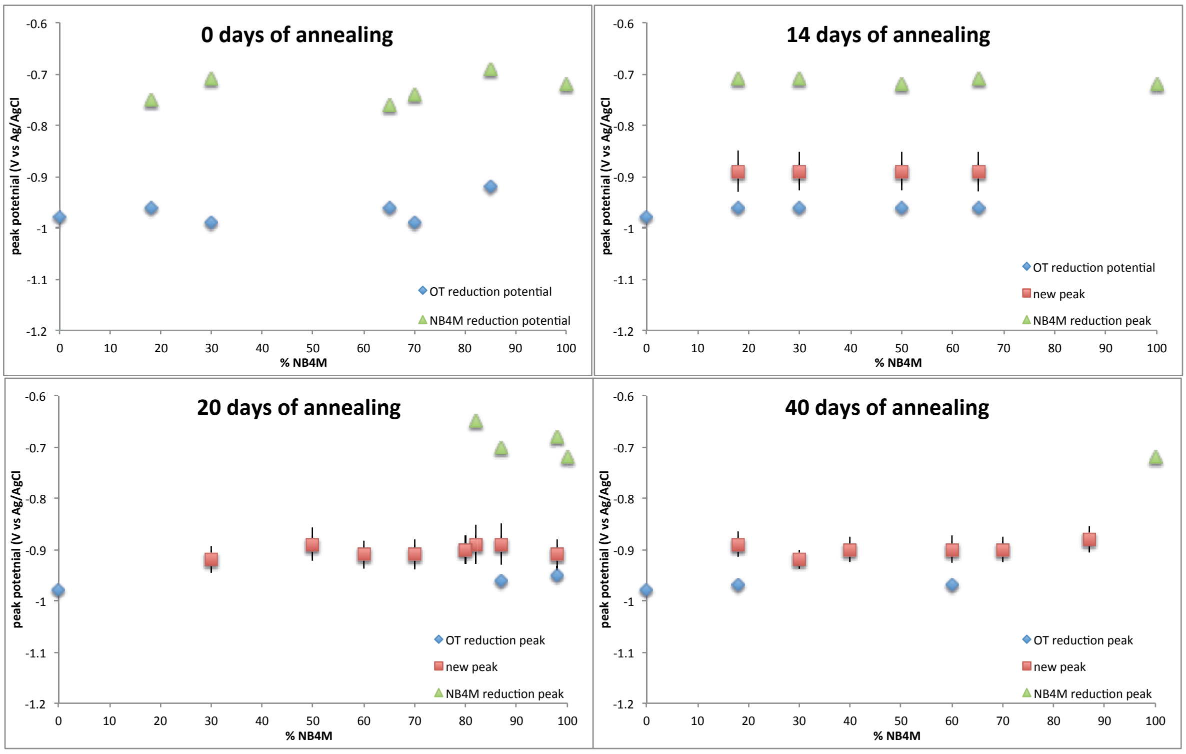

ApndxC Figure 8. Dependence of the peak potentials on the surface composition divided in 4 plots according to the annealing time. The error bars represent the +/-HWHM of the peak at the intermediate potential (new phase) according to the calculated values of FWHM after Gaussian fitting.

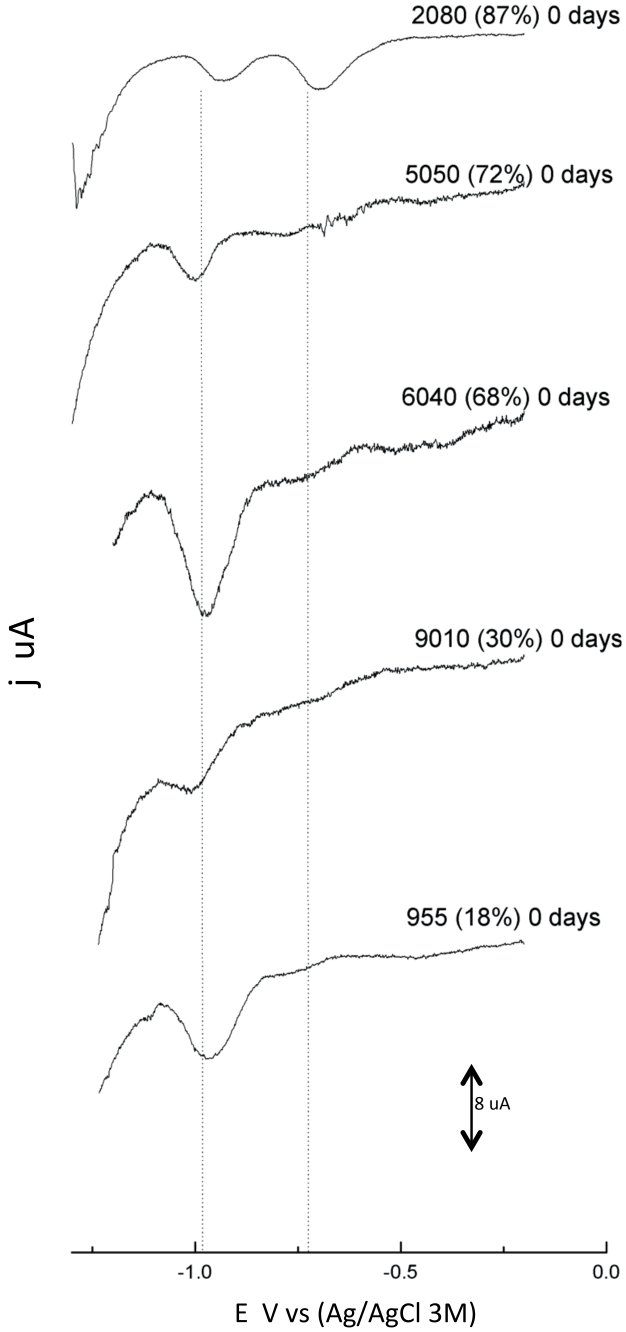

ApndxC Figure 9. oltammograms of the OT:NB4M binary SAMs, different surface compositions non-annealed. The two dotted lines indicate the desorption potential of the OT (left) and NB4M (right) single SAMs. Analysis in 0.1 KOH degassed electrolyte. Scan rate 50mV/s.

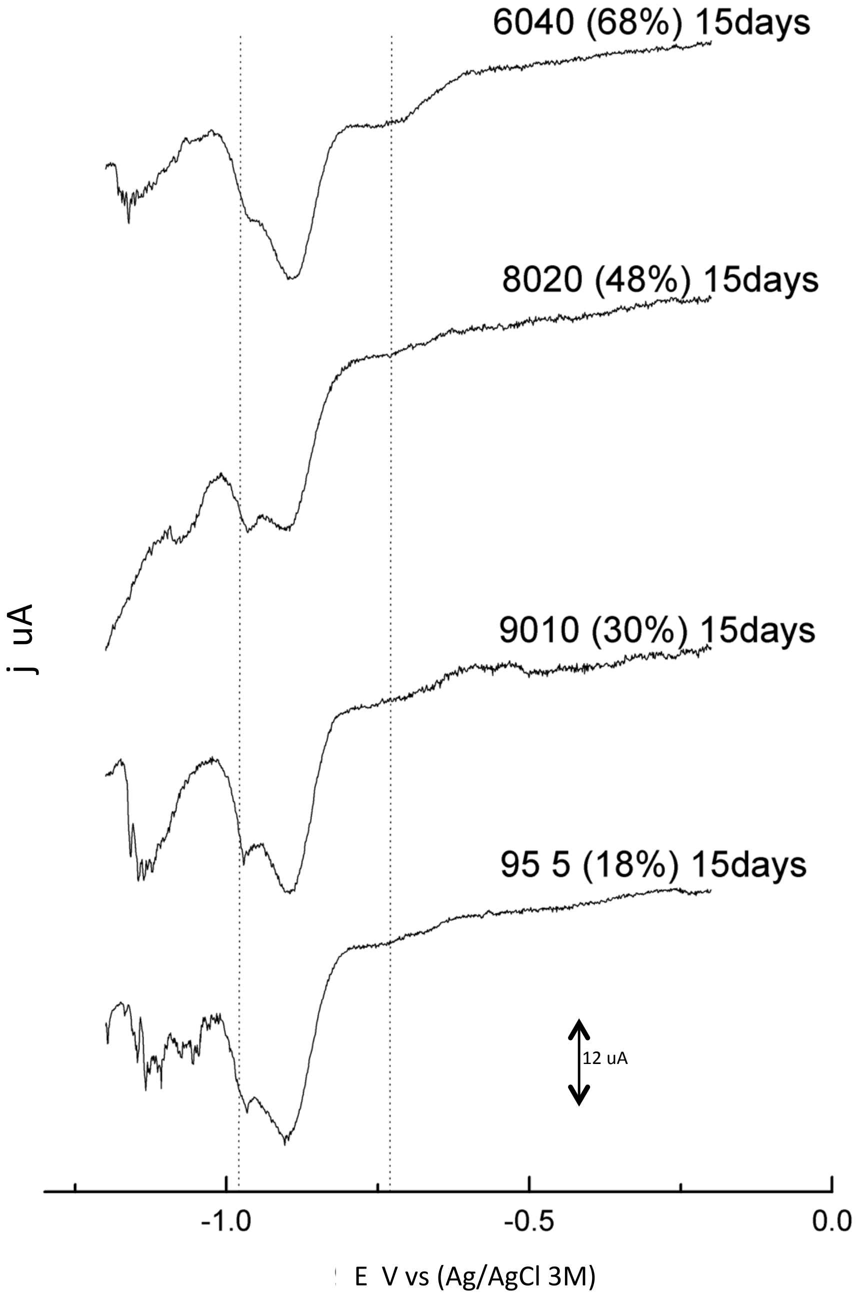

ApndxC Figure 10. Voltammograms of the OT:NB4M binary SAMs, different surface compositions annealed for 15 days. The two dotted lines indicate the desorption potential of the OT (left) and NB4M (right) single SAMs. Analysis in 0.1 KOH degassed electrolyte. Scan rate 50mV/s.

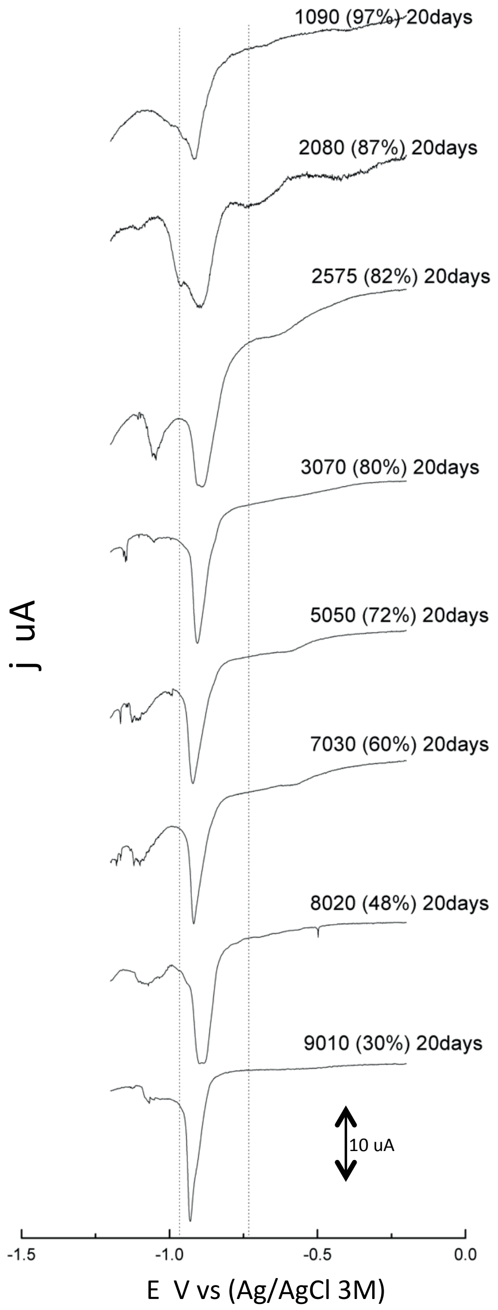

ApndxC Figure 11. Voltammograms of the OT:NB4M binary SAMs at different compositions annealed for 20 days. The two dotted lines indicate the desorption potential of the OT (left) and NB4M (right) single SAMs. Analysis in 0.1 KOH degassed electrolyte. Scan rate 50mV/s.

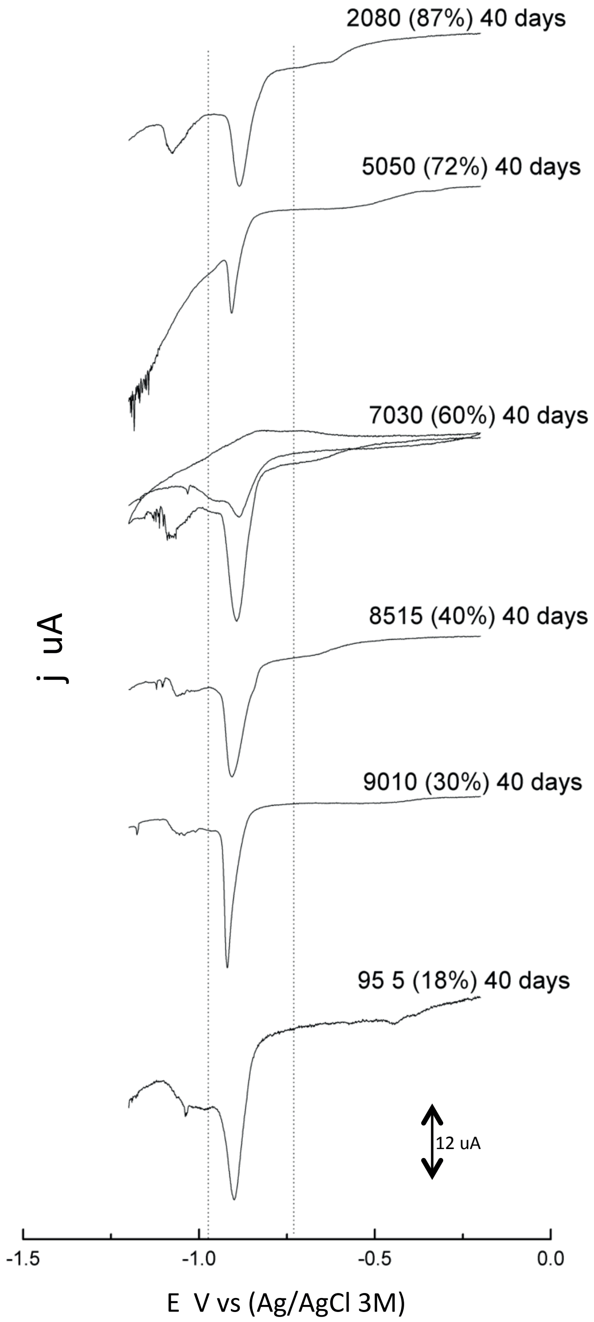

ApndxC Figure 12. Voltammograms of the OT:NB4M binary SAMs at different surface compositions, annealed for 40 days. The two dotted lines indicate the desorption potential of the OT (left) and NB4M (right) single SAMs. Analysis in 0.1 KOH degassed electrolyte. Scan rate 50mV/s.

Electroreductive desorption voltammograms of OT:MPA binary SAMs.

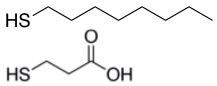

Plots of peak potential as a function of OT:MPA feed ratio in the SAM, at different annealing times

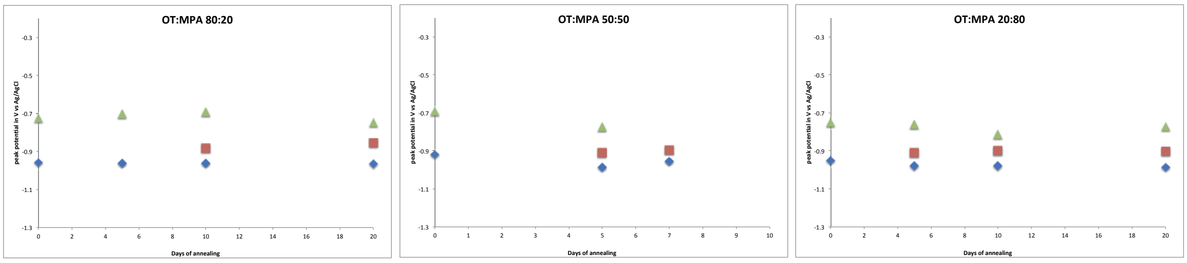

ApndxC Figure 13. Dependence of the peak potentials on the annealing time surface composition divided in 4 plots according to the feed ratio of the OT:MPA binary SAM.

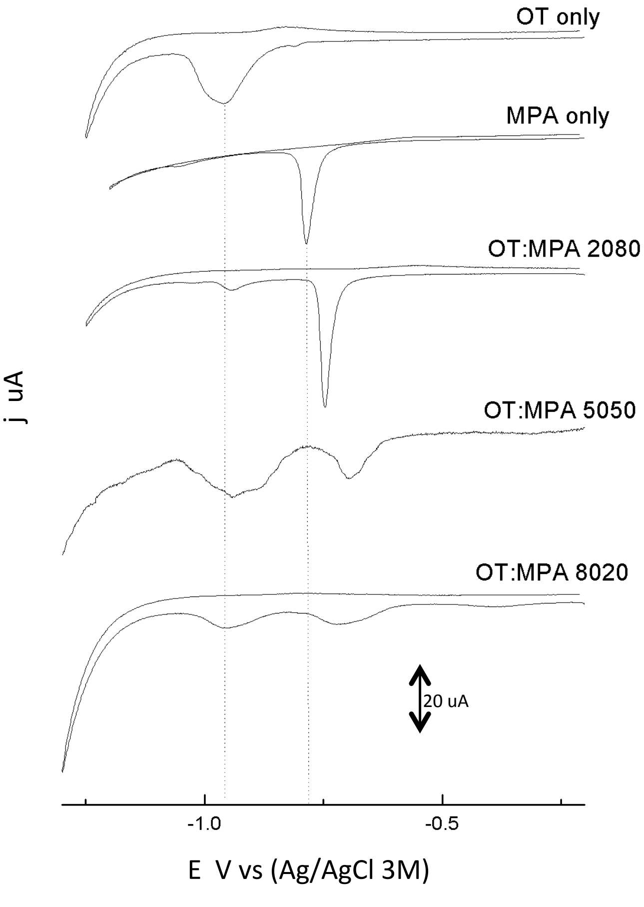

ApndxC Figure 14. Voltammograms of the OT:MPA binary SAMs at different surface compositions, annealed for 0 days. Analysis in 0.1 KOH degassed electrolyte. Scan rate 50mV/s.

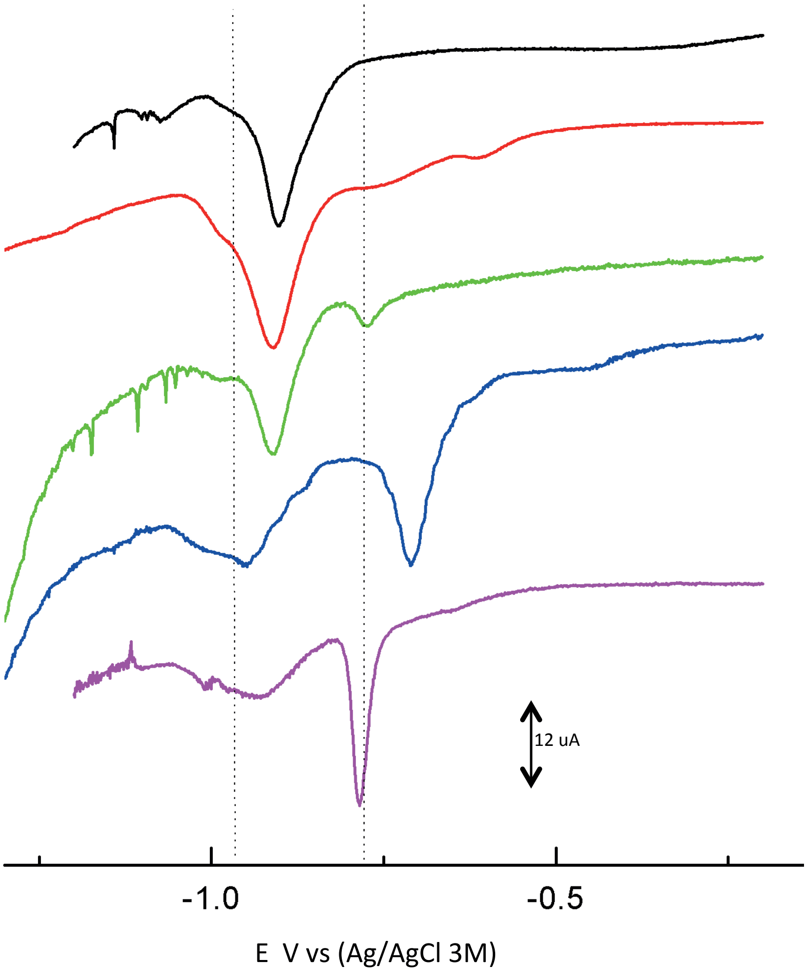

ApndxC Figure 15. Voltammograms of the OT:MPA binary SAMs at different surface compositions, annealed for 5 days. Analysis in 0.1 KOH degassed electrolyte. Scan rate 50mV/s.

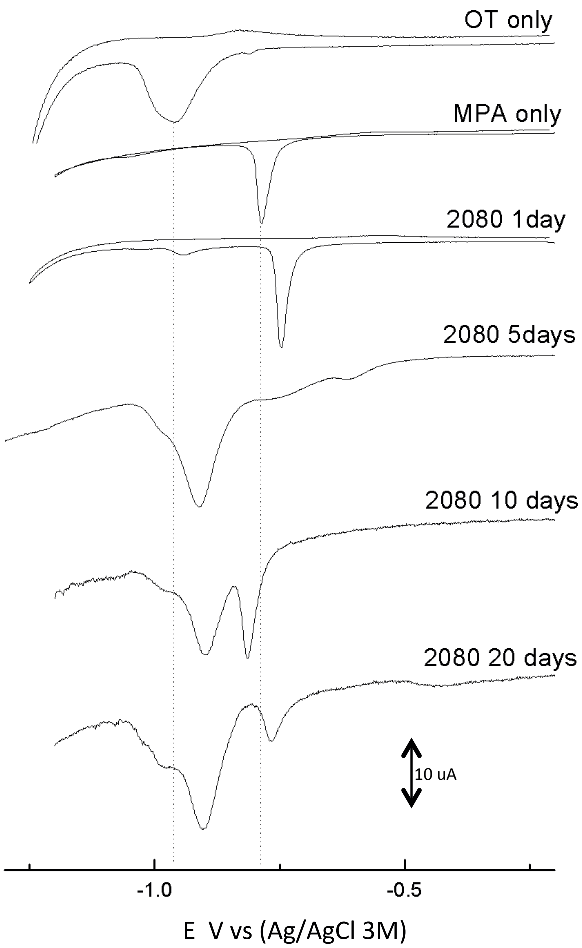

ApndxC Figure 16. Voltammograms of the OT:MPA binary SAMs at 2080 surface composition, annealed for various times. Analysis in 0.1 KOH degassed electrolyte. Scan rate 50mV/s.

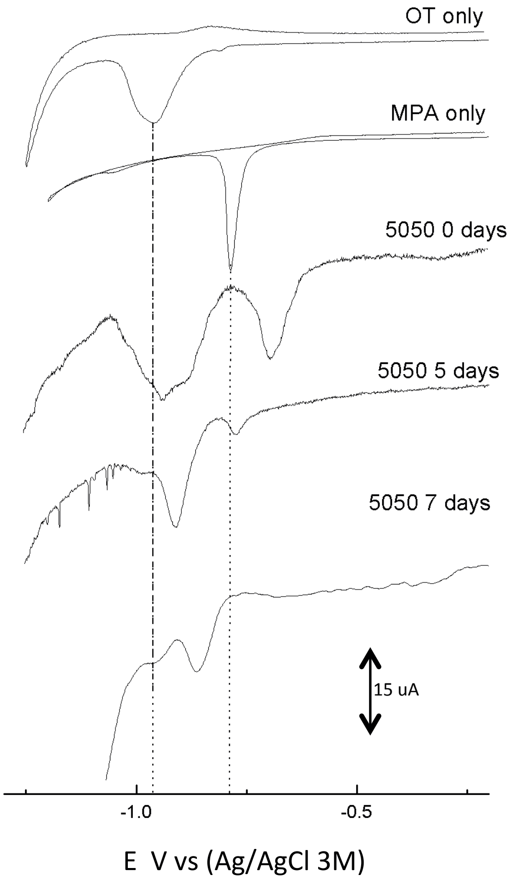

ApndxC Figure 17. Voltammograms of the OT:MPA binary SAMs at 5050 surface composition, annealed for various times. Analysis in 0.1 KOH degassed electrolyte. Scan rate 50mV/s.

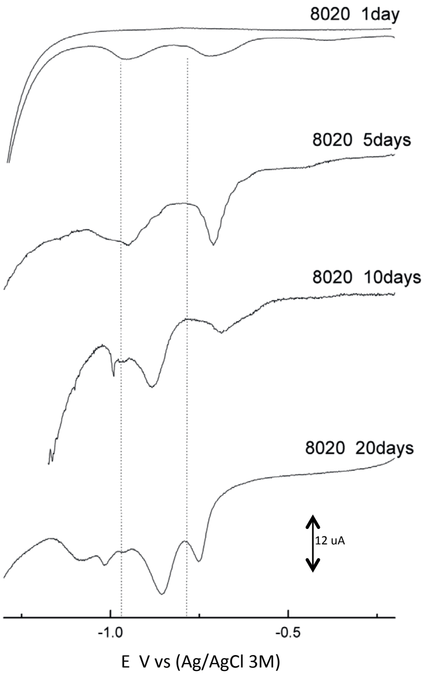

ApndxC Figure 18. Voltammograms of the OT:MPA binary SAMs at 8020 surface composition, annealed for various times. Analysis in 0.1 KOH degassed electrolyte. Scan rate 50mV/s.

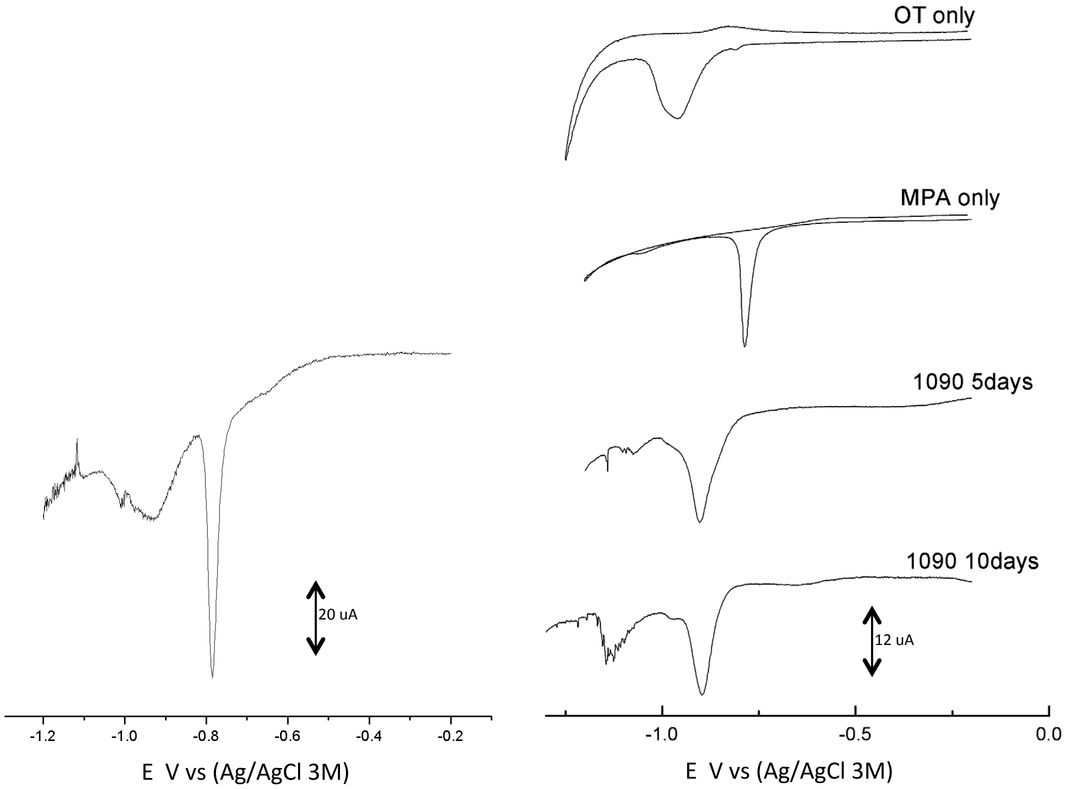

ApndxC Figure 19. OT:MPA 9010 at 5 days of annealling (left). OT:MPA 1090 at various annealling times (right)

CURRICULUM VITAE

NIKOLAOS NIANIAS *CHEMIST*

PERSONAL INFORMATION

Date of Birth	May 16, 1984
Place of Birth	Zurich, Switzerland

CONTACT INFORMATION

Home Address	Chemin de la Prairie 62, 1007, Lausanne
Telephone	+41 787050677
e-mail	nanonikonian@gmail.com

SCIENTIFIC EDUCATION

PhD-Doctoral Assistant	EDOC-EDMX Supramolecular Nanomaterials and Interfaces Laboratory Successfully defended at December 7th, 2017 ÉCOLE POLYTECHNIQUE FÉDÉRALE DE LAUSANNE School of Engineering - Institute of Materials
M.Sc. In Chemistry	Specialization CHEMISTRY AND POLYMER TECHNOLOGY February 2012 Aristotle University of Thessaloniki - Department of Chemistry **Master's Dissertation:** "Synthesis and study of syndiotactic polystyrene nanocomposites"
Degree in Chemistry	July 2010 Aristotle University of Thessaloniki - Department of Chemistry **Undergraduate Thesis:** "Synthesis and characterization of nanocomposite materials using biocompatible polymers and fumed silica nanoparticles. Application in controlled drug release"

PUBLICATIONS IN INTERNATIONAL SCIENTIFIC JOURNALS

7- Quy Ong, **Nikolaos Nianias**, Francesco Stellacci. "*Molecular-phase separation in binary self-assembled monolayers of thiols on gold surfaces*" (REVIEW), submitted at EPL (Europhysics Letters).

6- Roumeli, E, **Nianias, N**, Filippousi, M, Avgeropoulos, A., Chrissafis, K., Papageorgiou, G.Z., Bikiaris, D.N. "*Combined and distinct contributions of different carbon nano-forms in polypropylene*", Macromolecular Materials and Engineering, 2015, 300, 611–626

5- I. Grigoriadou, **N. Nianias**, A. Hoppe, Z. Terzopoulou, D. Bikiaris, J. Will, J. Hum, J.A. Roether, R. Detsch, A.R. Boccaccini. "*Evaluation of silica-nanotubes and strontium hydroxyapatite nanorods as appropriate nanoadditives for poly(butylene succinate) biodegradable polyester for biomedical applications*", Composites Part B: Engineering Volume 60, April 2014, (49–59)

4- G.Z. Papageorgiou, D.S. Achilias, **N.P. Nianias**, P. Trikalitis, D.N. Bikiaris. *"Effect of the type of nano-filler on the crystallization and mechanical properties of syndiotactic polystyrene based nanocomposites"*, Thermochimica Acta Volume 565, 10 August 2013, (82–94)

3- K. Chrissafis,E. Roumeli, K.M. Paraskevopoulos, **N. Nianias**, D.N. Bikiaris. "*Effect of different nanoparticles on thermal decomposition of poly(propylene sebacate)/nanocomposites: Evaluation of mechanisms using TGA, and TG-FTIR-GC/MS"*, Journal of Analytical and Applied Pyrolysis Volume 96, July 2012, (92–99)

2- Dimitrios N. Bikiaris, **Nikolaos P. Nianias**, Evrykleia G. Karagiannidou, Aristides Docoslis. *"Effect of different nanoparticles on the properties and enzymatic hydrolysis mechanism of aliphatic polyesters,"* Polymer Degradation and Stability, (2011) 1-13

1- K. Chrissafis, E. Pavlidou, K. M. Paraskevopoulos, T. Beslikas, **N. Nianias**, D. Bikiaris, "*Enhancing mechanical and thermal properties of PLLA ligaments with fumed silica nanoparticles and montmorillonite,"* Journal of Thermal Analysis and Calorimetry (2011) Vol. 105, No.1, 313-323

PUBLICATIONS IN BOOKS

1- Dimitris S. Achilias, Lefteris Andriotis, Ioannis A. Koutsidis, Dimitra A. Louka, **Nikolaos P.Nianias**, Panoraia Siafaka, Ioannis Tsagkalias and Georgia Tsintzou. "*Recent Advances in the Chemical Recycling of Polymers (PP, PS, LDPE, HDPE, PVC, PC, Nylon, PMMA)*". Material Recycling - Trends and Perspectives, Editor: Dimitris S. Achilias. InTech, March/2012

PRESENTATIONS IN INTERNATIONAL CONFERENCES

April 24 – 27/2012	Nikolaos Nianias, Dimitrios Bikiaris. "**Effect of different nanofiller on syndiotactic polystyrene properties"**. 7th International Conference on NANOSTRUCTURED POLYMERS AND NANOCOMPOSITES, Prague, Czech Republic.
August 29-31/2011	N. P. Nianias, E. G. Karagiannidou, D. N. Bikiaris. **"Effect of different nanoparticles on properties and enzymatic hydrolysis rate of an aliphatic polyester".** BIOPOL-2011, 3rd International Conference on Biodegradable and Biobased Polymers, Strasbourg, France.
July 24-27/2011	Nikolaos Nianias, Dimitrios Bikiaris, K. Chrissafis, E. Pavlidou. **"Polypropylene nanocomposites with enhanced mechanical properties, thermal conductivity and thermal stability".** MEDICTA 2011 – 10th Mediterranean Conference on Calorimetry and Thermal Analysis, Porto, Portugal.
August 28 /2011	N. Nianias, E. Pavlidou, K. Chrissafis, Dimitrios Bikiaris. "**Polypropylene nanocomposites with MWCNTs and/or Nanodiamonds prepared by melt mixing".** Microscopy Conference MC 2011, Kiel, Germany.
December 9-12/2011	N.Nianias, G. Papageorgiou, D.Bikiaris, D.Achilias. **"Crystallization studies of novel nanocomposite materials of syndiotactic polystyrene and various types of inorganic nanoparticles".** Xidas P., Giliopoulos D., Tsiomi M., Nianias N., Bikiaris D., Triantafillidis K. **"Advanced mono-,di- and three-dimensional nanostructures for the reinforcement of polymeric materials".** 21st Panhellenic Chemistry Conference, Thessaloniki, Greece

SCIENTIFIC INTERESTS

- Self-assembly
- Nanostructured Surfaces and Engineered Interfaces
- Fabrication and modification of Carbon-Based and Metal Nanostructures
- Conductive polymers and Nanowires
- Biomimetic Materials

TEACHING EXPERIENCE

Assistant in MX-Bachelor EPFL course: Surfaces and interfaces (MSE-304)

PARTICIPATION IN RESEARCH PROJECTS

Jan.2 012-Dec. 2013	Project Titles: **«Polymeric nanocomposite materials of high performance and versatile properties»**.Research Committee A.U.TH. **« Green composite materials for 3D object production»**. Research Committee A.U.TH. **« Development of innovative nanocomposite polymeric materials as scaffolds for bone tissue reconstruction».**Research Committee A.U.TH. **« Development of innovative nanocomposite polymeric materials as scaffolds for bone tissue reconstruction».** Scholarship program for the Promotion of Scientific Exchanges and Cooperation between Greece and Germany IKYDA 2012
June 2011-Dec. 2013	Project Title: **« Application of novel inorganic nanostructures for the development of polymer nanocomposites with improved properties»**. Research Committee A.U.TH.

ADDITIONAL SKILLS AND INTERESTS

KNOWLEDGE OF HANDLING SCIENTIFIC INSTRUMENTS

- SPM (Easyscan 2 STM, Bruker Multimode Nanoscope IIIA, MFP-3D, Cypher S AFM Asylum)
- Electrochemistry
- Laboratory scale batch polymerization reactor & CEM Discover Microwave reactor
- Melt mixing twin screw co-rotating extruder
- Electrospinning apparatus
- MALDI-TOF-MS (Axima Plus))
- Mechanical properties (Instron 3344 Dynamometer & Tinius Olsen impact test)
- Polymer Thermal Analysis (Perkin-Elmer Pyris Diamond DSC, Pyris TGA, Diamond DMA)
- X-Ray Diffractometer (Rigaku-MiniFlex II)
- Gel Permeation Chromatography (Varian PL-GPC 50 Plus)
- HPLC(Shimadzu-Prominence Modular HPLC)
- Melt flow index (Dynisco-LMI4000)

LANGUAGE SKILLS

GREEK	Native
ENGLISH	Fluent - Certificate of Proficiency and TOEFL iBT 94/120
FRENCH	Beginner

COMPUTER SKILLS

UBUNTU , OSXand Windows XP,7 *(Operating Systems)*
Basic, Pascal *(Programming Languages)*
ChemOffice suite, ACD/ChemSketch, HyperChem *(Chemistry software)*
Origin *(data analysis, graphing and programming)*
Gimp (graphics editing program)

MEMBERSHIPS

Member of the Swiss Chemical Society
Member of the Association of Greek Chemists.

OTHER SKILLS

Silver medallist in national youth athletics championship